Detection of Nitroaromatic Compounds through Fluorescence Quenching of Pyrene Labeled Starch Nanoparticles

by

Sanjay Rajnikant Patel

A thesis

presented to the University Of Waterloo

In fulfilment of the

Thesis requirement for the degree of

Master of Science

in

Chemistry

Waterloo, Ontario, Canada 2018

AUTHOR'S DECLARATION

I hereby declare that I am the sole author of this thesis. This is a true copy of the thesis, including any required final revisions, as accepted by my examiners.

I understand that my thesis may be made electronically available to the public.

Abstract

The aim of this research was to demonstrate the potential application of starch nanoparticles (SNPs) labeled with 1-pyrenebutyric acid (PBA) as the active component in optical sensors used for the detection of minute quantities of nitroaromatic compounds such as 2,4,6-trinitrotoluene (TNT). Pyrene-labeled SNPs (Py-SNPs) with pyrene content ranging from 0.06 to 39 mol% were prepared. Quenching of the Py-SNPs by nitromethane (NM), 4-mononitrotoluene (MNT), 2,4-dinitrotoluene (DNT), and TNT was investigated in dimethyl sulfoxide (DMSO) and water. The bimolecular quenching rate constant for Py-SNPs in DMSO (k_{qSNP}) remained constant with pyrene content and was found to equal 1.6 (± 0.1), 3.9 (± 0.2), 2.2 (± 0.2), and 1.6 (± 0.2) $M^{-1}.ns^{-1}$ for NM, MNT, DNT, and TNT, respectively, averaged across all Py-SNPs for a given quencher. These quenching experiments revealed that the quenching efficiency in DMSO increased according to the sequence MNT>DNT>TNT=NM, where MNT was the most efficient quencher and TNT and NM were the worst quenchers. Quenching studies conducted in water for Py-SNPs quenched by NM showed increased protective quenching with increased pyrene content, suggesting that hydrophobic aggregation of the pyrene labels induced a collapse of the Py-SNPs in water that hindered the diffusion of NM to access the pyrene labels. Hardly any diffusive quenching was observed in water for the quenching of the Py-SNPs by MNT, DNT, and TNT. Rather these quenchers targeted hydrophobic aggregates of pyrene labels, which emitted as excimer. The binding of the quenchers to the pyrene aggregates of the Py-SNPs increased with increasing pyrene content and followed the sequence TNT >> DNT > MNT. In addition to quenching studies conducted in solution, quenching studies were repeated with MNT, DNT, and TNT on solid films of Py-SNPs coated filter papers (Py-CFPs). Vapour quenching studies yielded response times of 0.48 (± 0.05) and 3.6 (± 0.3) min for air saturated with MNT and DNT, respectively. Detection limits for the quenching of Py-CFPs by MNT, DNT, and TNT deposited onto the filter paper were

found to equal 30 (± 9), 11 (± 5), and 1.4 (± 0.6) ng per mm^2. In terms of detection limits, these results place the Py-CFPs among the best optical sensors currently available for the detection of TNT.

Acknowledgements

I would like to thank Professor Jean Duhamel for giving me the opportunity to do a M. Sc. thesis under his supervision and for his constant support, guidance, and encouragement in the laboratory. I would like to also thank my committee members, Profs. Scott Taylor and Juewen Liu, for taking the time to read and edit my thesis. I would also like to give special thanks to Damin Kim and Lu Li from the Duhamel group, for their precious help in the laboratory, and also Bowen Zhang from the Taylor laboratory for supplying starch nanoparticles modified with styrene oxide. I would like to also thank all members from the Duhamel and Gauthier groups for making my time as a graduate student a fun and friendly experience. Special thanks must be given to EcoSynthetix for financial support, providing the research-grade starch nanoparticles that were used throughout this thesis, and also for extremely helpful discussions and continued guidance and advice for the project by Drs. Smeets, Mesnager, and Bloembergen. I also want to thank my parents and siblings for all their support throughout my M. Sc. degree.

Table of Contents

List of Figures

Abbreviations

DIC	*N*,*N*'-Diisopropylcarbodiimide
DMAP	4-Dimethylaminopyridine
DMF	*N*,*N*'-Dimethylformamide
DMSO	Dimethyl Sulfoxide
DNT	2,6-Dinitrotoluene
DS	Degree of Substitution
IMS	Ion Mobility Spectroscopy
MNT	4-Mononitrotoluene
NAC	Nitroaromatic compound
NM	Nitromethane
PBA	1-Pyrenebutyric acid
Py-CFPs	Py-SNP-Coated Cellulose Filter Papers
Py-SNPs	Pyrene-Labeled Starch Nanoparticles
SNPs	Starch Nanoparticles
SNP1	Starch Nanoparticles with a hydrodynamic diameter of 46 (± 3) nm
SNP2	Starch Nanoparticles with a hydrodynamic diameter of 8.3 (± 0.7) nm
SV	Stern-Volmer
THF	Tetrahydrofuran
TNT	2,4,6-Trinitrotoluene
UV-Vis	Ultraviolet-Visible

List of Symbols

F	Fluorescence intensity after exposure to quencher
F_o	Fluorescence intensity before the addition of quencher
h	Hill coefficient
k	Quencher concentration for the Hill equation where 50% quenching occurs
k_q	Bimolecular quenching rate constant for molecular pyrene
k_{qSNP}	Bimolecular quenching rate constant for Py-SNPs
K_s	Equilibrium constant for the binding of NACs to pyrene aggregates in water
$<\tau>_N$	Number average fluorescence lifetime at a given quencher concentration
$<\tau>_{No}$	Number average fluorescence lifetime before the addition of quencher
$<\tau>_{Wo}$	Weight average fluorescence lifetime before the addition of quencher
S_o	Zeroth electronic state
S_1	First electronic state
S_2	Second electronic state

Chapter 1

Introduction

1.0 Introduction

Nitroaromatic compounds (NACs) are well known for their use as explosives[1–3] and pesticides.[4,5] Unfortunately, NACs are also known to be mutagenic to humans and toxic to the environment.[4,6] Furthermore, as most NACs are explosives, they pose significant security risks in public areas. Consequently, the ability to detect their presence has become an urgent public need.[4] Current methods employed for the detection of NACs include ion mobility spectroscopy, mass spectroscopy, or canine units.[1–3] Although these methods offer high sensitivity, typically on the order of ppb and ppt, they suffer from at least one or more of the following drawbacks: high cost, non-portability, and complex instrumentation.[3,7] Owing to these disadvantages, the suitability of alternate detection methods based on surface enhanced Raman spectroscopy, electronic olfactory systems, and sensor techniques have been investigated.[3,8] Within the realm of sensor-based techniques, fluorescence has gained much popularity due to its lower requirements in terms of relatively simple instrumentation, portability, low cost, and high sensitivity.[2,9] In these experiments, electron-rich dyes are exposed to electron-poor NACs resulting in efficient quenching of the dyes. The luminophores that have been employed so far in fluorescence sensors include conjugated polymers,[2,3,8–15] nanodots,[2,8,16,17] metal complexes,[8,18] luminophores that undergo aggregation induced emission (AIEgens),[3,14,19–23] and pyrene.[10,24–27] Contrary to AIEgens whose fluorescence is dramatically enhanced upon aggregation in water, aggregation of pyrene induces pyrene excimer formation which shifts the purplish-blue fluorescence of the pyrene monomer (370 – 400 nm) to the green fluorescence of the excimer (450 – 600 nm).[28] Beside the luminophore, the nature of the substrate used in a fluorescence sensor must be carefully considered as it must ensure that the luminophores be readily accessible upon exposure to NACs. Consequently, substrates which offer an open structure are often selected for fluorescence sensors.

These include mesoporous silica films,[10,29–32] or thin films of microspheres,[26] nanofibers,[14,25,27] dendrimers,[33–35] and hyperbranched[11,36] or linear polymers[10,18,21,22,24,25,27,30,37–40] deposited on a glass, quartz, or paper substrate. However, the preparation of these fluorescent substrates is commonly based on multi-step syntheses that usually increase costs during the scale up process, limiting their potential applicability in an industrial setting. In this work, the fluorescence of pyrene-labeled starch nanoparticles (Py-SNPs) was employed to detect minute quantities of nitroaromatic compounds. Starch nanoparticles (SNPs) offer several advantages over the other polymeric scaffolds traditionally used in optical sensors. SNPs are derived from food grade starch. As such, SNPs represent a cost-effective and nontoxic nanosized material. Furthermore SNPs are already being employed industrially as natural alternatives to styrene butadiene latexes for paper coating.[41,42] As such, they strongly interact with cellulose and adsorb tightly onto the surface of the cellulosic fibers constituting paper. However the development of an optical sensor based on SNPs requires that they be fluorescently labeled. A wide array of fluorophores has been described in the scientific literature for the detection of NACs with the dye pyrene being one of them.[11,13,14,16,18,20,22,24,26,29,30,37,38,43–49]

In this work, pyrene was chosen as the fluorescent dye to label SNPs owing to its well-known photophysical properties[28] such as high quantum yield and large molar extinction coefficient which enable its detection at low concentrations, its ability to form excimers, and its hydrophobicity (solubility of pyrene equals 0.7 μM in water).[50] Labeling of SNPs with pyrene induces the formation of hydrophobic pyrene-rich microdomains in water that emit as excimer upon direct excitation. The hydrophobic microdomains of the pyrene-labeled SNPs (Py-SNPs) can be exploited to drive sparingly water-soluble NACs to them. Since most nitroaromatic compounds are well known quenchers of fluorescence, the hydrophobic microdomains generated by pyrenyl

aggregates within Py-SNPs adsorbed onto paper offer an inherent means to detect NACs in water by monitoring their sensitivity to fluorescence quenching.

1.1 Starch

Starch is the second most abundant biopolymer available on earth, typically found in many plants where it mainly serves as energy storage.[51–53] Starch consists of amylose and amylopectin, where amylose is a linear polysaccharide composed of anhydroglucose units connected via an α (1→4) linkage and amylopectin is a highly branched polysaccharide composed of anhydroglucose units connected via α (1→4) linkages with branching occurring via α (1→6) linkages.[51] Their structure is shown in Figure 1. Since starch can be isolated from a variety of sources such as peas, wheat, corn, potatoes, etc., the size and branching level of amylose and amylopectin vary.[51,52,54] In this thesis, the research grade starch nanoparticles (SNPs) obtained from EcoSynthetix were derived from corn starch, which is composed mainly of amylopectin. Starch, found as micron-sized granules in nature, is not typically dispersible in water. By contrast, the SNPs supplied by EcoSynthetix, namely SNP1 and SNP2 with a hydrodynamic diameter of, respectively, 46 (± 3) and 8.3 (± 0.7) nm,[55] were water dispersible. In addition to water dispersibility, the SNPs retained the numerous advantages of starch, such as their innate non-toxicity, environmentally friendly production free of organic solvents, and facile chemical modification and adsorption onto paper. An important industrial use for SNPs is as coating material to replace styrene butadiene and styrene acrylate latex in paper coating applications.[41,42] Consequently, the development of an optical sensor utilizing SNPs may represent a new industrial application for SNPs and could provide a cost effective means to detect NACs in settings where NAC detection is of the utmost importance such as in public spaces.

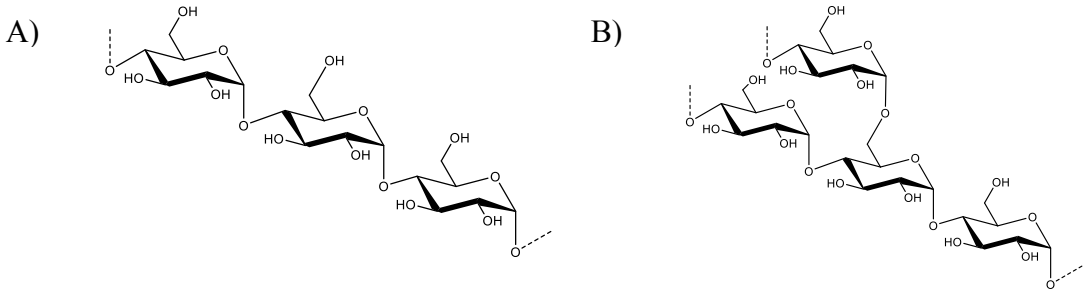

Figure 1. Chemical structure of amylose (A) and amylopectin (B).

The development of an optical sensor based on SNPs requires the fluorescent labeling of their polysaccharide scaffold. Therefore a brief introduction into fluorescence and the photochemical properties of the chosen fluorophore, pyrene, is provided hereafter.

1.2 Fluorescence

Fluorescence is a well-known photophysical phenomenon where the relaxation of an excited molecule to its ground-state is associated with the emission of a photon.[56] This process can be easily visualized with the Jablonski diagram shown in Figure 2.

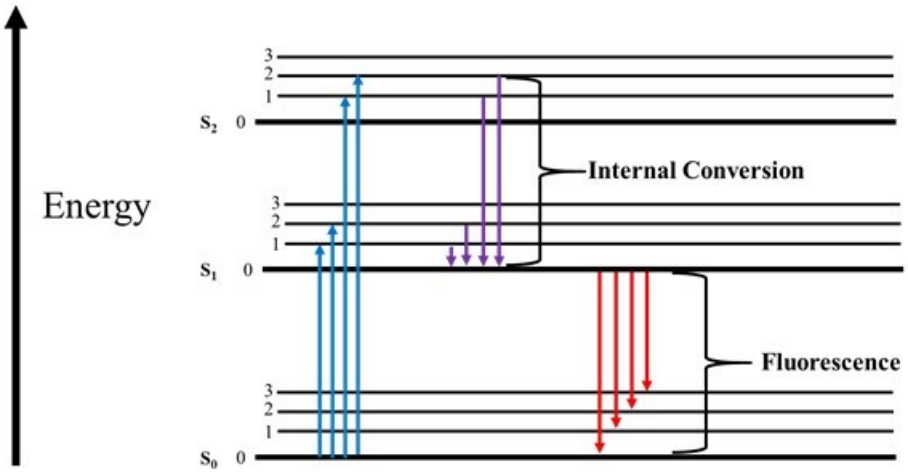

Figure 2. Jablonski diagram describing the fluorescence phenomenon

Fluorescence begins with the absorption of a photon of energy (hv), where h is Planck's constant and v is the frequency of the electromagnetic radiation.[56] Absorption of a photon by the fluorophore at an excitation wavelength, λ_{ex}, results in its excitation from the lowest vibrational level of the lowest electronic state (S_0^0) to one of the vibrational levels of a higher electronic state. This process typically occurs within 10^{-15} s.[56] Depending on the energy having been absorbed by the fluorophore, the excited molecule will reach one of the vibrational energy levels of a higher electronic state (S_1, S_2….). The excited fluorophore will undergo internal conversion, which is a process whereby the excited molecule relaxes down to the lowest vibrational energy level of the S_1 electronic state (S_1^0). Internal conversion typically occurs within 10^{-12} s. The molecule will then relax from S_1^0 back to one of the vibrational energy levels of the lowest electronic state, S_0, by emitting a photon at a wavelength, λ_{em}. The energy of a photon can be described using Planck's equation given as $E = \frac{h \times c}{\lambda}$, where E and λ are, respectively, the energy and wavelength of the photon and c is the speed of light.[56] E and λ being inversely proportional, a higher wavelength corresponds therefore to a lower energy. Since energy is lost via internal conversion (as seen in the Jablonski diagram), solvent relaxation, and various non-radiative processes, an energy larger than that corresponding to fluorescence is required to excite the fluorophore. The energy loss between the absorption and emission of a fluorophore is referred to as Stokes' shift.[56] In turn, this energy loss can be amplified or reduced depending on the ability of the local environment of the fluorophore to undergo molecular rearrangements that stabilize (or not) the dipole moment of the fluorophore as it transitions between its excited and ground states. Thus, the fluorescence signal is often found to respond to the polarity of the local environment experienced at the molecular level

by a fluorophore which makes fluorescence an excellent analytical tool to probe the behavior of fluorescently labeled macromolecules in solution and the solid state.

1.2.1 Pyrene

Numerous fluorophores are commercially available for fluorescence quenching studies. However, considering that this project was to develop a turn-off optical sensor for the detection of NACs, the dye to be employed in these studies needed to be carefully selected. Pyrene has many advantageous photophysical properties such as a long fluorescence lifetime (~400 ns in unaerated cyclohexane)[57] and a high quantum yield (0.31 in cyclohexane)[58] and large molar extinction coefficient (54,000 $M^{-1}.cm^{-1}$ in cyclohexane at 335.2 nm)[59] that enable its easy detection at micromolar concentrations due to its strong fluorescence signal. In addition to these well-known properties, pyrene can also form an excimer. An excimer is an excited complex between an excited and a ground-state fluorophore.[28] Many aromatic fluorophores, such as naphthalene or perylene, are known to form excimer, but their excimer fluorescence is either weak or overlaps the monomer fluorescence. Pyrene stands out compared to other fluorophores because it forms excimer efficiently and the fluorescence of the pyrene monomer and excimer do not overlap.[28] This enables one to monitor the fluorescence signal of the monomer and excimer independently providing two optical channels to probe the kinetics of pyrene excimer formation (PEF). Many of the special photophysical properties of pyrene are due to the fact that its 0-0 transition is symmetry forbidden. The symmetry forbidden 0-0 transition of pyrene results in the absence of overlap between the absorption and fluorescence spectra of pyrene which minimizes the inner filter effect when working at high pyrene concentration, the ability of pyrene to respond to the polarity of its local environment, and its long lifetime.[28] Furthermore, the quasi-absence of overlap between the

absorption and fluorescence spectra of pyrene implies that the energy of an excited pyrene cannot hop between different pyrene labels contrary to other dyes like naphthalene or perylene, even when the average distance between pyrene labels decreases as they approach each other during excimer formation.[28] In this work, 1-pyrenebutyric acid (Figure 3) was selected to fluorescently label the SNPs.[60,61]

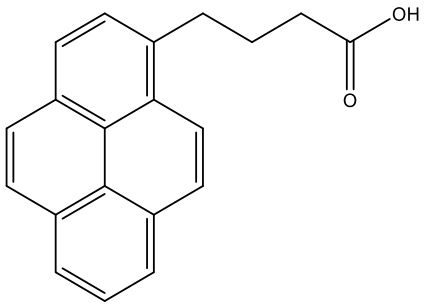

Figure 3. Chemical structure of 1-pyrenebutyric acid (PBA).

1.3 Quenching

This project was to assess the potential of Py-SNP-coated filter papers (Py-CFPs) as optical sensors for the detection of nitroaromatic compounds (NACs) by monitoring a decrease in fluorescence intensity of the Py-CFPs upon contact with NACs. As such, quenching played a key role in the design of the Py-CFP optical sensor. Quenching refers to any photophysical process leading to a decrease in the overall fluorescence intensity of a dye. The processes include fluorescence resonance energy transfer (FRET), electron transfer, or excimer formation, to name but a few. Quenching can occur in a dynamic manner by diffusive encounters between an excited dye and a quencher or in a static manner through the formation of a ground-state complex between a dye and a quencher. The former and latter processes are referred to as, respectively, dynamic and static quenching and are described in more details in the next section.

1.3.1 Dynamic Quenching

Dynamic quenching, also called collisional quenching, is a process whereby the quencher will diffuse through the solution and encounter an excited fluorophore. Upon contact between the quencher and the excited fluorophore, the excited fluorophore will undergo a non-radiative transition to the ground state without the emission of a photon. The Stern-Volmer (SV) equation given in Equation 1 describes quantitatively the decrease in fluorescence intensity and lifetime due to collisional quenching.

$$\frac{\tau_o}{\tau} = \frac{F_o}{F} = 1 + k_q \cdot \tau_o \cdot [Q] \tag{1}$$

In Equation 1, F and τ and F_o and τ_o are the fluorescence intensity and lifetime of the dye with and without quencher, respectively, $[Q]$ is the concentration of quencher added, and k_q is the bimolecular quenching rate constant. The bimolecular quenching rate constant reflects the efficiency of quenching. If quenching occurs in a purely dynamic manner, F_o/F plotted as a function of quencher concentration should yield a linear relationship. Furthermore, F_o/F should be equivalent to τ_o/τ and therefore, both plots should overlap.

1.4.1 Static Quenching

In contrast to dynamic quenching, static quenching occurs via the formation of a non-fluorescent complex between a fluorophore and the quencher. Excitation of this complex results in instantaneous quenching of the fluorophore. As such, fluorescence lifetime measurements report only on the non-complexed fluorophores and they are unaffected by the presence of the non-fluorescent complexes. Consequently the τ_o/τ ratio should equal unity and remain unchanged with quencher concentration. However, an overall decrease in the fluorescence intensity should be

observed with increasing quencher concentration in the steady-state fluorescence spectra, since more non-fluorescent complexes are generated with increasing quencher concentration, while the number of uncomplexed fluorescent species decreases. The SV equation given in Equation 1 can be modified according to Equation 2 to account for static quenching. If quenching occurs predominantly in a static manner, k_q approaches zero and a plot of F_o/F as a function of quencher concentration yields K_s, the equilibrium constant for the formation of the ground-state complex.

$$\frac{F_o}{F} = (1 + k_q \cdot \tau_o \cdot [Q]) \times (1 + K_S \cdot [Q]) \quad (2)$$

1.4 Thesis Outline

This thesis aims to demonstrate that Py-SNP-coated filter papers (Py-CFPs) can be employed as optical sensors. The research that was conducted to achieve this goal is presented in the following manner. This first chapter provided a brief introduction on NAC detection, SNPs, fluorescence, and quenching mechanisms. The experimental procedures and instrumentation used in this thesis are presented in Chapter 2. Chapter 3 reports the quenching experiments carried out on Py-SNPs in DMSO and water to assess the mode of quenching induced by different NACs in these solvents. Included in Chapter 3 are experiments where the fluorescence of Py-CFPs is quenched either by exposure to MNT, DNT, and naphthalene vapours or by MNT, DNT, TNT, and naphthalene adsorbed directly onto the Py-CFPs. The advantages and disadvantages of the Py-CFPs were then compared to those of other optical sensors described in the scientific literature. Chapter 4 reports on the attempts that were made to lower the detection limits achieved with the Py-CFPs in Chapter 3. Chapter 5 summarizes the key findings of this thesis and makes suggestions for future work.

Chapter 2:

Experimental Procedure

2.0 Experimental Procedures

Materials: Two research grade SNPs, namely SNP1 and SNP2 with hydrodynamic diameters of, respectively, 46 (± 3)[55] and 8.3 (± 0.7 nm),[55] were supplied by EcoSynthetix. They were dispersed by stirring the dry SNP powder in warm DMSO for 30 minutes to obtain a homogeneous dispersion. The SNPs in the DMSO dispersion were precipitated once in HPLC grade acetone to remove any remaining by-products resulting from their production. All chemicals were purchased directly from Sigma-Aldrich and used without further purification. Special care was applied when handling 2,4,6-trinitrotoluene (TNT) as it is an explosive. Only minuscule quantities of TNT were used in the dry state to conduct the quenching study on the Py-CFPs. After the quenching studies were conducted, the Py-CFPs were rinsed with organic solvents to remove traces of TNT. All other experiments used dilute solutions of TNT (< 1 g/L).

2.1 Synthesis of Pyrene Labeled Starch Nanoparticles

The pyrene-labeled starch nanoparticles and amylopectin (Py-SNPs and Py-Amy respectively) used in this research were synthesized according to the reaction scheme shown in Figure 4 which had been reported earlier for the pyrene-labeling of amylose.[61] The synthesis of Py(8)-SNP1 where 8 mol% of the anhydroglucose units of the SNP1 sample bore a pyrene label is described in more details hereafter. SNP1 (1.0 g, 6.2 mmol of anhydroglucose units) was dispersed in DMSO (30 mL) by stirring at 60 ^{o}C for 30 min. The dispersion was brought to room temperature and DMF (10 mL) was added. 1-Pyrenebutyric acid (PBA, 3.65 mmol) and 4-(dimethylamino)pyridine (DMAP, 0.88 mmol) were dissolved in the SNP1 dispersion. The mixture was placed in an ice bath while *N*,*N*'-diisopropylcarbodiimide (DIC, 0.848 mL, 5.4 mmol) was added dropwise under N_2 atmosphere. The reaction was allowed to proceed at room temperature for 48 hours under

nitrogen atmosphere. The Py-SNP1 sample was purified via 3-4 precipitations in tetrahydrofuran or methanol.

Fluorescence spectra of dilute Py-SNP dispersions in DMSO of the precipitated Py-SNPs ([*Py*] = 2.5×10^{-6} M) were acquired and the fluorescence intensity ratio (I_E/I_M) of the excimer over that of the monomer was determined after each precipitation. Since unattached PBA would emit as monomer, a constant I_E/I_M ratio after two successive precipitations indicated that all unattached PBA had been removed and that the fluorescence signal was solely due to PBA molecules covalently attached to the SNPs. The degree of substitution (DS) of the Py-SNPs was determined with Equations 3 and 4. In brief, the absorbance (*Abs*) at 346 nm of a dispersion prepared with a known massic concentration (m in $g.L^{-1}$) of Py-SNP in DMSO was measured. The number of moles of pyrene per gram of Py-SNP (λ_{Py}) was determined using Equation 3, where ε, the molar extinction coefficient of PBA in DMSO at 346 nm, equaled 41,400 $M^{-1}.cm^{-1}$ and l, the cuvette path length, was 1 cm. The molar fraction (x) of anhydroglucose units labeled with pyrene could then be calculated by applying Equation 4, where M_{Glu} and M_{Py} represented the molar mass of an unlabeled and pyrene-labeled anhydroglucose unit equal to 162 and 432 $g.mol^{-1}$, respectively. The method described above has been previously employed for pyrene content determination.[60,61]

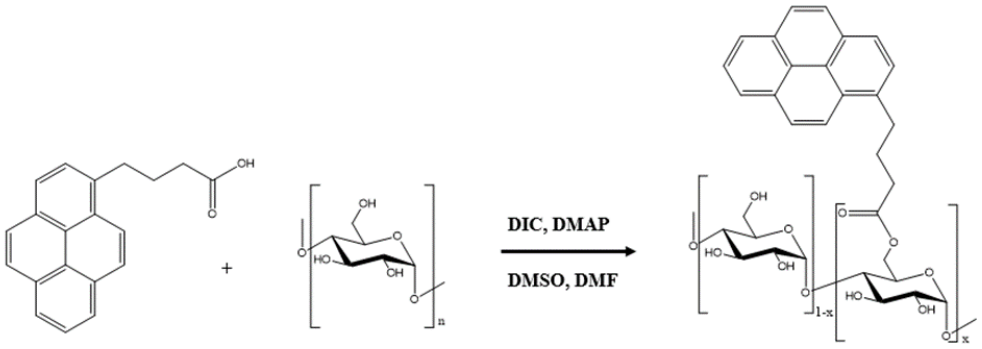

Figure 4. Labeling scheme of SNPs with 1-pyrenebutyric acid (PBA).

$$\lambda_{Py} = \frac{Abs}{m \cdot \varepsilon \cdot l} \tag{3}$$

$$x = \frac{M_{Glu}}{1/\lambda_{Py} + M_{Glu} - M_{Py}} \tag{4}$$

2.2 Quenching Studies

Quenching studies conducted in DMSO with nitromethane (NM), *p*-mononitrotoluene (MNT), and 2,4-dinitrotoluene (DNT) were carried out with a pyrene concentration of $2.4 \cdot 10^{-6}$ M while those conducted with TNT used a pyrene concentration of $1.2 \cdot 10^{-5}$ M, owing to the molar extinction coefficient of TNT which was significantly higher than that of NM, MNT, and DNT at 346 nm, the excitation wavelength for 1-pyrenebutyric acid. These pyrene concentrations were low enough to prevent any interaction between Py-SNPs. In each case, a Py-SNP dispersion was prepared and split in two halves. The desired volume of quencher solution in DMSO was added to one half and a same volume of DMSO without quencher was added to the other half. In so doing, the two halves of the Py-SNP dispersion in DMSO had the same Py-SNP concentration, but one was without quencher and the other was with quencher. Mixing different volumes of the two dispersions yielded the desired range of quencher concentration for the quenching study. This procedure ensured that increasing quencher concentrations did not dilute the Py-SNP dispersion so that a reduction in fluorescence intensity could be assigned to quenching only.

The quenching studies in water were conducted in the same manner. They were complicated by the fact that pyrene, MNT, DNT, and TNT were sparingly soluble in water. To circumvent this issue, a Py-SNP stock solution was prepared in DMSO with a pyrene concentration of $4.6 \cdot 10^{-4}$ M. The Py-SNP stock solution was then diluted with milliQ water to yield an aqueous Py-SNP dispersion with a final $2.6 \cdot 10^{-6}$ M pyrene concentration. All aqueous Py-SNP dispersions contained less than 1 wt% of DMSO. The Py-SNP aqueous dispersions were split into two halves,

and the quencher was added to only one half at a concentration that was lower than its saturation limit in water equal to 361 at 24 °C,[62] 204 at 24 °C,[62] and 115 mg/L at 23 °C,[63] also equivalent to molar concentrations of 2.6, 1.1, and 0.51 mM, for MNT, DNT, and TNT, respectively. The two aqueous dispersions containing the same Py-SNP concentration were mixed to adjust the quencher concentration for the quenching studies without affecting the Py-SNP concentration.

The fluorescence spectra and decays acquired with the Py-SNP dispersions without quencher were used to determine the fluorescence intensity (F_o) and lifetime (τ_o). The fluorescence intensity and decay of the Py-SNP dispersions with quencher were referred to as F and τ, respectively. Quenching studies with MNT, DNT, and TNT in DMSO were conducted with a triangular cell from Hellma in the front face geometry due to the strong absorbance of the solutions prepared with the nitroaromatic quenchers. All quenching studies in water were conducted using a normal geometry, since the NM, MNT, DNT, and TNT concentrations in water were sufficiently low that quencher absorption would not affect the steady-state fluorescence measurements.

The highest pyrene content for quenching studies with NM, MNT, and DNT in DMSO and water was 10 mol%. Owing to the limited stock of Py(10)-SNP1 sample, a new SNP1 sample was synthesized and its content was determined to be 11 mol%. Py(11)-SNP1 was used for quenching studies with TNT in DMSO and water. Additionally, this sample was used for subsequent Py-CFPs studies.

2.3 Py-SNP coated filter papers (Py-CFPs)

The filter papers were coated with Py-SNPs according to the drop method. In brief, a Py-SNP stock dispersion was prepared in DMSO with a pyrene concentration of $6.0 \cdot 10^{-5}$ M. The Py-SNP stock dispersion in DMSO (0.06 g) was then diluted with milliQ water (9 g), to make a Py-SNP stock dispersion in water that contained 0.7 wt% DMSO. The aqueous Py-SNP stock dispersion

was directly deposited onto a piece of filter paper resulting in a filter paper coated with approximately $1.6 \cdot 10^{-11}$ mol of pyrene per mm^2. The filter paper was dried in the dark under N_2 until constant mass (typically within an hour) was reached. A limit stock of Py(10)-SNP1 was available after conducting the solution-based quenching studies. As such a new Py-SNP1 sample, namely Py(11)-SNP1, was synthesized and used for a majority of the Py-CFP studies.

2.4 Quenching of Py-CFPs by NAC vapors

A given quantity of NAC, typically 10 (± 2) mg, was deposited at the bottom of a 20 mL disposable vial. The NAC at the bottom of the vial was covered by a cotton ball before capping the vial. The chemical was allowed to equilibrate at room temperature for 24 hours. The initial fluorescence intensity (F_o) of a 0.5 cm × 0.5 cm Py-CFP humidified with 5 μL of water was measured in the absence of chemical vapour. The Py-CFPs strip was quickly introduced to the 20 mL vial for a predetermined time and the fluorescence intensity after exposure to the chemical (F) was measured. Equation 5 provided a measure of the quenching efficiency (E_Q). E_Q was determined and plotted as a function of exposure time. The experimental data for MNT and DNT were well described by a hyperbola and were parameterized with a Michealis-Menten like equation, namely Equation 6 where t was the exposure time in minutes and k_m was the time where 50% quenching occurred. A more detailed description of Equation 6 and the determination of the error bars for k_m can be found in the appendix along with the fitted parameters for the response times (see Table 58A). The response time of MNT and DNT, and the error, were determined when 90% quenching had occurred.

$$E_Q = (1 - F/F_o) \times 100\% \quad (5)$$

$$E_Q = \frac{t}{k_m + t} \quad (6)$$

2.5 Quenching of Py-CFPs by NAC deposition

The Py-CFPs prepared by the drop method were humidified with water. The protocol described hereafter was for 1 × 1 cm^2 filter papers coated with Py(11)-SNP1. The Py-CFPs were humidified with water (10 μL). The humidified Py-CFPs were placed between two quartz plates and their fluorescence spectrum was acquired to obtain the fluorescence intensity without quencher ($^{W}F_o$). The Py-CFPs were dried. An organic solvent (OS), either pure HPLC grade ethanol or acetonitrile (10 μL), or 10 μL of a solution of MNT, DNT, TNT, or naphthalene in the same organic solvent, was deposited on the Py-CFPs. The organic solvent was evaporated under a gentle flow of nitrogen and a drop of water (10 μL) was added to drive the binding of the quencher to the pyrene aggregates. The humidified Py-CFPs were placed between two quartz plates and the fluorescence spectra of the Py-CFPs without ($^{OS}F_o$) and with (^{OS}F) quencher were acquired. In order to duplicate the same experimental protocol, a single application of organic solvent was applied to all Py-CFPs. For each quenching study, the $^{W}F_o$ and $^{OS}F_o$ intensities were recorded for four Py-CFPs prepared without quencher and their ratios were averaged to yield $<^{W}F_o/^{OS}F_o>$. The averaged ratio was found to equal 1.25 ± 0.05 reflecting enhanced excimer emission from the Py-CFPs before application of the organic solvent. The ratio ($^{W}F_o/^{OS}F$) obtained for each Py-CFP with quencher was compared to $<^{W}F_o/^{OS}F_o>$ by plotting the quantity $<^{W}F_o/^{OS}F_o>/(^{W}F_o/^{OS}F)$ as a function of the amount of quencher added to the Py-CFP expressed in ng of quencher per mm^2. All Py-CFP studies, unless otherwise specified, were conducted with Py(11)-SNP1 (SNP1 labeled with 11 mol% of 1-pyrenebutyric acid) on Whatman filter paper No. 1. The trends of $<^{W}F_o/^{OS}F_o>/(^{W}F_o/^{OS}F)$-*vs*-mass of quencher added were fitted to the Hill equation (Equation 7), where x represents the mass of quencher expressed in ng per mm^2, h reflects the steepness of the drop where quenching occurs, and k is the mass of quencher where 50% of the Py-CFP

fluorescence is quenched. A more detailed description of Hill's equation and error determination is provided in the Appendix (pages 141-142). All detection limits and fitted parameters of the Hill equation can be found in Table A59. All detection limits reported corresponded to the amount of quencher that was required to quench 90% of the fluorescence intensity of the Py-CFPs.

$$< {}^{W}F_0 / {}^{E}F_0 > /({}^{w}F_0 / {}^{E}F) = 1 - \frac{x^h}{x^h + k^h} \quad (7)$$

2.6 UV-Vis Absorption

A Varian Cary 100 Bio spectrophotometer was employed to acquire the absorption spectra of the Py-SNP dispersions and the quencher solutions. It was used to determine the pyrene concentration of the Py-SNP dispersions in DMSO from the absorbance at 346 nm using the molar extinction coefficient of 41,400 $M^{-1}.cm^{-1}$ for 1-pyrenebutyric acid in DMSO. Knowledge of the concentration of the pyrene labels was necessary to measure the pyrene content (λ_{Py}) of the Py-SNPs and ensure that the Py-SNP dispersions contained 2.4×10^{-6} M pyrene for most fluorescence quenching studies or 1.2×10^{-5} M pyrene for the TNT quenching study in DMSO.

2.7 Steady-State Fluorescence

A Photon Technology International spectrofluorometer equipped with a xenon arc lamp was employed to acquire the fluorescence spectra by exciting the dispersions or films at 346 nm and scanning the emission from 350 to 600 nm. Front face measurements were carried out with a quartz triangular cell from Hellma for the Py-SNP dispersions in DMSO quenched by the NAC quenchers and with a solid-state sample holder for the Py-CFPs. The excitation and emission slit-widths were set at 2 and 1 nm, respectively. The Py-SNP dispersions in water and DMSO were not degassed. The fluorescence intensity of the monomer (I_M) and excimer (I_E) were calculated using the area under the SSF spectrum from 373 to 379 nm and from 500 to 530 nm, respectively.

2.7 Time-Resolved Fluorescence

The monomer and excimer fluorescence decays of the Py-SNP dispersions in water and DMSO were acquired at an emission wavelength of, respectively, 375 and 510 nm using an IBH TC-SPC fluorometer in conjunction with a NanoLED-340 laser and an excitation monochromator to excite the dispersions at 346 nm. Additionally a cut-off filter at 370 and 495 nm was used during the acquisition of, respectively, the monomer and excimer fluorescence decays to prevent scattered light from reaching the detector. The decay of a LUDOX dispersion obtained by setting the excitation and emission wavelengths at 346 nm was employed as the instrument response function (IRF) in the decay analysis. All fluorescence decays had 15,000 counts at the decay maximum to ensure a satisfying signal-to-noise ratio. The fluorescence decays were analyzed with sums of two-to-three exponentials which were convoluted with the IRF. Pre-exponential factors and decay times were optimized with the Marquardt-Levenberg algorithm.[64] The fits were deemed satisfactory when the χ^2 parameter was smaller than 1.3 and the residuals and autocorrelation of the residuals were randomly distributed around zero. Pre-exponential factors and decay times retrieved from these analyses are listed in Tables A1-49 in the Appendix.

Chapter 3

Solution Quenching

Studies

3.0 Solution Quenching Studies

The goal of this project was to develop Py-SNP-coated filter papers (Py-CFPs) and demonstrate their potential application as optical sensors for the detection of nitroaromatic explosives such as TNT. The implementation of an optical sensor whose operation would be based on the fluorescence quenching in the solid state of Py-SNPs by NACs required that the actual fluorescence quenching mechanism be first investigated in solution. DMSO and water were selected to conduct these solution quenching studies. DMSO constituted an ideal solvent where the pyrenyl labels and all quenchers (NM, MNT, DNT, and TNT) were soluble and the SNPs could be easily dispersed. Quenching studies in DMSO yielded the bimolecular quenching rate constant for the Py-SNPs by the quenchers which provided a measure of their relative quenching efficiency. By contrast, only the SNPs were dispersible in water while the pyrene labels and the NACs were sparingly soluble. Consequently hydrophobic interactions between the pyrene labels and the NACs took place in water and this interaction could be probed through fluorescence quenching experiments. These different quenching mechanisms were carefully characterized for all the quenchers to prepare Py-CFPs that could be employed as optical sensors by taking advantage of the quenching of excited pyrene aggregates by NACs. But before conducting the fluorescence quenching experiments, the effect that the absorption of the quenchers might have on the fluorescence of the Py-SNP dispersions needed to be investigated.

3.1 Comparison of the photophysical properties of the quenchers and 1-pyrenebutyric acid

Since the purpose of this study was to develop a fluorescent paper-based sensor for the detection of nitrated compounds through a decrease in fluorescence intensity induced by quenching, the photophysical properties of the different quenchers needed to be carefully examined. Indeed, a decrease in fluorescence intensity is not always the result of quenching. For instance, introduction

of a chemical that absorbs where the fluorophore absorbs and/or emits can also lead to a decrease in fluorescence intensity. In order to assess the importance of reabsorption by the quenchers on the fluorescence of the Py-SNP dispersions, the extent of overlap between the absorption spectra of the quenchers and the absorption and emission spectra of the pyrene derivative used to prepare the Py-SNPs was determined. The molar extinction coefficient spectrum of each quencher in DMSO and water was obtained by dividing the absorbance in the absorption spectra by the concentration of the quenchers since the pathlength of the cell equaled 1 cm. To illustrate the extent of overlap between spectra, the molar extinction coefficient spectra of the quenchers in DMSO and water were plotted in, respectively, Figures 5A and B together with the spectra of the molar extinction coefficient and the normalized fluorescence of 1-pyrenebutyric acid used to prepare the Py-SNPs. As shown in Figure 5, NM had a low absorbance in DMSO and water at both 346 nm and 375 nm which were the wavelengths for, respectively, the excitation (λ_{ex}) and emission (λ_{em}) of the pyrene monomer. At the highest NM concentration of 20 mM used in the quenching experiments, the absorbance at λ_{ex} and λ_{em} would equal 0.05 and 0.004, respectively in DMSO. Such a low absobance suggested that an NM concentration of 20 mM and lower would not induce re-absorption. However this was not the case for MNT, DNT, and TNT which, at their highest concentrations of 6.0, 5.0, and 4.5 mM used for the quenching experiments in DMSO, had absorptions of 1.7 and 0.8, 3.5 and 1.4, 4.3 and 1.5 at λ_{ex} and λ_{em}, respectively. Such high absorptions are known to result in substantial re-absorption effects in fluorescence studies. To mitigate this issue, front face geometry was employed. Since similar molar extinction coefficients were found in water and DMSO for all quenchers, re-absorption would also be a problem for Py-SNP dispersions in water, if a same quencher concentration was used. Fortunately, the limited solubility of MNT, DNT, and TNT in water resulted in maximum concentrations of 0.3, 0.1, and

0.01 mM, respectively. Such low concentrations ensured that no re-absorption would induce any artefact in the fluorescence experiments even at the highest quencher concentration used in the quenching studies for the aqueous Py-SNP dispersions.

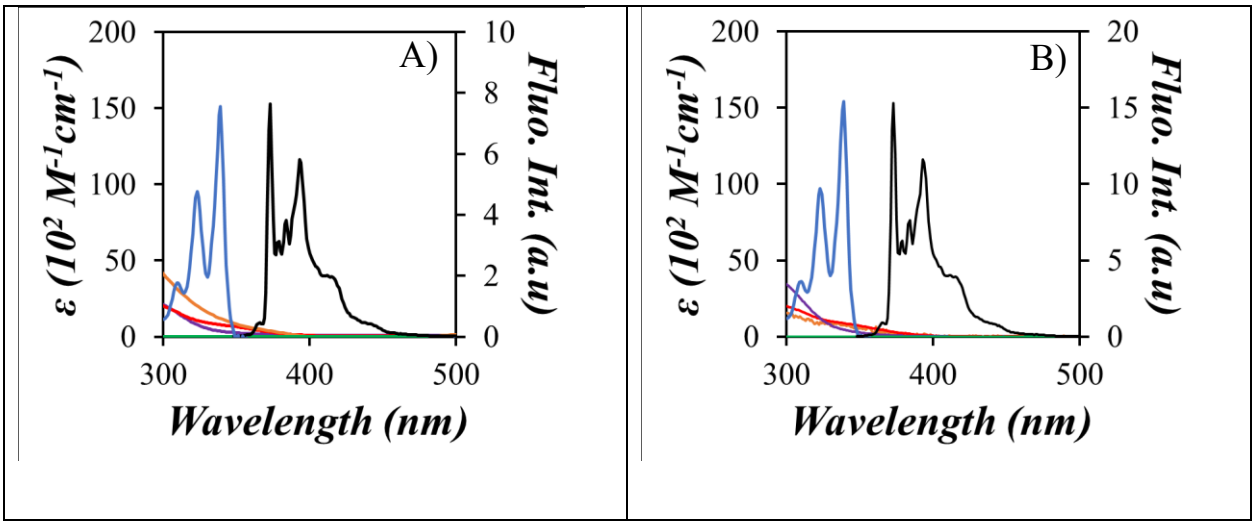

Figure 5. Spectra of the molar extinction coefficient of NM (, low value along the x-axis), MNT ( ), DNT ( ), and TNT ( ), and the normalized absorption ( ) and fluorescence ( ) spectra of 1-pyrenebutyric acid in A) DMSO and B) water.

3.2 Quenching Studies in DMSO

As mentioned earlier, DMSO is a good solvent for the Py-SNPs and all quenchers. Thus dynamic quenching between the pyrene labels was expected to occur in this solvent. This was indeed observed as described hereafter.

3.2.1 Quenching of pyrene and Py-SNP1 by nitromethane in DMSO

Figures 6A and B illustrate the effect that an increase in NM concentration had on the fluorescence spectra and decays of pyrene, respectively. The fluorescence intensity decreased, and the fluorescence decays shortened with an increase in quencher concentration. The fluorescence decays of pyrene in DMSO were quasi monoexponential, exhibiting a 95% pre-exponential contribution with a long decay time that was attributed to the lifetime of molecular pyrene (see

Table A1). The fluorescence intensity with (F) and without (F_o) quencher as well as the number average decay time of the pyrene solution with ($<\tau>_N$) and without ($<\tau>_{No}$) quencher were calculated from the fluorescence spectra and decays shown in Figures 6A and B, respectively. F_o, F, $<\tau>_{No}$, and $<\tau>_N$ were used to calculate the ratios F_o/F and $<\tau>_{No}/<\tau>_N$ which were plotted in Figure 6C as a function of NM concentration. The plots shown in Figure 6C were linear as expected for a Stern-Volmer plot. These trends were fitted to Equation 6 where k_q is the rate constant for the quenching of pyrene by NM and $<\tau>_{Wo}$ is the weight average lifetime of pyrene without quencher. A derivation of Equation 8 is provided in SI. According to Equation 8 which was derived for perfectly dynamic quenching, F_o/F should equal $<\tau>_{No}/<\tau>_N$. However, $<\tau>_{No}/<\tau>_N$ was found to be slightly smaller than F_o/F in Figure 6C, probably because of residual static quenching. Fortunately, lifetime measurements are unaffected by static quenching[56] and the slope of the $<\tau>_{No}/<\tau>_N$-vs-$[Q]$ plot was used to determine k_q, found to be 2.9 (± 0.03)×10^9 $M^{-1}.s^{-1}$ for molecular pyrene in DMSO.

$$\frac{<\tau>_{No}}{<\tau>_N} = \frac{F_o}{F} = 1 + k_q <\tau>_{Wo} [Q] \qquad (8)$$

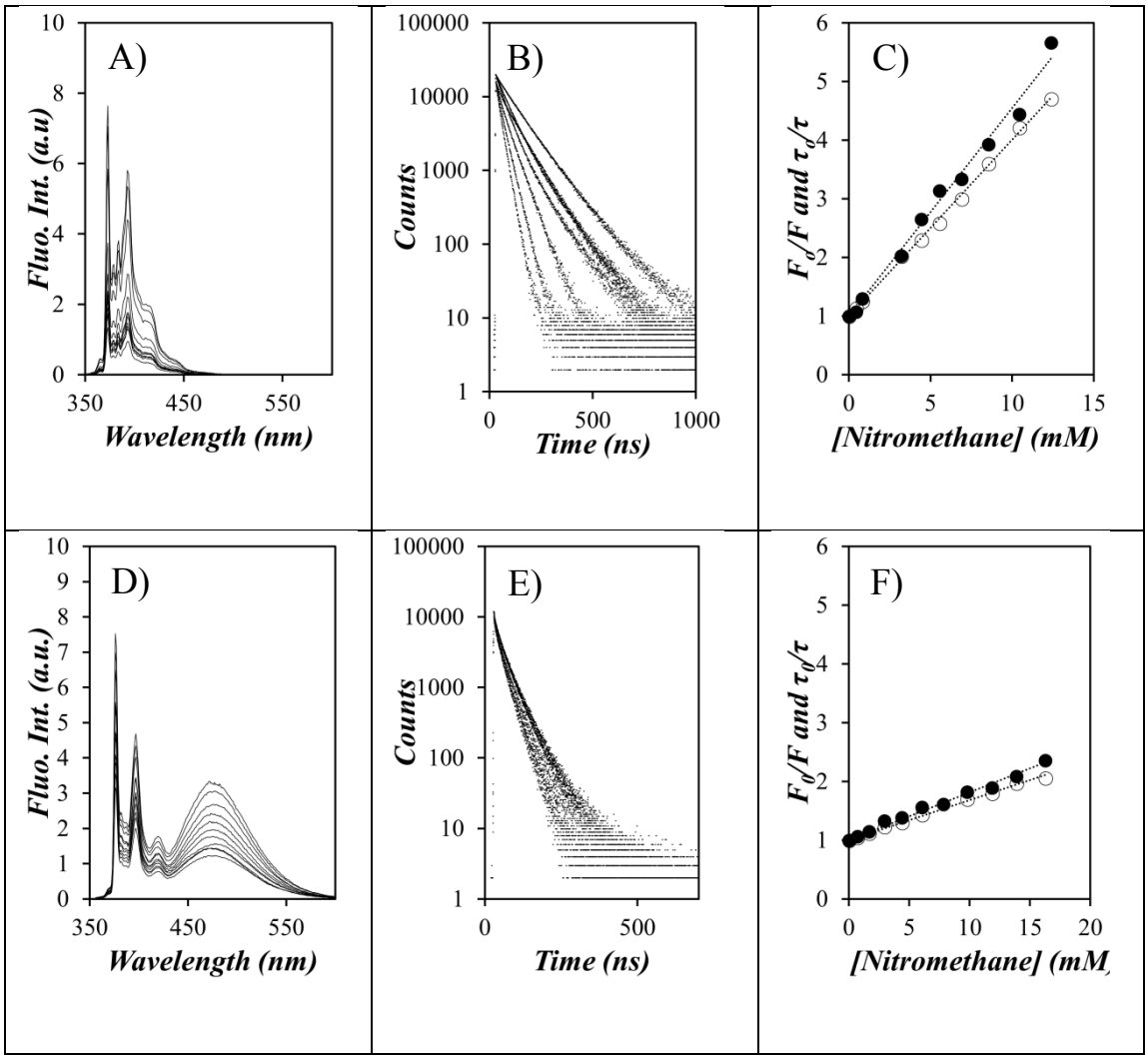

Figure 6. Fluorescence spectra of A) pyrene (λ_{ex} = 338 nm) and D) Py(10)-SNP1 (λ_{ex} = 346 nm) with increasing NM concentration. Time-resolved fluorescence decays of the monomer of B) pyrene (λ_{ex} = 338 nm, λ_{em} = 375 nm) and E) Py(10)-SNP1 (λ_{ex} = 346 nm, λ_{em} = 375 nm) with increasing concentration of NM. Stern-Volmer plots for (●) steady-state and (○) time-resolved fluorescence for C) pyrene and F) Py(10)-SNP1. Solvent = DMSO. [*Py*] = 2.4×10^{-6} M.

These quenching experiments were repeated for all Py-SNP1 samples, and the results obtained for Py(10)-SNP1 are shown in Figure 6D-F. The main differences were that the

fluorescence spectra showed excimer fluorescence as would be expected from the high pyrene content of Py(10)-SNP1 and the monomer decays were clearly multiexponential due to the random labeling of the SNPs with 1-pyrenebutyric acid. All the fluorescence data obtained with the Py-SNP1 samples are presented in Tables A50-A57. The Stern-Volmer plots were generated and F_o/F and $<\tau>_{No}/<\tau>_N$ were found to increase linearly as a function of quencher concentration. However, F_o/F was found to be slightly larger than $<\tau>_{No}/<\tau>_N$, the difference between F_o/F and $<\tau>_{No}/<\tau>_N$ decreasing with increasing pyrene content. The small difference between F_o/F and $<\tau>_{No}/<\tau>_N$ was most certainly the result of static quenching due to complexation between NM and the pyrenyl labels. However, increasing the pyrene content is known to lead to more pyrene aggregation in DMSO which might induce the binding of NM to the pyrene aggregates, thus reducing the likelihood of having NM binding to isolated pyrenyl labels at high pyrene content for the Py-SNP1 samples. Analysis of the Stern-Volmer plots based on the $<\tau>_{No}/<\tau>_N$ ratio were linear and could be analyzed to yield $k_{q,SNP}$ for the quenching of the pyrenyl labels of the Py-SNP1 samples by NM. The $k_{q,SNP}$ values for all Py-SNP1 samples and the k_q values for pyrene quenched by NM were presented in Figure 8.

3.2.2 Quenching of pyrene and Py-SNP1s by MNT, DNT, and TNT in DMSO

As observed for the quenching of the Py-SNP1s by NM in DMSO, a decrease in the fluorescence intensity and a reduction in the lifetime was observed with increasing 4-mononitrotoluene (MNT) concentration (see Figures 7A and B). The resulting Stern-Volmer plot, given in Figure 7C, yielded an exponential increase in the F_o/F ratio with increasing MNT concentration, while the $<\tau>_{No}/<\tau>_N$ ratios increased linearly. The upward curvature in the F_o/F ratios was attributed to the absorption of MNT (see Figure 5). Similar trends in the Stern-Volmer plots were obtained for quenching studies conducted with DNT and TNT. Since lifetime measurements were unaffected by the

absorption of the quenchers, the $<\tau>_{No}/<\tau>_{N}$ ratios were employed to determine the k_q and k_{qSNP} values for MNT, DNT, and TNT. For molecular pyrene in DMSO, the k_q values were found to equal 5.81 (± 0.13), 5.35 (± 0.13), and 5.33 (± 0.07) $\cdot 10^9$ $M^{-1}s^{-1}$, respectively, indicating that the number of nitro substituents on the NACs has little effect on the quenching of pyrene in this solvent.

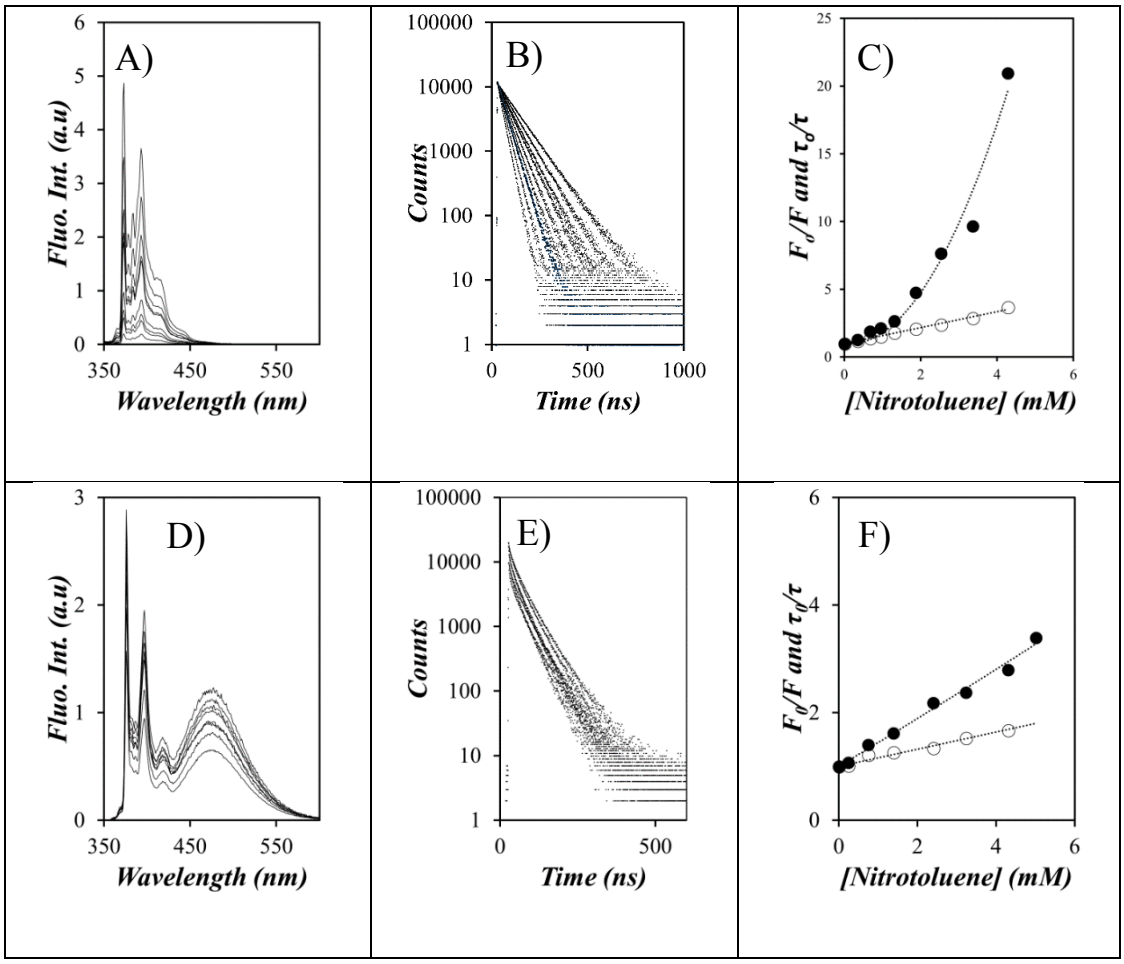

Figure 7. Fluorescence spectra of A) pyrene and D) Py(10)-SNP1 with increasing MNT concentration. Time-resolved fluorescence decays (λ_{em} = 375 nm) of the monomer of B) pyrene and E) Py(10)-SNP1 with increasing concentration of MNT. Stern-Volmer plots for (●) steady-state and (○) time-resolved fluorescence for C) pyrene and F) Py(10)-SNP1. Solvent = DMSO; λ_{ex} = 338 and 346 nm for pyrene and Py(10)-SNP1, respectively.

3.2.3 Comparison of the k_q and k_{qSNP} values obtained in DMSO

The fluorescence quenching experiments were repeated for Py-SNP1 samples with different pyrene contents which were quenched with NM, MNT, DNT, and TNT. The $<\tau>_{No}/<\tau>_{N}$ ratios were used to build the Stern-Volmer plots. They all yielded straight lines whose slope was used to determine the k_q and k_{qSNP} values presented in Figure 8. k_{qSNP} was found to remain constant regardless of the degree of substitution (DS) of the Py-SNP1 samples. This observation confirmed that the pyrene labels were accessible to the solvent, and thus the quencher, independently of the pyrene content. As mentioned earlier, k_q for molecular pyrene was found to equal 2.91 (± 0.03), 5.8 (± 0.1), 5.4 (± 0.1), and 5.33 (±0.07) $\cdot 10^9$ $M^{-1}s^{-1}$ for NM, MNT, DNT and TNT, respectively. k_{qSNP} averaged across all Py-SNP1s was determined to equal 1.6 (± 0.1), 3.9 (± 0.2), 2.2 (± 0.2) and 1.6 (± 0.2) $\cdot 10^9$ $M^{-1}s^{-1}$ for NM, MNT, DNT, and TNT, respectively. For any given quencher, k_q for molecular pyrene was consistently higher than k_{qSNP} for the pyrene labels bound to the SNPs. Since k_q is proportional to the sum of the diffusion coefficients of both the pyrene labels and quencher,[56] and since the covalent attachment of the pyrenyl labels to the SNPs brought the diffusion of the labels to a halt compared to the free pyrene molecules, k_{qSNP} would be expected to take a lower value than k_q, as observed experimentally. The quenching efficiency for the NACs towards the Py-SNPs in DMSO followed the sequence MNT>DNT>TNT whereby each addition of a nitro group to the benzene ring resulted in a decrease in quenching efficiency. Since quenching of pyrene by NACs is believed to occur via electron transfer from an electron-rich excited pyrene to an electron-poor NAC, addition of a nitro-group to a NAC would be expected to result in a more electron-poor molecule yielding more efficient quenching. However, such a trend was not supported by the k_q values obtained for molecular pyrene in DMSO which showed that the number of nitro-groups on a NAC had little effect on the quenching efficiency. We suspect that the

different trend observed for the quenching of molecular pyrene and the Py-SNPs might be due to hydrogen-bonding between the nitro groups of the NACs and the hydroxyls of the SNPs, a NAC with more nitro-groups would generate stronger H-bonds with the SNPs, thereby reducing the quencher mobility and causing a reduction in k_{qSNP} as observed in Figure 8.

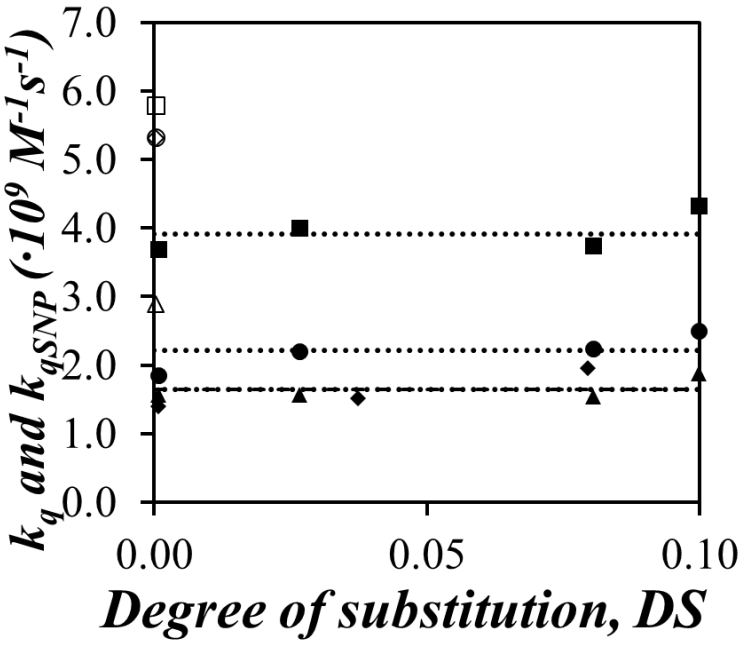

Figure 8. Plot of k_q (hollow symbols) and k_{qSNP} (filled symbols) as a function of DS for NM (△, ▲), MNT, (□, ■), DNT (○, ●) and TNT (◇, ◆) in DMSO.

3.3 Quenching Studies in Water

In water, the hydrophobic pyrenyl labels formed pyrene aggregates whose enhanced hydrophobicity was expected to drive the binding of sparingly soluble NACs and facilitate quenching. Consequently, the quenching studies carried out with pyrene and the Py-SNP1s in DMSO with NM, MNT, DNT, and TNT were repeated in water.

3.3.1 Quenching of pyrene and Py-SNP1 samples by NM in water

Similar to the quenching studies conducted in DMSO, a decrease in the fluorescence intensity and lifetime of the pyrene monomer was observed with the addition of NM to the Py-SNP1 dispersions. The F_o/F ratio remained just slightly larger than the $<\tau>_{No}/<\tau>_N$ ratio and both ratios increased linearly with increasing NM concentration indicating that quenching was dynamic in nature. Linear Stern-Volmer plots were obtained for all Py-SNP1 samples except for those with a DS of 0.08 and higher (see Figure 9). For these latter Py-SNP1 samples, the F_o/F and $<\tau>_{No}/<\tau>_N$ ratios reached a plateau at high NM concentrations (see Table A54). This downwards curvature in a Stern-Volmer plot is indicative of protective quenching whereby a fraction of the pyrenyl labels has become inaccessible to the quencher. Equation 9 was applied to determine k_{qSNP} and f_a, the fraction of pyrene labels that are accessible to NM for the Py-SNP1 samples in water quenched by NM.[56] The resulting k_{qSNP} and f_a values were plotted as a function of DS in Figure 9B and C, respectively. As previously observed in DMSO, k_{qSNP} remained constant, within experimental error, regardless of the pyrene content and was found to equal 2.1 ($\pm$ 0.5) $\cdot 10^9$ $M^{-1}s^{-1}$ in Figure 9B. The molar fraction f_a, shown in Figure 9C, decreased with increasing DS, indicating that the pyrene labels were less accessible. With a solubility limit of ~ 0.7 μM in water,[50] pyrene and its derivatives are very hydrophobic. Consequently, the pyrenyl labels of Py-SNP1 samples were expected to form aggregates in water, as supported by the absence of a risetime in all excimer decays acquired for the Py-SNP1 samples in water (see Tables A54 to A57). The decrease in f_a with increasing DS suggested that hydrophobic aggregation of the pyrenyl labels reduced accessibility of the isolated pyrene labels to the quencher in solution, possibly because of a tightening of the interior of the SNPs that increased with increasing DS.

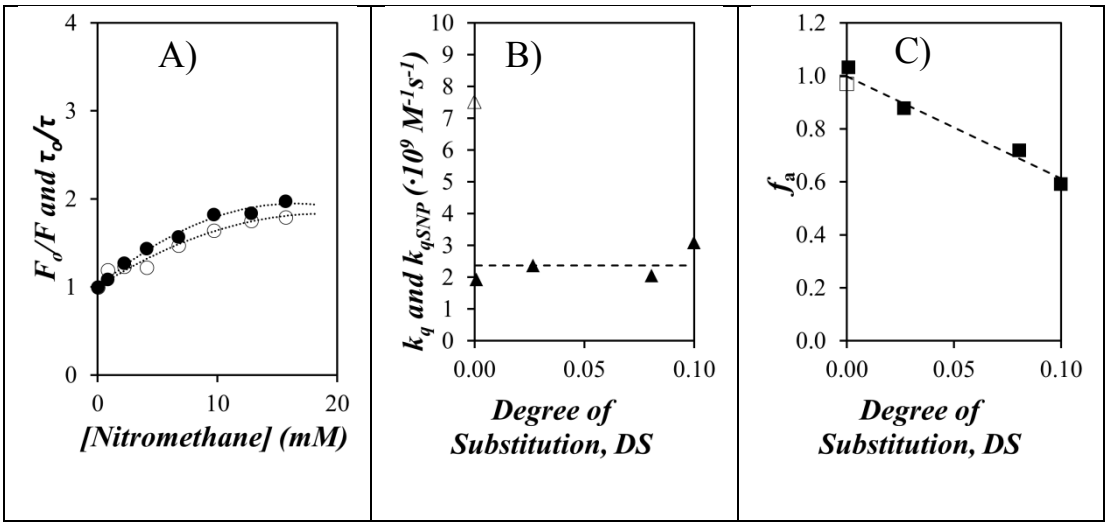

Figure 9. A) Stern-Volmer plot for Py(8)-SNP1 quenched by nitromethane, (●) F_o/F and (○) $<\tau>_{No}/<\tau>_N$ ratios. B) k_q (△) for molecular pyrene and k_{qSNP} (▲) for Py-SNP1 plotted as a function of DS. C) f_a plotted as a function of DS for molecular pyrene (□) and Py-SNP1 (■).

$$\frac{<\tau>_{No}}{<\tau>_{No}-<\tau>_N}=\frac{1}{f_a<\tau>_{Wo}k_q}\frac{1}{[Q]}+\frac{1}{f_a} \qquad (9)$$

3.3.2 Quenching of pyrene excimer and Py-SNP1 samples by MNT, DNT, and TNT in water

The quenching studies were conducted with the Py-SNP1 samples in the presence of MNT, DNT, and TNT. However since the NACs were sparingly soluble in water,[62,63] the quencher concentrations used in water were about 50 times lower than those used for NM in DMSO and water. Under such dilute quencher concentrations, little change in the fluorescence intensity, and thus little quenching was observed for molecular pyrene and Py(0.06)-SNP (see Figures 10A-C). However, for the Py-SNP1 samples with a DS of 0.0265 and higher, a substantial decrease in the excimer fluorescence intensity was observed (Figure 10D), accompanied by a less pronounced change in the monomer fluorescence. Furthermore, the fluorescence decays for the pyrene monomer (Figure 10E) and excimer (Figure 10F) showed hardly any difference with increasing

concentration of MNT, DNT, and TNT, resulting in a constant $<\tau>_{No}/<\tau>_{N}$ ratio that remained near unity. These results were a clear demonstration that quenching took place in a static manner through ground-state associations between the pyrenyl labels, either isolated or aggregated, and the NACs. It is worth pointing out that the low MNT, DNT, and TNT concentrations used in the experiments whose results were presented in Figure 10 rule out re-absorption by the quenchers as the cause for the reduction in fluorescence intensity. When a combination of static and dynamic quenching is at play, Equation 10 can be used. In the present case however, the absence of significant dynamic quenching, inferred from the unchanged fluorescence decays, implied that k_{qSNP} approached zero over the range of quencher concentrations. Since the Stern-Volmer plots based on F_o/F in Figure 10F for the excimer yielded a straight line, Equation 10 was applied with $k_{qSNP} = 0$ $M^{-1}.s^{-1}$ to yield K_S, the equilibrium constant for the formation of ground-state complexes between pyrene and the quenchers, from the slope of the plot. Similar trends were observed for all quenching studies carried out with the Py-SNP1 samples having a DS of 2.65 or higher for MNT, DNT, or TNT. In all cases, the slopes of the Stern-Volmer plots obtained for the pyrene excimer were determined to obtain K_S which was plotted as a function of the DS of the Py-SNP1 samples in Figure 11.

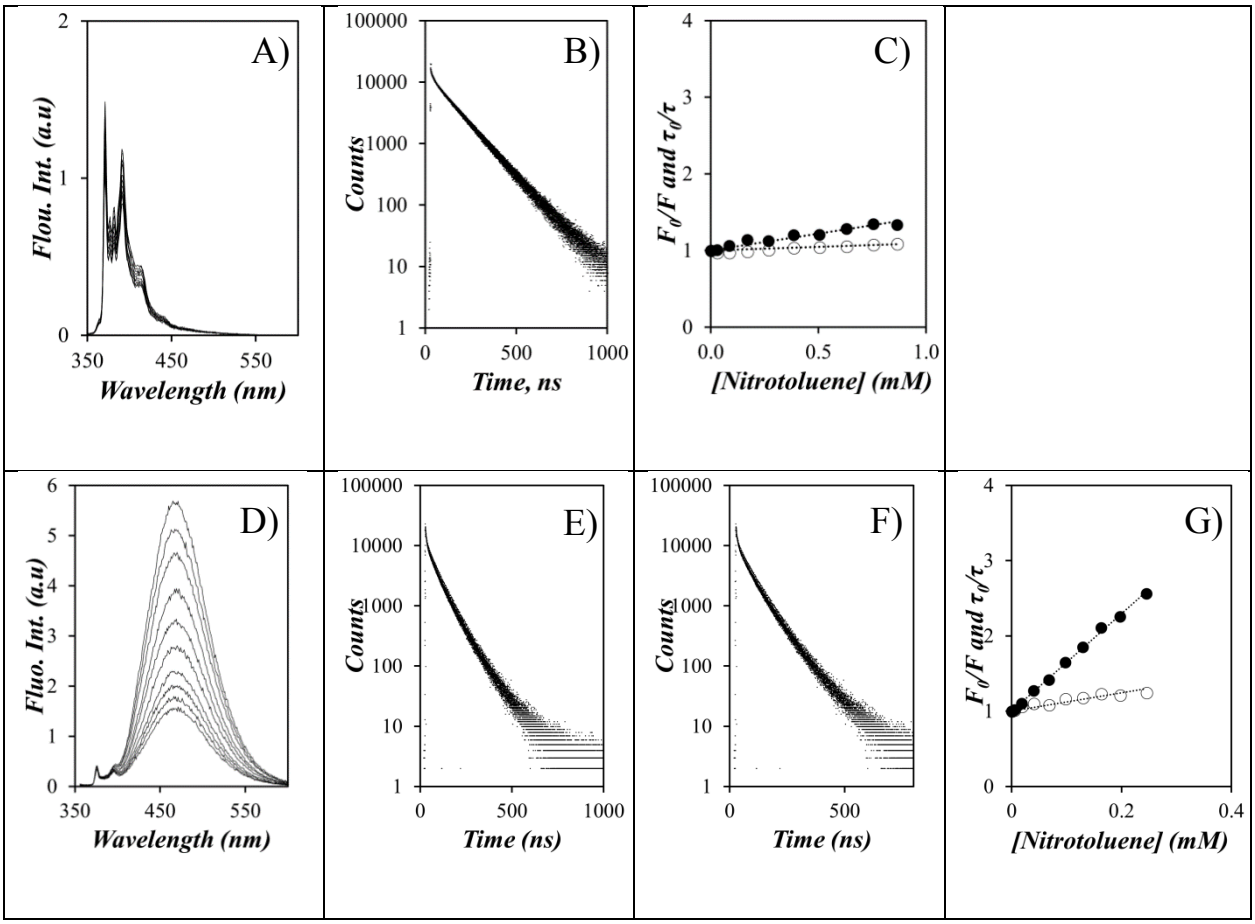

Figure 10. A) Fluorescence spectra, B) fluorescence decays, and C) Stern-Volmer plot of molecular pyrene quenched by MNT in water. D) Fluorescence spectra, fluorescence decays of E) the monomer acquired at 375 nm and F) the excimer acquired at 510 nm, and G) Stern-Volmer plot for Py(10)-SNP1 quenched by MNT in water. In C) and G) (●) and (○) are for the F_o/F and $\langle\tau\rangle_{No}/\langle\tau\rangle_N$ ratios, respectively.

$$\frac{F_o}{F} = (1 + k_{qSNP} < \tau >_{No} [Q]) \times (1 + K_S[Q]) \qquad (10)$$

The trends shown in Figure 11 indicate that an increase in pyrene content resulted in an exponential increase in K_S. This observation was certainly a result of the formation of more hydrophobic microdomains at higher DS, which favored the binding of MNT, DNT, and TNT to the pyrenyl aggregates. Interestingly, K_S for DNT was about twice as large compared to MNT and K_S for TNT was close to an order of magnitude higher compared to DNT. Consequently, the quenching efficiency of the NACs based on the K_S values followed the sequence TNT>DNT>MNT, opposite to the trend observed for the k_{qSNP} values in DMSO. The solubility of TNT (115 mg/L),[63] DNT (204 mg/L),[62] and MNT (361 mg/L)[62] in water were not sufficiently different to explain the much larger K_S values obtained for TNT. Rather the third nitro group of TNT seems to induce a much stronger affinity between TNT and the pyrenyl aggregates.

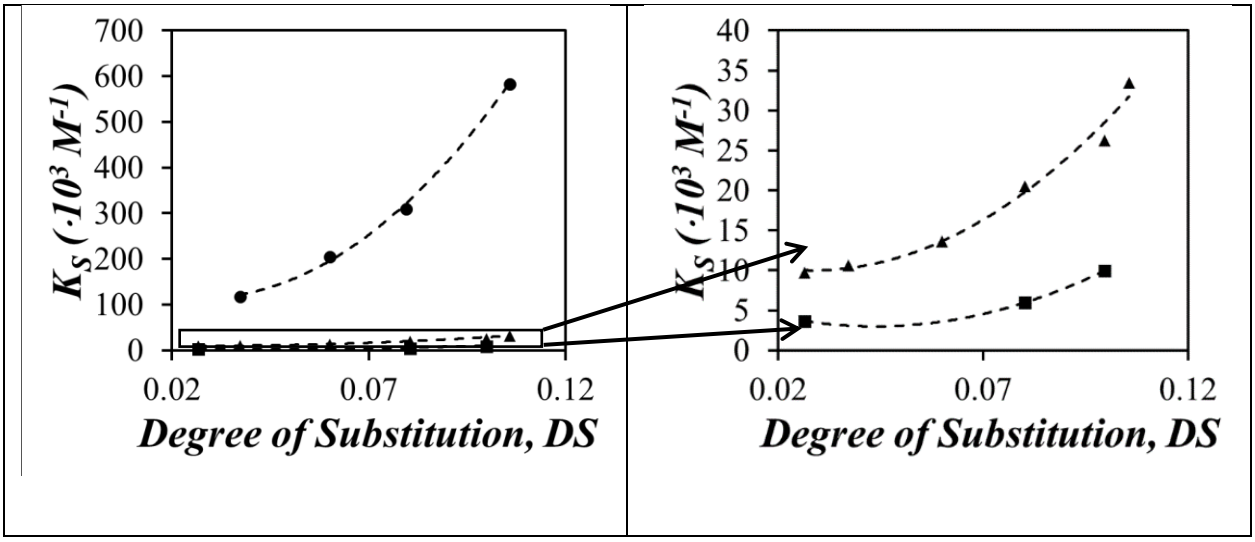

Figure 11. Plot of K_s as a function of DS for MNT (■), DNT (▲), and TNT (●).

3.4. Comparison of DMSO and Water Quenching Studies

Although the main objective of this project was to develop Py-SNP-coated filter papers (Py-CFPs) and demonstrate their potential as optical sensors for the detection of NACs, the quenching efficiencies of the quenchers were first evaluated in solution using DMSO and water as solvents. In DMSO, where quenchers, pyrene labels, and SNPs were soluble, the quenching efficiency for

the Py-SNP1 samples was found to increase according to the sequence MNT>DNT>NM~TNT, where MNT was the best and NM and TNT were the worst performing quenchers. Furthermore, it was found that no targeted (i.e. static) quenching occurred in DMSO and that quenching occurred predominantly in a dynamic manner. Interestingly, the quenching studies in water yielded a trend that was opposite to that observed in DMSO for the three NACs studied. In water, TNT was the most efficient quencher and MNT the worst. Visual inspection of the fluorescence spectra indicated that NACs targeted the pyrene aggregates in water since a pronounced decrease was observed for the fluorescence intensity in the excimer region. Furthermore, the overlapping fluorescence decays of the monomer and excimer acquired with the aqueous Py-SNP dispersions quenched by MNT, DNT, and TNT implied that quenching occurred predominantly in a static manner through the formation of ground-state complexes between NAC quenchers and pyrene aggregates. Since quenching studies conducted in water suggested that higher pyrene contents resulted in stronger binding based on the K_S values shown in Figure 11, Py(11)-SNP1 with the highest pyrene content was used to prepare Py-SNP-coated filter papers (Py-CFPs) to generate optical sensors whose fluorescence quenching was monitored for different NACs.

3.5 Quenching Studies of Py-CFP

After having demonstrated the substantial enhancement in quenching efficiency by NACs upon forming pyrene aggregates in water, Py-CFPs were prepared according to the procedure outlined in the Experimental section and their quenching by different NACs was evaluated. These quenching experiments were conducted in a manner that was either qualitative by exposing the Py-CFPs to NAC vapors or quantitative by adsorbing a known amount of NACs and monitoring the extent of quenching experienced by the Py-CFPs. The results of these studies are presented hereafter.

3.5.1 Vapour Quenching Studies of Py-CFPs

Having characterized how NACs quenched the fluorescence of molecular pyrene and Py-SNPs in DMSO and water, quenching studies of Py-SNPs adsorbed at the surface of Whatman No1 filter paper were carried out. All quenching studies presented in Chapter 3 with Py-CFPs were conducted with SNP1 labeled with 11 mol% pyrene. The efficiency of many optical sensors for NACs have been characterized by monitoring their response time upon exposure to NAC vapours.[11,14,15,27,32,36,38,46,50,69] As such, vapour quenching studies were conducted on Py-CFPs by exposing them to a headspace saturated with NAC vapours and monitoring the quenching efficiency ($E_Q = (1 - F_1/F_o)\times 100\%$, see Equation 5) as a function of exposure time.

Before vapor quenching studies were conducted, the stability of the Py-CFPs upon irradiation with UV-light needed to be investigated since the Py-CFPs were going to be irradiated at least twice, before and after exposure to NAC vapors. To this end, the quenching efficiency was monitored for a single Py-CFP ($1\times 1 cm^2$) as a function of the number of irradiations of light at 346 nm. Each irradiation of light had a duration of 30 seconds, which is the time needed to acquire a fluorescence spectrum. When plotted against the number of 30-s irradiations, E_Q was found to increase linearly with increasing irradiation number. This trend indicates that the fluorescence intensity of Py-CFPs decreases with each irradiation by light at 346 nm. This decrease was attributed to the degradation of the Py-CFPs and not quenching. It is worth noting that the protocol employed hereafter for all Py-CFP studies required only two irradiations which should correspond to a maximum 5% decrease in the fluorescence intensity. Since all reported detection limits with the Py-CFPs corresponded to 90% quenching, the small 5 % decrease in fluorescence intensity due to photobleaching will be less than the error bars on the detection limits.

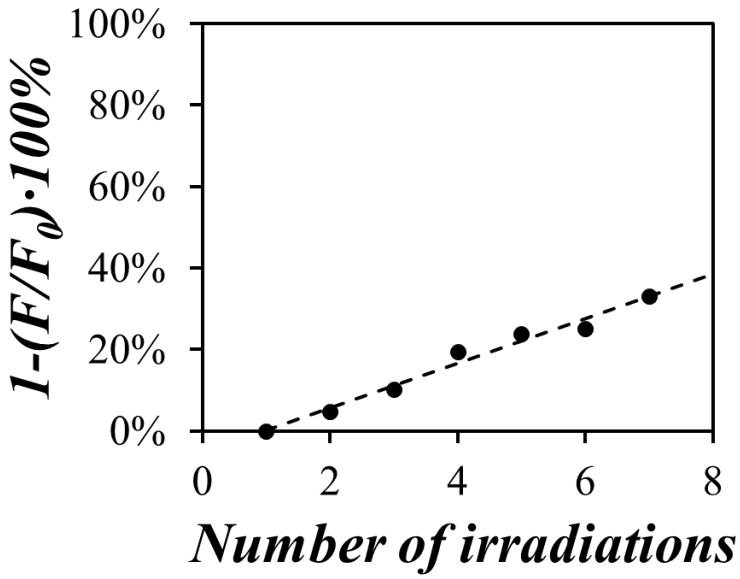

Figure 12. Plot of the quenching efficiency of Py-CFPs as a function of the number of 30 s irradiations at 346 nm in the absence of NACs.

Having assessed the stability of the Py-CFPs upon irradiation by light, vapor quenching studies were conducted. Although vapour studies are commonly used to determine the response time of optical sensors, the procedures that are being applied in the scientific literature vary from study to study. In this work, the response time represented the time taken for a Py-CFP to lose 90% of its original fluorescence intensity. The vapour studies were conducted with MNT, DNT, and naphthalene, but TNT was excluded for the time being due to the following reason. TNT has a low vapour pressure, commonly reported as $5.5 \cdot 10^{-6}$ mmHg at 25 °C,[65] would require that a large mass of TNT be placed inside the vial to saturate its head space within a reasonable experimental time. Unfortunately, the high cost of TNT would make such vapour quenching study prohibitively expensive and it was not attempted. The quenching efficiency (E_Q) of the vapor quenching studies conducted with MNT, DNT, and naphthalene was plotted as a function of exposure time in Figure 13. As time elapsed, it approached 100% for MNT and DNT, yielding response times of 0.48

(± 0.05) and 3.6 (± 0.4) minutes, respectively. Vapour pressures for MNT and DNT are usually reported in the literature as $4.9 \cdot 10^{-2}$ and $6.2 \cdot 10^{-4}$ mmHg at 25°C, respectively.[65] The 100-fold larger vapor pressure of MNT suggests that its concentration in the head space of the vial would be much larger compared to DNT, resulting in a significantly faster response time for MNT. This was indeed observed in Figure 13.

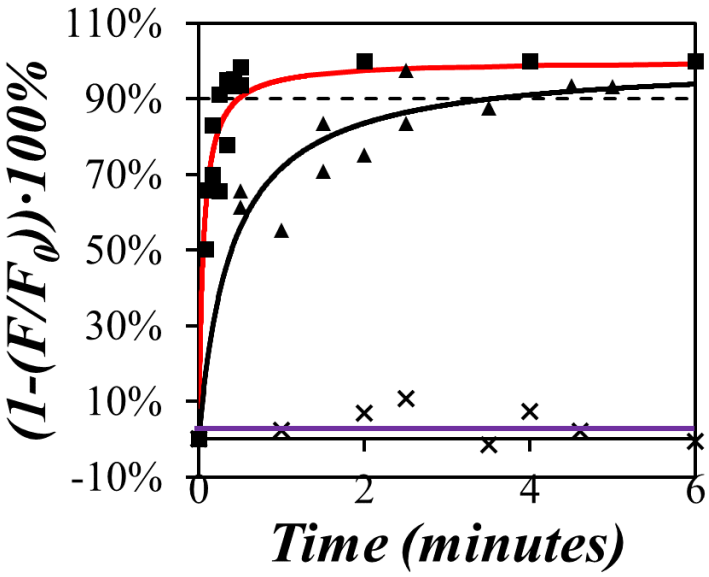

Figure 13: Plot of quenching efficiency as a function of exposure time for Py-CFPs exposed to MNT (■), DNT (▲), and naphthalene (✖) vapours. The dash line indicates the efficiency where 90% quenching occurs. All studies were conducted with 10 (± 2) mg of chemical.

In addition to vapour quenching studies conducted with MNT and DNT, similar experiments were performed with naphthalene to investigate the selectivity of the Py-CFPs towards NACs. As shown in Figure 13, exposure of Py-CFPs to naphthalene resulted in no significant quenching suggesting that Py-CFPs exhibited some selectivity towards NACs.

To the best of our knowledge, 0.5 minute was the fastest response time reported in a DNT vapor study for reaching 80% quenching with a 90 nm thick pyrene-doped polyether sulfone film.[26]

This is faster than our response time for DNT found to equal 3.6 (± 0.4) minutes for 90 % quenching. However, a substantially shorter response time of 1.6 (± 0.2) minutes would have been obtained for 80% quenching efficiency. This response time is actually much better than most of those reported in the literature. For example, an electro-spun poly(triphenyl ethene) film with a thickness of 1.6 ± 0.06 μm, was found to have a response of 4 minutes with only 75% quenching.[22] Compared to our response time (1.6 ± 0.2 minutes), Py-CFPs respond twice more quickly to DNT vapours for the same level of quenching. A response time of 5 minutes with 100%[39] and 87%[45] of fluorescence quenching, and thus similar to the response time obtained for the Py-CFPs, was found for films prepared by spin coating AIE-active pentipycene-derived polymers and organically modified silica doped with pyrene, respectively. To the best of our knowledge, the largest response time for DNT vapors was found to equal 16 hrs to achieve 95% fluorescence quenching with an electrochemically etched n-type silicon wafer doped with phosphorous. From this broad range of response times to DNT vapour, it can be argued that the Py-CFP films display a response that is competitive among the best response times reported in the scientific literature.[22,25,39,45,46]

Although vapour quenching studies are commonplace, and invaluable to assess how quickly optical sensors respond to minute quantities of NACs, there are 3 main problems typically associated with them. First the mass of quencher actually adsorbed onto the film cannot be determined without a more complex protocol in which temperature, flow rate, volume of the cell used, and additional parameters must be carefully controlled. Second vapour quenching studies reported in the literature apply different experimental protocols, making a direct comparison of the various response times quite challenging. Finally, almost all vapor quenching studies suffer from the same flaw, that introduction of the film acting as an optical sensor to the head space saturated with NAC vapors requires to unseal the container, allowing some of the NAC vapor to escape, and

resulting in the head space being no longer saturated. Therefore, the response time reported in a given vapor study should also account for the time required for the NAC vapor to re-saturate the head space of the container which depends, among other parameters, on the headspace volume. A proper report of the detection limit of a given NAC for an optical sensor should provide the lowest possible mass of quencher adsorbed onto a film that can still be detected. The next section of this thesis describes how the drop method, where the mass of a given NAC adsorbed onto a Py-CFP is carefully measured, was applied to determine the detection limit of these optical sensors.

3.5.2 Quenching Studies by adsorbing known quencher quantities to Py-CFPs

The main problem associated with vapour quenching studies is that the amount of quencher adsorbed onto an optical sensor is impossible to determine in a simple direct manner. By contrast, this next section focuses on quenching studies conducted by applying the drop method on Py-CFPs prepared with SNP1 labeled with 11 mol% of 1-pyrenebutyric acid (Py(11)-SNP1), as described in Chapter 2. In brief, increasing amounts of NACs were deposited onto the Py-CFPs and their fluorescence was recorded to yield the quantity $<{}^{W}F_o/{}^{OS}F_o>/({}^{W}F_o/{}^{OS}F)$ which was plotted as a function of the amount of quencher deposited on the paper and expressed in ng of quencher per mm^2 of filter paper. A plot of $<{}^{W}F_o/{}^{OS}F_o>/({}^{W}F_o/{}^{OS}F)$ as a function of the mass of quencher per mm^2 is shown in Figure 14. The nice overlap observed for all the trends obtained with different sizes of Py-CFPs demonstrated that the detection limit, defined as the mass of NAC per mm^2 of Py-CFP resulting in 90% quenching, was independent of the area of filter paper used, as long as the results were reported in terms of mass of NAC per unit surface. Interestingly, Figure 14 also suggested that a smaller mass of quencher could be detected simply by reducing the paper size. All following quenching studies were conducted with 1×1 cm^2 filter papers coated with Py(11)-SNP1.

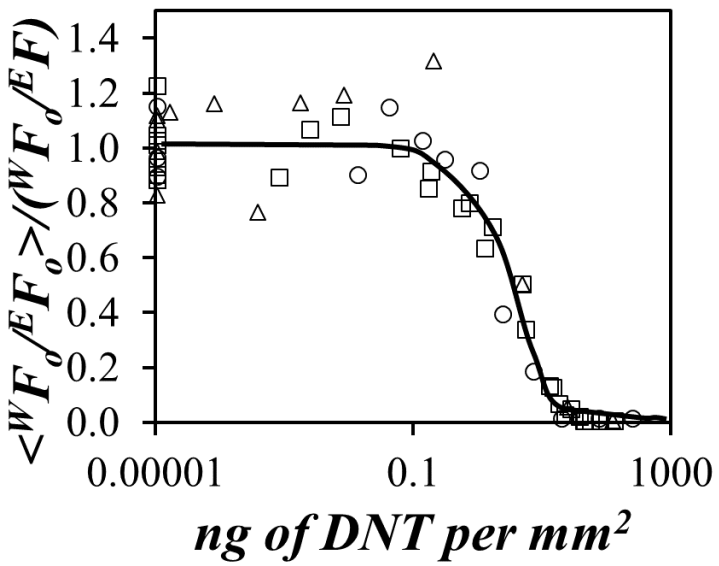

Figure 14: Plot of $<{}^{W}F_o/{}^{E}F_o>/({}^{W}F_o/{}^{E}F)$ as a function of the amount of DNT expressed in ng/mm^2 deposited on the Py-CFPs with sizes of (□) 1 × 1,(△) 0.5 × 0.5, and (○) 0.1 × 0.4 cm^2. The curve above was drawn as a mean to guide the eye only and was not parameterized by the Hill equation.

Experiments similar to those conducted with DNT in Figure 14 were also conducted for Py-CFPs quenched by MNT, DNT, and TNT to assess their detection limits. The results of these studies were presented in Figure 15. The sigmoidal trends shown in Figure 15 reflected a rapid decrease in the fluorescence of the Py-CFPs after the mass of quencher adsorbed per unit area of Py-CFP reached a threshold. The trends were fitted with the Hill equation (see Equation 7) which was used to simply parametrize the data. It is noteworthy to mention that the Hill equation could only reach a value of 0, corresponding to complete quenching of the Py-CFP, at infinitely high quencher concentration. As such, the detection limits reported in this thesis corresponded to the mass of NAC per unit surface of Py-CFP where the fluorescence intensity was reduced by 90%. Based on the trends shown in Figure 15, detection limits of 30 (± 9), 11 (± 5), and 1.4 (± 0.6) ng

per mm^2 were obtained for MNT, DNT, and TNT, respectively. Interestingly, the detection limit of TNT was about 7 and 19-fold lower compared to those of DNT and MNT, respectively. The decrease in the detection limit for the Py-CFPs mirrored the trend found with K_s for the Py-SNPs in water (see Figure 11) which was significantly higher for TNT than for MNT and DNT. Since the Py-CFPs were impregnated with 10 μL of water, the agreement between the trends obtained for the binding of the NACs onto the Py-SNPs in water and onto the humid Py-CFPs was reassuring. Furthermore to demonstrate the selectivity of the Py-CFPs toward NACs, naphthalene, a non-nitrated aromatic compound, was deposited onto a series of Py-CFPs. Within experimental error, no quenching was observed for naphthalene in Figure 15, thus confirming that Py-CFPs showed some selectivity towards NACs.

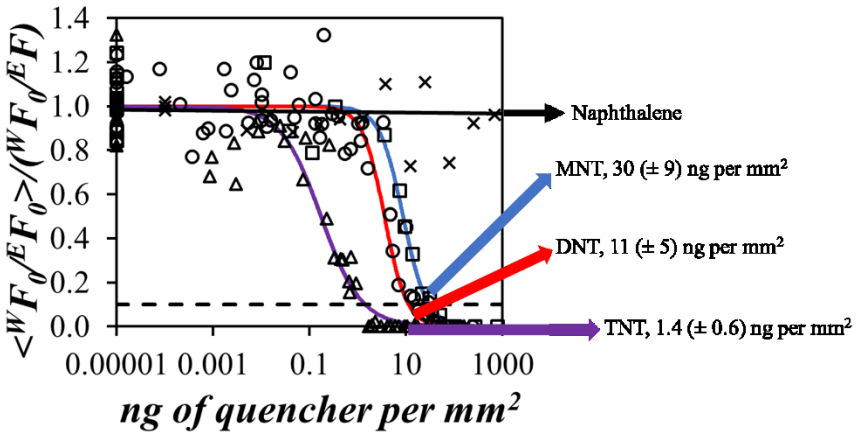

Figure 15. Plot of $<{}^{W}F_o/{}^{E}F_o>/({}^{W}F_o/{}^{E}F)$ as a function of the mass of chemical adsorbed onto the Py-CFPs expressed in ng/mm^2 for (×) naphthalene, (□) MNT, (○) DNT, and (△) TNT.

Figure 16 shows the actual change in color experienced by a 1 × 1 cm^2 Py-CFP upon irradiation with a hand-held UV-lamp after exposure to 2 ng per mm^2 of TNT. The clear difference in fluorescence signal, combined with the sharp transition around the detection limit indicated in

Figure 15, should enable the rapid assessment of whether a Py-CFP has come in contact, or not, with minute quantities of NACs. Furthermore, most of the fluorescence intensity could be recovered after simply dipping the Py-CFP in ethanol to remove the TNT.

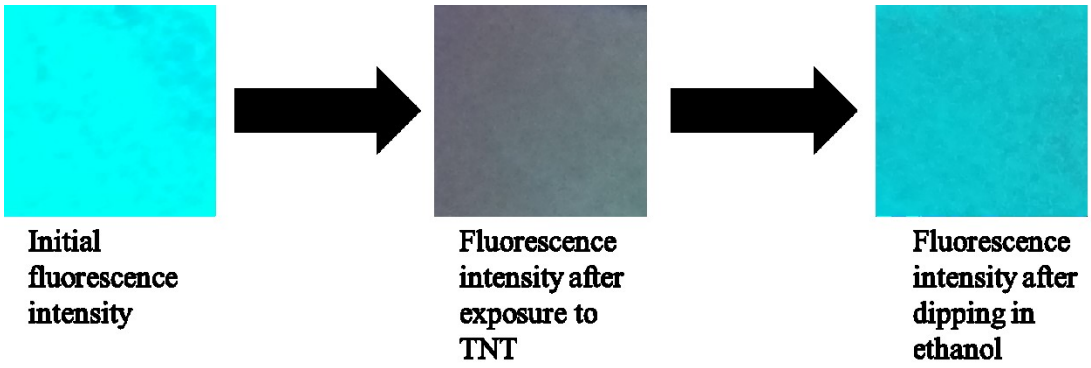

Figure 16. Visual representation of the actual fluorescence intensity change upon exposure to 2 ng per mm^2 of TNT and the recovery in fluorescence intensity after dipping the filter paper in ethanol under the irradiation of a hand-held UV-lamp.

3.5.3 Comparison of the performance of Py-CFPs to that of other optical sensors

Although much work has been reported previously in the literature, no standard has been agreed upon on how quenching studies should be conducted and reported. For instance, detection limits are typically reported in parts per million (ppm) of quencher adsorbed onto the optical sensor, molar concentrations in mol/L of a quencher solution into which an optical sensor was immersed, or response times for an optical sensor to be quenched by a variable amount, to name but a few of the parameters being employed. This makes direct comparison between different scientific reports quite challenging. Some detection limits and SV constants (K_{SV}) reported in the literature for TNT and other NACs have been summarized in Table A57. The detection limit reported in this work for TNT equaled 1.4 (± 0.6) ng per mm^2 for Py-CFPs coated with Py(11)-SNP1. Very few scientific reports determine the detection limits in terms of quencher mass per unit area. One report

found a detection limit for TNT of 1 ng per mm^2 by using a poly(triphenyl ethene) film spray coated onto Whatman filter paper.[22] It should be noted that the detection of the poly(triphenyl ethene) paper sensor was only determined by visual inspection and the polymer was electro-sprayed onto paper contaminated with NACs, compared to Py-CFPs where experimental data was parametrized and quencher was added onto paper that had been coated with Py-SNPs beforehand. Another similar paper found a detection limit of 0.2 ng per mm^2 for picric acid (PA) using a polyaniline coated filter paper.[37] However the detection limit of PA was determined using an infrared camera, and the mass of quencher per unit area was determined by dipping a known area of a gloved finger into a PA solution with a known concentration and volume and subsequently pressing the contaminated finger onto the polyaniline film. Nevertheless, the reported detection limits of 1 ng/mm^2 for TNT[22] and 0.2 ng/mm^2 PA[37] were comparable in magnitude to the detection limit determined of 1.4 (±0.6) ng/mm^2 for TNT using Py-CFP films. However, as mentioned earlier, the synthesis of Py-SNPs used to prepare the Py-CFPs is significantly simpler compared to the polymers used in all other optical sensors.[22,37] Furthermore, substrates with an open structure such as dendrimers are highly valued for the preparation of optical sensors since they are believed to promote interactions with the chemical of interest. Unfortunately, dendrimers are prohibitively expensive compared to the SNPs, which are roughly two orders of magnitude more cost-effective than dendrimers ($100/g). In addition to Py-CFPs having comparable detection limits as many other paper sensors, the K_s values for the binding of NACs to the Py-SNPs in water were found to be similar as, if not better than, those reported in the literature for other substrates used to prepare optical sensors (Table A60). Unfortunately, it is difficult to compare the K_s values directly for a given polymer, as the K_s value reported in this report depends on pyrene content and many scientific reports determine K_{sv} values. It was worth noting however, that the Py(3.7)-SNP1 sample

had a K_S value of 119 (± 1.6) $\cdot 10^3$ M^{-1} for TNT, which was similar to those reported in the literature for TNT, typically found to be in the 1 - $5 \cdot 10^5$ M^{-1} range.[13,20,25,49] The K_S value of the Py-SNPs having a larger pyrene content was much larger as illustrated in Figure 11, suggesting that an even better detection limit and response time could be obtained with these Py-SNPs.

Chapter 4

Optimization of Py-CFPs

4.0 Optimization of Py-CFP Detection Limits

Since the quenching studies reported in Chapter 3 demonstrated that NACs bind strongly to the pyrene aggregates generated by Py(11)-SNPs in water, quenching studies were conducted with filter papers coated with Py(11)-SNP1. Although an excellent detection limit of 1.4 (±0.6) ng per mm^2 was determined for TNT, suitable adjustments of other experimental parameters might enable an even lower detection limit. This section describes several attempts at improving the detection limit of the Py-CFPs to TNT by adjusting the pyrene content and the size of the Py-SNPs and hydrophobically modifying the Py-SNPs with styrene oxide. So far, none of these attempts were successful at achieving a significantly lower detection limit of the Py-CFPs. The following studies were conducted with DNT since it was available in much larger quantities compared to TNT.

4.1 Effect of the Pyrene Content of the Py-SNPs

The first experimental parameter that was optimized was the pyrene content of the Py-SNP1. The quenching studies conducted in water demonstrated in Figure 11 that an increase in pyrene content resulted in an exponential increase in K_S, the equilibrium constant for the binding of NACs to pyrene aggregates. Consequently, an increase in pyrene content of Py-SNP1 would be expected to result in a lower detection limit. As such, quenching studies were conducted on a series of Py-CFPs prepared with SNP1 labeled with 1, 4, 6, 8, 11, and 36 mol% of pyrene. The result of these quenching studies, shown in Figure 17, suggests the existence of two quenching regimes. Py-CFPs prepared with Py-SNPs having a pyrene content greater than or equal to 8 mol% yield similar sigmoidal curves with similar detection limits, within experimental error (see Figure 17B). In other words, a 3-fold increase in pyrene content from 11 to 36 mol% resulted in no substantial decrease in the detection limit. Consequently, increasing the pyrene content of the Py-SNPs does not seem to increase the number of pyrene aggregates because more pyrene aggregates would

compartmentalise the NACs among different pyrene aggregates leading to a larger detection limit. Rather the increase in pyrene content must result in larger pyrene aggregates which promote the binding of the NACs to the pyrene aggregates, as predicted from the exponential increase in K_S with pyrene content found in Figure 11. While stronger binding takes place, the same number of quenchers are required to bind to each pyrene aggregate to ensure 90 % quenching of the Py-CFP. If the K_S value obtained for Py(8)-SNP is sufficient to ensure quantitative binding of NACs to the pyrene aggregates and results in 90% quenching of the Py-CFPs, then increasing the pyrene content further will not improve the detection limit much as observed in Figure 17. By contrast, lowering the pyrene content of the Py-SNPs from 8 mol% to 6, 4 and 1 mol% lowers K_S and reduces the binding of DNT to the pyrene aggregates resulting in a higher detection limit.

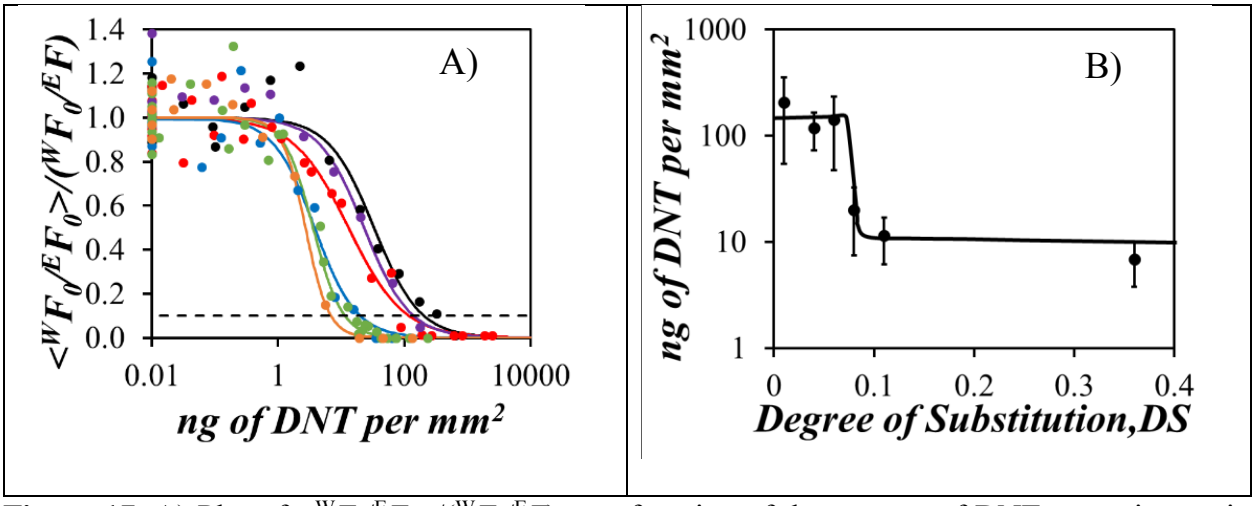

Figure 17. A) Plot of $<{}^{W}F_o/{}^{E}F_o>/({}^{W}F_o/{}^{E}F)$ as a function of the amount of DNT per unit area in ng/mm^2 for Py-SNP1 samples with pyrene conte nts of (━, ●) 1, (━, ●) 4 (━, ●) 6, (━, ●) 8, (━, ●) 11, and (━, ●) 36 mol% and B) detection limit in ng of DNT per unit area in ng/mm^2 as a function of DS. All curves in Figure 17A were fitted with the Hill equation and the *h* and *k* parameters can be found in Table A59 in the appendix. All experiments were conducted with a paper density of pyrene labels of $1.6 \cdot 10^{-11}$ mol pyrene per mm^2. The dash line represents the detection limit where $<{}^{W}F_o/{}^{E}F_o>/({}^{W}F_o/{}^{E}F)$ equals 0.1.

4.2 Effect of Particle Size on the Detection Limit

The second parameter investigated to decrease the detection limit of the Py-CFPs was the size of the particles used to prepare the Py-SNPs. To this end, amylopectin (D_h= 244 (± 49) nm, determined by intrinsic viscosity measurements conducted by Damin Kim, a graduate student in the Duhamel lab, and the known relationship between intrinsic viscosity and D_h, SNP-1 (46 (± 3) nm)[55] and SNP-2 (8.3 (± 0.7) nm)[55] were labeled with a same pyrene content of 6 mol%. These samples were used to prepare Py-CFPs whose quenching efficiencies were compared at a same surface density of pyrene labels. Shown in Figure 18A, a decrease in particle size from 244 (± 49) nm to 8.3 (± 0.7) nm[55] resulted in little change in the detection limit, within experimental error. Particle size did not affect the detection limit either when working at much higher pyrene content with Py(36)-SNP1 and Py(39)-SNP2. The detection limit was lower due to the high pyrene content, an effect that was established in Figure 17, but hardly any change in detection limit could be found with different particle size at higher pyrene contents. Based on these results, it appears that the size of the Py-SNPs used to prepare Py-CFPs had little effect on their detection limit.

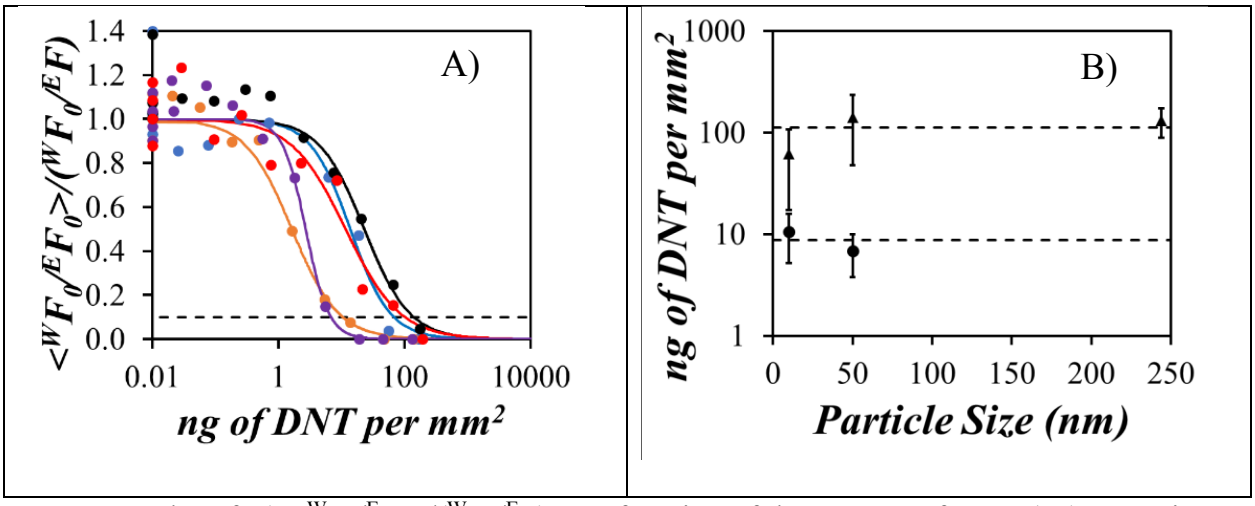

Figure 18. Plot of A) $<{}^{W}F_o/{}^{E}F_o>/({}^{W}F_o/{}^{E}F)$ as a function of the amount of DNT (ng) per unit area (mm^2) deposited for (●) Py(6)-Amylopectin,(●) Py(6)-SNP1, and (●) Py(6)-SNP2,(●) Py(36)-SNP1, and (●) Py(39)-SNP2 and B) detection limits expressed in mass of DNT (ng) per unit area (mm^2) as a function of particle size for pyrene contents of (▲) 6 and (●) 36 mol%. All Py-CFPs used in these experiments had a pyrene surface concentration of $1.6 \cdot 10^{-11}$ mol pyrene per mm^2.

4.3. Effect of Further Hydrophobic Modification

Although changes in pyrene content and particle size did not decrease the detection limit in any substantial manner, further hydrophobic modifications of the Py-SNPs might achieve lower detection limits. In theory, further hydrophobic modification of Py-SNPs should generate more hydrophobic microdomains, thereby driving the binding of the sparingly water-soluble NACs. To this end, an SNP1 sample was modified by Bowei Zhang, a graduate student in Prof. Taylor's laboratory, with 10 mol% styrene oxide to generate Sty(10)-SNP1. Styrene is a well-known hydrophobic monomer. The Sty(10)-SNP1 was labeled with 3.7 and 15 mol% PBA to yield Py(4)-Sty(10)-SNP1 and Py(15)-Sty(10)-SNP1s, respectively. The detection limit was found to decrease from 118 (±45) for Py(4)-SNP1 to 32 (±17) ng per mm^2 for Py(4)-Sty(10)-SNP1. This suggested that styrene modification improved the detection limit for the low pyrene-content samples. Unfortunately, no change in detection limit was observed for the higher pyrene content samples

with Py(11)-SNP1 and Py(15)-Sty(10)-SNP1 yielding detection limits of 11 (±5) and 28 (±20) ng of DNT per mm^2. However it should also be noted that styrene is more water soluble (300 mg/L at 25 °C)[66] compared to pyrene (0.135 mg/L at 25 °C).[67] Consequently, the little change in detection limit observed between the Py(11)-SNP1 and Py(15)-Sty(10)-SNP1 samples might have been the result of an insufficient level of styrene (only 10 mol%) modification on the SNPs compared to the already high pyrene content. In the case of the Py(4)-Sty(10)-SNP1 sample, addition of 10 mol% styrene oxide doubled the weight fraction of hydrophobic material from 6 to 12 wt%. In effect, the 10 mol% styrene oxide modification of Py(4)-Sty(10)-SNP1 generated a hydrophobically modified SNP (HMSNP) with a hydrophobic content equivalent to that of Py(8)-SNP1, thus turning Py(4)-SNP1 from a poor to a good detection limit in Figure 17. By comparison, addition of 10 mol% styrene oxide to Py(15)-SNP1 turned this particle into a HMSNP having a hydrophobic content equivalent to Py(20)-SNP1. Based on Figure 17, both particles belonged to the family of Py-SNPs having a low detection limit around 10 ng/mm^2 as found experimentally for Py(11)-SNP1 and Py(15)-Sty(10)-SNP1 within experimental error. Consequently, styrene oxide modification was not expected to improve the detection limit of Py-CFPs prepared with Py-SNPs having a pyrene content greater than 8 mol%.

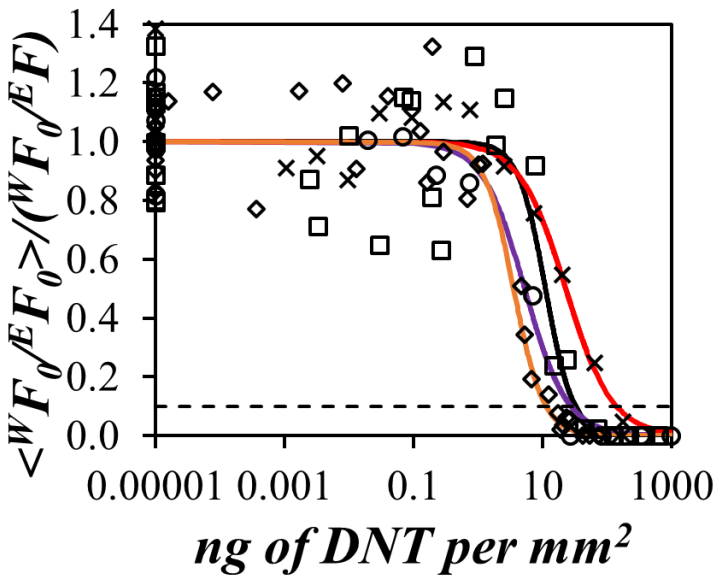

Figure 19. Plot of $<{}^{W}F_o/{}^{E}F_o>/({}^{W}F_o/{}^{E}F)$ as a function of the amount of DNT (ng) per unit area (mm^2) deposited for Py-CFPs coated with Py(4)-SNP1 (—,×), Py(4)-Sty(10)-SNP1 (—, □), Py(11)-SNP1 (—, ○), and Py(15)-Sty(10)-SNP1 (—, ◇). All Py-CFPs had a same pyrene surface concentration of $1.6 \cdot 10^{-11}$ mol pyrene per mm^2.

4.4 Conclusions of Optimization Attempts

The experiments carried out in Chapter 4 investigated the effect that pyrene content, particle size, and hydrophobic modification of the SNPs had on the detection limits of the corresponding Py-CFPs. While the detection limit was little affected by particle size, it depended strongly on pyrene content and hydrophobic modification. In fact, two regimes in detection limit were obtained in Figure 16 depending on the pyrene content of the Py-SNPs. Py-SNPs with pyrene contents below 8 mol% had a high detection limit above 100 ng DNT per mm^2. The detection limit decreased to about 10 ng of DNT per mm^2 for Py-SNPs having a pyrene content higher than 8 mol%. This decrease was attributed to the extensive formation of pyrene aggregates that drove the binding of NACs. Most interestingly, the hydrophobicity of the SNPs could also be increased by reacting

them with styrene oxide, resulting in similar detection limit as for a Py-SNP having an equivalent hydrophobic content. The ability to replace some of the pyrene labels by styrene oxide matters considering the difference in price between styrene oxide ($ 0.16/g) versus 1-pyrenebutyric acid ($ 48/g) based on the Aldrich catalog. The use of styrene oxide to prepare Py-CFPs might thus provide a means to lower the cost of these optical sensors while not affecting their detection limit.

Chapter 5

Conclusions and Future Work

5.0 Conclusions and Future Work

The end goal of this research was to develop and demonstrate the potential applicability of Py-CFPs to detect NACs. Py-SNPs with various DS were synthesized and their photophysical properties were characterized in solution and when adsorbed onto filter paper. Pyrene aggregates, which were formed through associations between the pyrene labels covalently attached onto the SNPs, emitted as excimer and generated hydrophobic microdomains in the presence of water. These hydrophobic microdomains were expected to drive the binding of hydrophobic NACs such as TNT, a well-known explosive, to the fluorescent pyrene aggregates. In turn, targeted binding of NACs was to result in targeted quenching of the excimer fluorescence emitted by the pyrene aggregates. A brief summary of the main conclusions reached in this thesis is presented hereafter.

MNT, DNT, and TNT were selected as NACs of interest, as they are well-known explosives and explosive by-products. Furthermore, quenching studies in solution also made use of NM, a nitrated fluorescence quencher that was not aromatic. The first sets of quenching studies were conducted in DMSO, to determine the efficiency of quenching in an ideal solvent where all components (pyrene labels, SNPs, and quenchers) were soluble. Based on the k_q values retrieved from the fluorescence quenching experiments, quenching in DMSO was strongest for MNT (3.9 ($\pm$ 0.2)$\cdot 10^9$ $M^{-1}s^{-1}$), followed by DNT (2.2 ($\pm$ 0.2)$\cdot 10^9$ $M^{-1}s^{-1}$), and weakest for TNT=NM (1.6 ($\pm$0.2 and 0.1, respectively) $\cdot 10^9$ $M^{-1}s^{-1}$). The next set of quenching studies were conducted in water, to demonstrate that NACs targeted the pyrene aggregates. Significantly more pyrene aggregates were generated in water compared to in DMSO based on the large increase observed in the I_E/I_M ratio when the solvent used to prepare the Py-SNP dispersions was switched from DMSO to water. Furthermore, the hydrophobic microdomains generated by the pyrene labels induced the targeted binding of NACs. Interestingly, an opposite trend in quencher efficiency was

observed in water compared to that found in DMSO, where TNT and MNT were the most and least efficient quencher, respectively, while DNT had an intermediate quenching efficiency. Interestingly, NM quenching studies showed no specific interactions with the pyrene aggregates. However they revealed that protective quenching took place for the fluorescence of the pyrene monomer in Py-SNPs with higher pyrene content, indicating that increased hydrophobic associations led to the formation of microdomains in the Py-SNPs that were not accessible to the solvent, and thus the NM quencher.

In addition to the quenching studies in solution, studies were also carried out on Py-CFPs with MNT and DNT vapours. Rapid response times of 0.48 (± 0.05) and 3.6 (± 0.3) minutes were found to reach 90% quenching of the fluorescence intensity of the Py-CFPs by MNT and DNT vapors, respectively. Further quenching studies were also performed on Py-CFPs in a much more quantitative manner, where a known mass of quencher was directly deposited onto the films. Detection limits of 30 (± 9), 11 (± 5), and 1.4 (± 0.6) ng per mm^2 were found for MNT, DNT, and TNT, respectively. This last point constitutes the main contribution from this thesis where a systematic quenching study of Py-SNPs was implemented to obtain quantitative detection limits expressed in ng of quencher per mm^2. This information is hardly ever reported in the scientific literature. When compared to the detection limits and response times available in a handful of reports,[22,25,30,37,39,45,46] the detection limits and response times obtained with the Py-CFPs were found to be either similar, but often much better. Furthermore, whereas the supports employed to attach the dyes typically employed in optical sensors usually involve complex multistep synthesis or expensive substrates such as dendrimers, the research grade SNPs used as substrate in the present application were safe and cost effective which establishes SNPs as important elements for the preparation of optical sensors for NAC detection.

Although, the detection limit for the Py-CFPs established in this thesis was promising, it could be further improved through further chemical modification and optimization. Preliminary experiments conducted to that effect showed that the size of the SNPs used to prepare the Py-SNPs employed in the preparation of the Py-CFPs had no effect on their detection limit. The main factor found to substantially lower the detection limit of the Py-CFPs was their hydrophobic content. A threshold was found whereby Py-SNPs labeled with less and more than 8 mol% pyrene had a detection limit on the order of 100 and 10 ng/mm^2, respectively. Most interestingly, adjusting the hydrophobic content by grafting styrene oxide instead of 1-pyrenebutyric acid brought the detection limit down to 10 ng/mm^2 as long as the overall hydrophobic content of the particles was larger than 11 wt%. Being able to replace some of the expensive pyrene labels by grafting cost effective styrene oxide while maintaining a low detection limit would certainly constitute a future line of research to follow.

Taking advantage of styrene having both a hydrophobic and aromatic character, more Py-Sty-SNPs should be generated where both pyrene and styrene content should be systematically adjusted and the detection limit of the resulting Py-Sty-CFPs should be evaluated. These experiments would establish how little pyrene can be employed to generate Py-Sty-CFPs having as low as possible a detection limit.

Another aspect that should be investigated would be the specific pyrene-labeling of the SNP surface, since it is the SNP surface that is most accessible to NACs. One way this could be achieved would be to prepare a water in toluene emulsion where the aqueous phase could be loaded with SNPs. Pyrene-labeling of the SNPs could only be achieved at the water-toluene interface, the pyrene labels being effectively excluded from the water-swollen interior of the SNPs due to their hydrophobicity. The resulting Py-SNPs would be expected to have fascinating properties in water.

Their hydrophobic pyrene labels located at the SNP surface would try to avoid exposure from water by locating in the SNP interior which would result in a profound rearrangement of their macromolecular conformation. The pyrene labels would not be able to be buried deep inside the SNPs however due to their highly branched interior. They would be close to the surface and accessible to the solvent which would secure easy quenching. Thus it would be interesting to investigate whether such Py-SNPs would result in lower detection limits for the corresponding Py-CFPs.

An investigation should be conducted by selecting different substrates to adsorb Py-SNPs. Substrate porosity, roughness, or wettability could improve the detection limit. In addition to further modification and optimization, quenching studies should be conducted on Py-CFPs with other common explosives such as picric acid or nitroglycerin to further demonstrate Py-CFPs selectivity towards NACs.

While further optimization and selectivity studies must be conducted in the future with the Py-CFPs, it is clear that this thesis has demonstrated the potential use of Py-SNPs for the detection minute quantities of NACs. It has established that with little optimization, Py-CFPs can be employed as cost effective and sensitive optical sensors.

Reference

(1) Ewing, R. G.; Atkinson, D. A.; Eiceman, G. A.; Ewing, G. J. A Critical Review of Ion Mobility Spectrometry for the Detection of Explosives and Explosive Related Compounds. *Talanta* **2001**, *54*, 515–529.

(2) Caygill, J. S.; Davis, F.; Higson, S. P. J. Current Trends in Explosive Detection Techniques. *Talanta* **2012**, *88*, 14–29.

(3) Akhgari, F.; Fattahi, H.; Oskoei, Y. M. Recent Advances in Nanomaterial-Based Sensors for Detection of Trace Nitroaromatic Explosives. *Sens. Actuators, B* **2015**, *221*, 867–878.

(4) Ju, K.-S.; Parales, R. E. Nitroaromatic Compounds, from Synthesis to Biodegradation. *Microbiol. Mol. Biol. Rev.* **2010**, *74*, 250–272.

(5) Pereira, T. R.; Laird, D. A.; Johnston, C. T.; Teppen, B. J.; Boyd, S. A. Mechanism of Dinitrophenol Herbicide Sorption by Smectites in Aqueous Suspensions at Varying PH. *Soil Sci. Soc. Am. J.* **2007**, *71*, 1476–1481.

(6) Kalderis, D.; Juhasz, A. L.; Boopathy, R.; Comfort, S. Soils Contaminated with Explosives: Environmental Fate and Evaluation of State-of-the-Art Remediation Processes. *Pure Appl. Chem.* **2011**, *83*, 1407–1484.

(7) Ma, Y.; Wang, S.; Wang, L. Nanomaterials for Luminescence Detection of Nitroaromatic Explosives. *TrAC, Trends Anal. Chem.* **2015**, *65*, 13–21.

(8) Yinon, J. Detection of Explosives by Electronic Noses. *Anal. Chem.* **2003**, *75*, 98-105.

(9) Toal, S. J.; Trogler, W. C. Polymer Sensors for Nitroaromatic Explosives Detection. *J. Mater. Chem.* **2006**, *16*, 2871–2883.

(10) Beyazkilic, P.; Yildirim, A.; Bayindir, M. Formation of Pyrene Excimers in Mesoporous Ormosil Thin Films for Visual Detection of Nitro-Explosives. *ACS Appl. Mater. Interfaces* **2014**, *6*, 4997–5004.

(11) Zheng, B.; Li, Y.; Tao, F.; Cui, Y.; Li, T. Enhanced Superquenching of the Hyperbranched Conjugated Polymer for the Detection of Nitroaromatic Explosives. *Sens. Actuators, B* **2017**, *241*, 357–363.

(12) Ma, X. S.; Wang, D. H.; Cui, Y. Z.; Tao, F. R.; Wang, Y. T.; Li, T. D. A Novel Hydrophilic Conjugated Polymer Containing Hydroxyl Groups: Syntheses and Sensing Performance for NACs in Aqueous Solution. *Sens. Actuators, B* **2017**, *251*, 851–857.

(13) Xu, B.; Wu, X.; Li, H.; Tong, H.; Wang, L. Selective Detection of TNT and Picric Acid by Conjugated Polymer Film Sensors with Donor-Acceptor Architecture. *Macromolecules* **2011**, *44*, 5089–5092.

(14) Long, Y.; Chen, H.; Yang, Y.; Wang, H.; Yang, Y.; Li, N.; Li, K.; Pei, J.; Liu, F. Electrospun Nanofibrous Film Doped with a Conjugated Polymer for DNT Fluorescence Sensor. *Macromolecules* **2009**, *42*, 6501–6509.

(15) Zhang, Y.; Shen, P.; He, B.; Luo, W.; Zhao, Z.; Tang, B. Z. New Fluorescent Through-Space Conjugated Polymers: Synthesis, Optical Properties and Explosive Detection. *Polym. Chem.* **2018**, *9*, 558–564.

(16) Tian, X.; Peng, H.; Li, Y.; Yang, C.; Zhou, Z.; Wang, Y. Highly Sensitive and Selective Paper Sensor Based on Carbon Quantum Dots for Visual Detection of TNT Residues in Groundwater. *Sens. Actuators, B* **2017**, *243*, 1002–1009.

(17) Bhatia, S. *Natural Polymer Drug Delivery System*. Springer, 2016, pp 33-93.

(18) Aparna, R. S.; Anjali Devi, J. S.; Sachidanandan, P.; George, S. Polyethylene Imine Capped Copper Nanoclusters - Fluorescent and Colorimetric Onsite Sensor for the Trace Level Detection of TNT. *Sens. Actuators, B* **2018**, *254*, 811–819.

(19) Chang, C. P.; Chao, C. Y.; Huang, J. H.; Li, A. K.; Hsu, C. S.; Lin, M. S.; Hsieh, B. R.; Su, A. C. Fluorescent Conjugated Polymer Films as TNT Chemosensors. *Synth. Met.* **2004**, *144*, 297–301.

(20) Li, D.; Liu, J.; Kwok, R. T. K.; Liang, Z.; Tang, B. Z.; Yu, J. Supersensitive Detection of Explosives by Recyclable AIE Luminogen-Functionalized Mesoporous Materials. *Chem. Commun.* **2012**, *48*, 7167–7169.

(21) Dong, W.; Fei, T.; Scherf, U. Conjugated Polymers Containing Tetraphenylethylene in the Backbones and Side-Chains for Highly Sensitive TNT Detection. *RSC Adv.* **2018**, *8*, 5760–5767.

(22) Zhou, H.; Wang, X.; Lin, T. T.; Song, J.; Tang, B. Z.; Xu, J. Poly(Triphenyl Ethene) and Poly(Tetraphenyl Ethene): Synthesis, Aggregation-Induced Emission Property and Application as Paper Sensors for Effective Nitro-Compounds Detection. *Polym. Chem.* **2016**, *7*, 6309–6317.

(23) Liu, X. G.; Tao, C. L.; Yu, H. Q.; Chen, B.; Liu, Z.; Zhu, G. P.; Zhao, Z.; Shen, L.; Tang, B. Z. A New Luminescent Metal-Organic Framework Based on Dicarboxyl-Substituted Tetraphenylethene for Efficient Detection of Nitro-Containing Explosives and Antibiotics in Aqueous Media. *J. Mater. Chem. C* **2018**, *6*, 2983–2988.

(24) He, G.; Yan, N.; Yang, J.; Wang, H.; Ding, L.; Yin, S.; Fang, Y. Pyrene-Containing Conjugated Polymer-Based Fluorescent Films for Highly Sensitive and Selective Sensing of TNT in Aqueous Medium. *Macromolecules* **2011**, *44*, 4759–4766.

(25) Sun, X.; Liu, Y.; Shaw, G.; Carrier, A.; Dey, S.; Zhao, J.; Lei, Y. Fundamental Study of Electrospun Pyrene-Polyethersulfone Nanofibers Using Mixed Solvents for Sensitive and Selective Explosives Detection in Aqueous Solution. *ACS Appl. Mater. Interfaces* **2015**, *7*, 13189–13197.

(26) Turhan, H.; Tukenmez, E.; Karagoz, B.; Bicak, N. Highly Fluorescent Sensing of Nitroaromatic Explosives in Aqueous Media Using Pyrene-Linked PBEMA Microspheres. *Talanta* **2018**, *179*, 107–114.

(27) Senthamizhan, A.; Celebioglu, A.; Bayir, S.; Gorur, M.; Doganci, E.; Yilmaz, F.; Uyar, T. Highly Fluorescent Pyrene-Functional Polystyrene Copolymer Nanofibers for Enhanced Sensing Performance of TNT. *ACS Appl. Mater. Interfaces* **2015**, *7*, 21038–21046.

(28) Duhamel, J. New Insights in the Study of Pyrene Excimer Fluorescence to Characterize Macromolecules and Their Supramolecular Assemblies in Solution. *Langmuir* **2012**, *28*, 6527–6538.

(29) Yildirim, A.; Budunoglu, H.; Deniz, H.; Guler, M. O.; Bayindir, M. Template-Free Synthesis of Organically Modified Silica Mesoporous Thin Films for TNT Sensing. *ACS Appl. Mater. Interfaces* **2010**, *2*, 2892–2897.

(30) Tao, T.; Gan, Y.; Yu, J.; Huang, W. Chemical Tuning Aggregation-Induced Emission Properties with the Number of Cyano and Ester Groups in the Same Dibenzo [b , d] Thiophene Skeleton for Effective Detection of Explosives. *Sens. Actuators, B* **2018**, *257*, 303–311.

(31) Tao, S.; Yin, J.; Li, G. High-Performance TNT Chemosensory Materials Based on Nanocomposites with Bimodal Porous Structures. *J. Mater. Chem.* **2008**, *18*, 4872–4878.

(32) Possamai, G.; Menna, E.; Maggini, M.; Carano, M.; Marcaccio, M.; Paolucci, F.; Guldi, D.

M.; Swartz, A. Rhenium(I) and Ruthenium(II) Complexes with a Crown-Linked Methanofullerene Ligand: Synthesis, Electrochemistry and Photophysical Characterization. *Photochem. Photobiol. Sci.* **2006**, *5*, 1154–1164.

(33) Astruc, D.; Boisselier, E.; Ornelas, C. Dendrimers Designed for Functions: From Physical, Photophysical, and Supramolecular Properties to Applications in Sensing, Catalysis, Molecular Electronics, Photonics, and Nanomedicine. *Chem. Rev.* **2010**, *110*, 1857–1959.

(34) Soršak, E.; Valh, J. V.; Urek, S. K.; Lobnik, A. Application of PAMAM Dendrimers in Optical Sensing. *Analyst* **2015**, *140*, 976–989.

(35) Tang, G.; Chen, S. S. Y.; Shaw, P. E.; Hegedus, K.; Wang, X.; Burn, P. L.; Meredith, P. Fluorescent Carbazole Dendrimers for the Detection of Explosives. *Polym. Chem.* **2011**, *2*, 2360-2368.

(36) Tao, S.; Li, G.; Zhu, H. Metalloporphyrins as Sensing Elements for the Rapid Detection of Trace TNT Vapor. *J. Mater. Chem.* **2006**, *16*, 4521–4528.

(37) Huang, S.; He, Q.; Xu, S.; Wang, L. Polyaniline-Based Photothermal Paper Sensor for Sensitive and Selective Detection of 2,4,6-Trinitrotoluene. *Anal. Chem.* **2015**, *87*, 5451–5456.

(38) Lu, W.; Zhang, J.; Huang, Y.; Théato, P.; Huang, Q.; Chen, T. Self-Diffusion Driven Ultrafast Detection of Ppm-Level Nitroaromatic Pollutants in Aqueous Media Using a Hydrophilic Fluorescent Paper Sensor. *ACS Appl. Mater. Interfaces* **2017**, *9*, 23884–23893.

(39) Yang, J. S.; Swager, T. M. Fluorescent Porous Polymer Films as TNT Chemosensors: Electronic and Structural Effects. *J. Am. Chem. Soc.* **1998**, *120*, 11864–11873.

(40) Almassio, M. F.; Romagnoli, M. J.; Del Rosso, P. G.; Schvval, A. B.; Garay, R. O. Distyrylbenzene-Based Segmented Conjugated Polymers: Synthesis, Thin Film

Morphology and Chemosensing of Hydrophobic and Hydrophilic Nitroaromatics in Aqueous Media. *Polymer* **2017**, *113*, 167–179.

(41) Bloembergen, S.; Vanegdom, E.; Wildi, R. H.; Mclennan, I. J.; Lee, D. I.; Klass, C. P.; van Leeuwen, J. Biolatex Binders for Paper and Paperboard Applications. *J. Pulp Pap. Sci.* **2011**, *36*, 151–161.

(42) Ballegooie, V. P.; Greenall, P.; Bloembergen, S.; Dejong, R. EcoSphere® Biolatex® Binders : Next Generation Solutions for Today's Paper Coating Industry. World Pulp & Paper **2011**, 100–104.

(43) Campo, J. C.; Perez, M. A.; Barragan, N.; Blanco, C.; Viera, J. C.; Grillo, G. Sol-Gel Based Oxygen Sensor and Luminescence Lifetime Based Instrumentation. *IEEE Sens.* **2002**, *1*, 388–392.

(44) Kumar, A.; Pandith, A.; Kim, H. S. Pyrene-Appended Imidazolium Probe for 2,4,6-Trinitrophenol in Water. *Sens. Actuators, B* **2016**, *231*, 293–301.

(45) Gillanders, R. N.; Campbell, I. A.; Glackin, J. M. E.; Samuel, I. D. W.; Turnbull, G. A. Ormosil-Coated Conjugated Polymers for the Detection of Explosives in Aqueous Environments. *Talanta* **2018**, *179*, 426–429.

(46) Content, S.; Trogler, W. C.; Sailor, M. J. Detection of Nitrobenzene, DNT, and TNT Vapors by Quenching of Porous Silicon Photoluminescence. *Chem. - Eur. J.* **2000**, *6*, 2205–2213.

(47) Kovalev, I. S.; Taniya, O. S.; Slovesnova, N. V.; Kim, G. A.; Santra, S.; Zyryanov, G. V.; Kopchuk, D. S.; Majee, A.; Charushin, V. N.; Chupakhin, O. N. Fluorescent Detection of 2,4-DNT and 2,4,6-TNT in Aqueous Media by Using Simple Water-Soluble Pyrene Derivatives. *Chem. - Asian J.* **2016**, *11*, 775–781.

(48) Ma, X.; Tao, F.; Zhang, Y.; Li, T.; Raymo, F. M.; Cui, Y. Detection of Nitroaromatic

Explosives by a 3D Hyperbranched Σ–π Conjugated Polymer Based on a POSS Scaffold. *J. Mater. Chem. A* **2017**, *5*, 14343–14354.

(49) Liu, J.; Zhong, Y.; Lu, P.; Hong, Y.; Lam, J. W. Y.; Faisal, M.; Yu, Y.; Wong, K. S.; Tang, B. Z. A Superamplification Effect in the Detection of Explosives by a Fluorescent Hyperbranched Poly(Silylenephenylene) with Aggregation-Enhanced Emission Characteristics. *Polym. Chem.* **2010**, *1*, 426-429.

(50) Yekta, A.; Duhamel, J.; Brochard, P.; Adiwidjaja, H.; Winnik, M. A. A Fluorescent-Probe Study of Micelle-like Cluster Formation in Aqueous-Solutions of Hydrophobically Modified Poly(Ethylene Oxide). *Macromolecules* **1993**, *26*, 1829–1836.

(51) Kim, H. Y.; Park, S. S.; Lim, S. T. Preparation, Characterization and Utilization of Starch Nanoparticles. *Colloids Surf. B* **2015**, *126*, 607–620.

(52) Tester, R. F.; Karkalas, J.; Qi, X. Starch - Composition, Fine Structure and Architecture. *J. Cereal Sci*. **2004**, *39*, 151–165.

(53) Le Corre, D.; Bras, J.; Dufresne, A. Starch Nanoparticles: A Review. *Biomacromolecules* **2010**, *11*, 1139–1153.

(54) Singh, N.; Singh, J.; Kaur, L.; Sodhi, N. S.; Gill, B. S. Morphological, Thermal and Rheological Properties of Starches from Different Botanical Sources. *Food Chem*. **2003**, *81*, 219–231.

(55) Kim, D.; Amos, R.; Gauthier, M.; Duhamel, J. Applications of Pyrene Fluorescence to the Characterization of Hydrophobically Modified Starch Nanoparticles. *Langmuir* **2018**, *34*, 8611–8621.

(56) Lakowicz, J. R. *Principles of Fluorescence Spectroscopy*; 3rd ed. Baltimore: Springer, 2006.

(57) Birks, J. B.; Dyson, D. J.; Munro, I. H. Excimer' Fluorescence. II. Lifetime Studies of Pyrene Solutions. *Proc. R. Soc. A Math. Phys. Eng. Sci.* **1963**, *275*, 575–588.

(58) Williams, A. T. R.; Winfield, S. A.; Miller, J. N. Relative Fluorescence Quantum Yields Using a Computer-Controlled Luminescence Spectrometer*. *Analyst* **1983**, *108*, 1067–1071.

(59) Berlman, I. B. *Handbook of Fluorescence Spectra of Aromatic Molecules,* 2nd ed. New York: Academic Press, 1971.

(60) Yi, W. Characterization of Starch Nanoparticles by Fluorescence Techniques, M.Sc. Thesis, University of Waterloo,Waterloo, Canada, 2014.

(61) Li, L.; Duhamel, J. Conformation of Pyrene-Labeled Amylose in DMSO Characterized with the Fluorescence Blob Model. *Macromolecules* **2016**, *49*, 7965–7974.

(62) Luning Prak, D. J.; O'Sullivan, D. W. Solubility of 4-Nitrotoluene, 2,6-Dinitrotoluene, 2,3-Dinitrotoluene, and 1,3,5-Trinitrobenzene in Pure Water and Seawater. *J. Chem. Eng. Data* **2007**, *52*, 2446–2450.

(63) Phelan, J. M.; Barnett, J. L. Solubility of 2 , 4-Dinitrotoluene and 2 , 4 , 6-Trinitrotoluene in Water. *J. Chem. Eng. Data* **2001**, *46*, 375–376.

(64) Press, W.; Flannery, B.; Teukolsky, S.; Vetterling, W. *Numerical Recipes in Fortran 77: The Art of Scientific Computing*; Cambridge University Press, **1992**, 523-528.

(65) Östmark, H.; Wallin, S.; Ghee, H. Vapor Pressure of Explosives : A Critical Review. *Propellants, Explos. Pyrotech.* **2012**, *37*, 12-23.

(66) Lide, D. R. *CRC Handbook of Chemistry and Physics,* 88th ed. Boca Raton: CRC press, 1999, pp 85-115.

(67) Miller, M. M.; Huang, G. L.; Shiu, W. Y,; Mackay, D., W. S. P. Relationships between

Octanol-Water Partition Coefficient and Aqueous Solubility. *Environ. Sci. Technol.* **1985**, *19*, 522–529.

(68) Giri, D.; Islam, S. N.; Patra, S. K. Synthesis and Characterization of 1,2,3-Triazole Appended Polythiophene Based Reusable Fluorescent Probe for the Efficient Detection of Trace Nitroaromatics. *Polymer* **2018**, *134*, 242–253.

(69) Xu, B.; Wu, X.; Li, H.; Tong, H.; Wang, L. Selective Detection of TNT and Picric Acid by Conjugated Polymer Film Sensors with Donor-Acceptor Architecture. *Macromolecules* **2011**, *44*, 5089–5092.

(70) Kou, S. C.; Cherayil, B. J.; Min, W.; English, B. P.; Xie, X. S. Single-Molecule Michaelis−Menten Equations. *J. Phys. Chem. B.* **2005**, *109*, 19068–19081.

(71) Weiss, J. N. The Hill Equation Revisited: Uses and Misuses. *FASEB J.* **1997**, *11*, 835–841.

Appendices

Quenching Studies Conducted in DMSO:

Table A1. Normalized preexponential factors and decay times retrieved from the analysis of the fluorescence decays of molecular pyrene quenched by nitrotmethane in DMSO. λ_{ex}= 338 nm and λ_{em}= 375 nm.

[Nitromethane] (mM)	a_1	τ_1 (ns)	a_2	τ_2 (ns)	χ^2
0.00	0.06	19.9	0.94	104	1.18
0.43	0.08	12.8	0.92	93	1.20
0.82	0.08	9.4	0.92	85	1.14
1.53	0.08	12.4	0.92	74	1.17
2.18	0.52	56	0.49	76	1.03
3.20	0.11	15.9	0.89	53	1.15
4.43	0.10	11.0	0.90	47	1.15
5.54	0.10	8.2	0.90	42	1.05
6.90	0.13	6.3	0.88	37	1.16
8.54	0.12	6.8	0.88	31	1.19
10.43	0.12	3.7	0.88	26.3	1.13
12.39	0.12	5.6	0.88	23.1	1.08

Table A2. Normalized preexponential factors and decay times retrieved from the analysis of the monomer fluorescence decays of Py(0.06)-SNP quenched by nitromethane in DMSO. λ_{ex}= 346 nm and λ_{em}= 375 nm.

[Nitromethane] (mM)	a_1	τ_1 (ns)	a_2	τ_2 (ns)	χ^2
0.00	0.13	37	0.87	96	1.10
0.43	0.13	34	0.87	90	1.08
1.32	0.18	25.0	0.82	81	1.09
2.56	0.21	24.7	0.79	71	1.20
4.04	0.26	26.5	0.74	66	1.16
5.74	0.29	22.2	0.72	56	1.09
7.70	0.34	20.3	0.67	48	1.11
9.76	0.39	20.3	0.61	45	1.09
11.91	0.45	18.1	0.55	39	1.12
15.19	0.45	16.2	0.56	35	1.16
18.18	0.37	14.3	0.61	34	1.19

Table A3. Normalized preexponential factors and decay times retrieved from the analysis of the monomer fluorescence decays of Py(2.65)-SNP quenched by nitromethane in DMSO. λ_{ex}= 346 nm and λ_{em}= 375 nm.

[Nitromethane] (mM)	a_1	τ_1 (ns)	a_2	τ_2 (ns)	χ^2
0.00	0.23	25.6	0.77	78	1.01
0.35	0.24	26.7	0.76	75	1.11
1.08	0.25	25.8	0.75	71	1.21
2.15	0.24	21.9	0.76	62	1.01
3.11	0.24	22.5	0.77	57	1.12
4.53	0.28	22.1	0.72	53	1.09
6.17	0.26	19.1	0.74	46	1.17
7.99	0.32	19.1	0.68	42	1.18
10.04	0.33	17.5	0.67	38	1.22
12.23	0.35	16.1	0.65	33	1.14

Table A4. Normalized preexponential factors and decay times retrieved from the analysis of the monomer fluorescence decays of Py(8.65)-SNP quenched by nitromethane in DMSO. λ_{ex}= 346 nm and λ_{em}= 375 nm.

[Nitromethane] (mM)	a_1	τ_1 (ns)	a_2	τ_2 (ns)	a_3	τ_3 (ns)	χ^2
0.00	0.23	6.1	0.42	28.4	0.35	59	1.07
0.49	0.22	6.8	0.39	26.0	0.39	53	1.06
1.51	0.23	6.3	0.42	24.8	0.35	49	1.01
2.82	0.20	4.1	0.38	20.1	0.42	44	0.90
4.25	0.17	3.4	0.36	16.7	0.47	39	1.06
6.06	0.18	4.4	0.35	16.6	0.47	35	0.94
7.97	0.20	4.2	0.37	17.0	0.43	34	1.05
10.04	0.26	6.0	0.55	21.8	0.20	36	1.09
12.26	0.18	3.5	0.37	13.9	0.45	27.2	0.91
14.55	0.18	3.8	0.39	13.4	0.48	25.5	0.98
16.69	0.20	3.8	0.41	13.6	0.39	23.9	1.14

Table A5. Normalized preexponential factors and decay times retrieved from the analysis of the monomer fluorescence decays of Py(10)-SNP quenched by nitromethane in DMSO. λ_{ex}= 346 nm and λ_{em}= 375 nm.

[Nitromethane] (mM)	a_1	τ_1 (ns)	a_2	τ_2 (ns)	χ^2
0.00	0.50	16.0	0.50	48	1.11
0.69	0.47	15.3	0.54	44	1.02
1.66	0.45	13.8	0.55	41	1.19
2.93	0.43	12.3	0.57	36	1.08
4.38	0.42	11.9	0.58	34	1.15
6.06	0.41	10.1	0.59	31	1.10
7.83	-	-	-	-	-
9.77	0.39	8.3	0.61	25.7	1.06
11.84	0.40	8.3	0.60	24.1	1.19
13.86	0.39	7.4	0.61	21.8	1.14
16.25	0.42	7.8	0.58	21.1	1.11

Table A6. Normalized preexponential factors and decay times retrieved from the analysis of the fluorescence decays of free pyrene quenched by nitrotoluene in DMSO. λ_{ex}= 338 nm and λ_{em}= 375 nm.

[Nitrotoluene] (mM)	a_1	τ_1 (ns)	a_2	τ_2 (ns)	χ^2
0.00	0.04	4.9	0.96	102	0.98
0.35	0.11	45	0.89	87	1.16
0.67	0.08	32	0.92	74	1.21
0.95	0.08	29.8	0.92	68	1.14
1.31	0.09	18.7	0.91	58	1.16
1.87	0.08	15.7	0.92	50	1.15
2.53	0.08	10.7	0.92	44	1.24
3.36	0.12	17.4	0.87	37	1.12
4.28	0.12	6.8	0.88	29.2	1.21

Table A7. Normalized preexponential factors and decay times retrieved from the analysis of the fluorescence decays of Py(0.06)-SNP quenched by nitrotoluene in DMSO. λ_{ex}= 346 nm and λ_{em}= 375 nm.

[Nitrotoluene] mM	a_1	τ_1 (ns)	a_2	τ_2 (ns)	χ^2
0	0.15	23.0	0.85	95	1.28
0.66	0.20	26.3	0.80	79	1.22
1.16	0.25	31.0	0.75	72	1.14
1.96	0.32	29.7	0.68	63	1.19
2.87	0.43	28.3	0.57	58	1.27
4.18	0.47	25.7	0.53	53	1.00
4.52	0.56	25.9	0.44	52	1.20
5.43	0.62	24.2	0.38	49	1.21
3.94	0.57	20.8	0.43	45	1.23

Table A8. Normalized preexponential factors and decay times retrieved from the analysis of the monomer fluorescence decays of Py(2.65)-SNP quenched by nitrotoluene in DMSO. λ_{ex}= 346 nm and λ_{em}= 375 nm.

[Nitrotoluene] (mM)	a_1	τ_1 (ns)	a_2	τ_2 (ns)	a_3	τ_3 (ns)	χ^2
0.00	0.15	18.4	0.52	62	0.33	94	1.04
0.19	0.17	9.8	0.49	54	0.34	91	1.02
0.27	0.15	17.7	0.54	58	0.31	83	1.28
0.66	0.17	19.2	0.52	57	0.31	76	1.16
0.74	0.16	12.3	0.61	53	0.23	88	1.07
1.32	0.18	17.3	0.52	50	0.30	68	1.18
1.48	0.14	6.0	0.43	36	0.43	62	1.01
2.22	0.08	6.9	0.31	25.7	0.61	50	1.07
2.50	0.16	5.9	0.54	33	0.30	54	0.93
3.20	0.12	6.5	0.40	27.7	0.47	46	1.01
3.52	0.15	7.5	0.42	26.4	0.43	43	1.05

Table A9. Normalized preexponential factors and decay times retrieved from the analysis of the monomer fluorescence decays of Py(8.65)-SNP quenched by nitrotoluene in DMSO. λ_{ex}= 346 nm and λ_{em}= 375 nm.

[Nitrotoluene] (mM)	a_1	τ_1 (ns)	a_2	τ_2 (ns)	a_3	τ_3 (ns)	χ^2
0.00	0.47	16.6	0.54	53	-	-	0.99
0.17	0.44	15.1	0.56	50	-	-	1.06
0.31	0.46	15.2	0.54	48	-	-	1.01
0.60	0.48	16.4	0.53	49	-	-	0.90
1.06	0.36	8.8	0.64	41	-	-	1.06
1.60	0.40	11.3	0.60	41	-	-	0.94
2.22	0.39	10.0	0.61	38	-	-	1.05
2.83	0.17	2.3	0.31	12.2	0.52	36	1.19
3.43	0.17	3.1	0.34	14.4	0.48	36	0.91
4.00	0.22	4.6	0.37	17.7	0.41	36	0.98

Table A10. Normalized preexponential factors and decay times retrieved from the analysis of the monomer fluorescence decays of Py(10)-SNP quenched by nitrotoluene in DMSO. λ_{ex}= 346 nm and λ_{em}= 375 nm.

[Nitrotoluene] (mM)	a_1	τ_1 (ns)	a_2	τ_2 (ns)	a_3	τ_3 (ns)	χ^2
0.00	0.33	9.0	0.50	32	0.17	54	1.14
0.24	0.37	10.8	0.50	33	0.14	53	1.14
0.75	0.25	3.7	0.36	18.0	0.39	40	1.06
1.39	0.24	3.4	0.34	16.2	0.42	38	1.20
2.40	0.23	3.9	0.34	15.3	0.44	34	0.98
3.23	0.27	3.3	0.36	15.3	0.37	32	1.18
4.30	0.28	3.7	0.34	14.5	0.38	28.5	1.15
5.01	0.36	2.1	0.29	11.4	0.35	27.5	0.91

Table A11. Normalized preexponential factors and decay times retrieved from the analysis of the monomer fluorescence decays of pyrene quenched by dinitrotoluene in DMSO. λ_{ex}= 338 nm and λ_{em}= 375 nm.

[Dinitrotoluene] (mM)	a_1	τ_1(ns)	a_1	τ_2 (ns)	χ^2
0.0	0.04	24.1	0.96	103	1.01
0.1	0.22	73	0.78	100	1.10
0.4	0.11	37	0.90	90	1.17
0.8	0.11	22.8	0.90	72	1.10
1.3	0.12	25.3	0.88	66	1.17
1.9	0.14	18.6	0.86	53	1.20
2.5	0.15	15.5	0.85	46	1.17

Table A12. Normalized preexponential factors and decay times retrieved from the analysis of the monomer fluorescence decays of Py(0.06)-SNPs quenched by dinitrotoluene in DMSO. λ_{ex}= 346 nm and λ_{em}= 375 nm.

[Dinitrotoluene] (mM)	a_1	τ_1 (ns)	a_2	τ_2 (ns)	χ^2
0.0	0.15	25.0	0.85	96	1.18
0.1	0.15	28.6	0.85	95	0.99
0.5	0.17	29.9	0.83	90	1.11
0.9	0.18	24.0	0.82	85	1.09
1.4	0.23	29.9	0.78	80	1.04
2.1	0.26	31	0.74	75	1.06
2.8	0.30	28.4	0.70	70	1.21
3.6	0.34	28.3	0.67	65	0.99

Table A13. Normalized preexponential factors and decay times retrieved from the analysis of the monomer fluorescence decays of Py(2.65)-SNPs quenched by dinitrotoluene in DMSO. λ_{ex}= 346 nm and λ_{em}= 375 nm.

[Dinitrotoluene] (mM)	a_1	τ_1 (ns)	a_2	τ_2 (ns)	a_3	τ_3 (ns)	χ^2
0.0	0.09	8.0	0.22	38	0.69	80	1.03
0.2	0.11	10.9	0.29	48	0.60	80	1.15
0.5	0.08	5.7	0.24	34	0.68	74	1.11
0.9	0.10	5.0	0.26	36	0.64	72	1.14
1.5	0.12	8.3	0.33	40	0.56	68	1.12
2.1	0.11	6.2	0.32	34	0.57	63	1.06
2.7	0.16	10.2	0.60	45	0.24	66	1.09

Table A14. Normalized preexponential factors and decay times retrieved from the analysis of the monomer fluorescence decays of Py(8.65)-SNPs quenched by dinitrotoluene in DMSO. λ_{ex}= 346 nm and λ_{em}= 375 nm.

[Dinitrotoluene] (mM)	a_1	τ_1 (ns)	a_2	τ_2 (ns)	χ^2
0.0	0.25	36	0.75	81	1.09
0.1	0.26	35	0.74	79	1.24
0.4	0.25	32	0.75	75	1.17
0.8	0.27	34	0.73	72	1.17
1.3	0.27	30	0.73	67	1.05
1.9	0.30	31	0.70	63	1.08
2.5	0.35	33	0.65	61	1.12
3.1	0.33	29.9	0.67	58	1.18
3.7	0.37	29.3	0.63	55	0.96
4.2	0.30	23.1	0.70	50	0.96

Table A15. Normalized preexponential factors and decay times retrieved from the analysis of the monomer fluorescence decays of Py(10)-SNPs quenched by dinitrotoluene in DMSO. λ_{ex}= 346 nm and λ_{em}= 375 nm.

[Dinitrotoluene] (mM)	a_1	τ_1 (ns)	a_2	τ_2 (ns)	χ^2
0.0	0.50	21.0	0.50	49	1.12
0.2	0.51	20.9	0.49	47	1.24
0.5	0.47	17.9	0.53	45	1.07
0.8	0.51	19.3	0.50	44	1.11
1.4	0.46	17.2	0.54	41	1.05
2.0	0.47	16.9	0.53	39	0.95
2.7	0.50	17.0	0.50	39	1.03

Table A16. Normalized preexponential factors and decay times retrieved from the analysis of the fluorescence decays of molecular pyrene quenched by trinitrotoluene in DMSO. λ_{ex}= 338 nm and λ_{em}= 375 nm.

[TNT] (mM)	a_1	τ_1 (ns)	a_2	τ_2 (ns)	χ^2
0.00	0.04	43	0.96	106	1.07
0.55	0.07	29.8	0.93	80	0.92
0.90	0.49	60	0.51	76	1.04
1.37	0.07	13.8	0.93	60	1.18
1.97	0.09	12.4	0.91	50	1.27
2.71	0.12	20.2	0.87	43	1.19
3.48	0.10	7.4	0.90	35	1.27
4.09	0.82	29.5	0.18	42	1.22
4.45	0.26	20.8	0.74	32	1.09

Table A17. Normalized preexponential factors and decay times retrieved from the analysis of the monomer fluorescence decays of Py(0.06)-SNPs quenched by trinitrotoluene in DMSO. λ_{ex}= 346 nm and λ_{em}= 375 nm.

[TNT] (mM)	a_1	τ_1 (ns)	a_2	τ_2 (ns)	a_3	τ_3 (ns)	χ^2
0.00	0.13	21.9	0.87	94	-	-	1.09
0.12	0.16	22.8	0.84	92	-	-	1.17
0.32	0.20	26.7	0.80	90	-	-	1.17
0.63	0.24	28.7	0.76	88	-	-	1.21
0.96	0.30	28.0	0.70	86	-	-	1.22
1.36	0.34	25.8	0.66	82	-	-	1.13
1.72	0.20	13.4	0.34	45	0.46	85	1.11
2.00	0.15	7.3	0.35	35	0.50	81	1.17

Table A18. Normalized preexponential factors and decay times retrieved from the analysis of the monomer fluorescence decays of Py(3.72)-SNPs quenched by trinitrotoluene in DMSO. λ_{ex}= 346 nm and λ_{em}= 375 nm.

[TNT] (mM)	a_1	τ_1 (ns)	a_2	τ_2 (ns)	a_3	τ_3 (ns)	χ^2
0.00	0.17	3.5	0.29	31	0.54	72	1.03
0.20	0.17	6.5	0.30	35	0.54	70	1.01
0.58	0.18	10.2	0.34	40	0.48	68	1.05
1.06	0.14	7.1	0.30	32	0.56	62	1.15
1.56	0.15	5.2	0.30	30	0.55	58	1.18
2.05	0.16	7.6	0.30	31	0.54	55	1.15

Table A19. Normalized preexponential factors and decay times retrieved from the analysis of the monomer fluorescence decays of Py(7.95)-SNPs quenched by trinitrotoluene in DMSO. λ_{ex}= 346 nm and λ_{em}= 375 nm.

[TNT] (mM)	a_1	τ_1 (ns)	a_2	τ_2 (ns)	a_3	τ_3 (ns)	χ^2
0.00	0.23	6.1	0.39	25.6	0.38	52	1.11
0.41	0.21	3.2	0.37	19.8	0.42	47	0.99
1.10	0.22	7.3	0.38	24.6	0.40	46	1.16
1.82	0.25	8.6	0.39	25.9	0.36	44	1.14
2.73	0.22	6.1	0.39	21.6	0.39	40	1.05
3.34	0.25	6.3	0.46	23.5	0.30	41	1.17

Quenching Studies Conducted in Water:

Table A20. Normalized preexponential factors and decay times retrieved from the analysis of the fluorescence decays of molecular pyrene quenched by nitromethane in water. λ_{ex}= 338 nm and λ_{em}= 375 nm.

[Nitromethane] (mM)	a_1	τ_1 (ns)	a_2	τ_2 (ns)	χ^2
0.00	0.21	16.5	0.80	132	1.16
0.65	0.25	20.4	0.75	94	1.24
1.74	0.27	16.7	0.72	55	1.06
3.00	0.22	10.9	0.78	36	1.15
4.60	0.21	9.7	0.79	26.8	1.20
6.55	0.24	9.3	0.76	20.9	1.07

Table A21. Normalized preexponential factors and decay times retrieved from the analysis of the monomer fluorescence decays of Py(0.06)-SNP quenched by nitromethane in water. λ_{ex}= 346 nm and λ_{em}= 375 nm.

[Nitromethane] (mM)	a_1	τ_1 (ns)	a_2	τ_2 (ns)	χ^2
0.00	0.15	51	0.85	142	1.09
0.55	0.26	48	0.74	123	1.03
1.65	0.29	46	0.71	117	1.07
3.31	0.35	44	0.66	107	1.09
5.30	0.38	33	0.62	88	1.13
7.47	0.42	25.8	0.58	73	1.16
9.75	0.44	20.4	0.56	61	1.07
11.98	0.46	16.5	0.54	53	1.15
14.37	0.51	15.5	0.49	46	1.21
16.60	0.52	13.6	0.49	42	1.02

Table A22. Normalized preexponential factors and decay times retrieved from the analysis of the monomer fluorescence decays of Py(2.65)-SNP quenched by nitromethane in water. λ_{ex}= 346 nm and λ_{em}= 375 nm.

[Nitromethane] (mM)	a_1	τ_1 (ns)	a_2	τ_2 (ns)	a_3	τ_3 (ns)	χ^2
0.00	0.21	8.7	0.31	50	0.48	116	1.13
0.69	0.24	6.8	0.31	46	0.44	104	1.11
1.33	0.22	5.7	0.33	42	0.44	95	1.07
1.96	0.23	4.8	0.33	38	0.44	88	1.19
3.13	0.20	5.4	0.39	36	0.41	80	1.11
4.90	0.25	3.2	0.33	24.6	0.43	64	1.10
7.01	0.22	4.6	0.39	26.1	0.39	58	1.16
9.33	0.30	2.4	0.34	20.6	0.36	51	1.18
11.84	0.25	5.3	0.46	24.3	0.29	50	1.19
14.25	0.29	5.5	0.46	24.4	0.25	47	1.11
16.69	0.27	3.7	0.41	18.5	0.31	40	1.19

Table A23. Normalized preexponential factors and decay times retrieved from the analysis of the excimer fluorescence decays of Py(2.65)-SNP quenched by nitromethane in water. λ_{ex}= 346 nm and λ_{em}= 510 nm.

[Nitromethane] (mM)	a_1	τ_1 (ns)	a_2	τ_2 (ns)	a_3	τ_3 (ns)	χ^2
0.00	0.44	5.4	0.37	54	0.19	98	1.07
0.69	0.43	5.5	0.34	51	0.23	93	1.11
1.33	0.44	5.1	0.31	49	0.25	88	1.05
1.96	0.43	5.1	0.29	46	0.29	84	1.11
3.13	0.46	5.2	0.32	48	0.23	84	1.15
4.90	0.43	5.7	0.34	45	0.24	80	1.02
7.01	0.45	4.9	0.28	40	0.26	73	1.07
9.33	0.45	4.9	0.29	38	0.26	72	1.11
11.84	0.44	4.9	0.30	36	0.25	69	1.17
14.25	0.48	5.0	0.31	35	0.24	67	1.14
16.69	0.46	4.8	0.32	34	0.22	66	1.11

Table A24. Normalized preexponential factors and decay times retrieved from the analysis of the monomer fluorescence decays of Py(8.65)-SNP quenched by nitromethane in water. λ_{ex}= 346 nm and λ_{em}= 375 nm.

[Nitromethane] (mM)	a_1	τ_1 (ns)	a_2	τ_2 (ns)	a_3	τ_3 (ns)	a_4	τ_4 (ns)	χ^2
0.00	0.54	1.4	0.22	10.6	0.16	37	0.08	90	1.11
0.81	0.48	4.8	0.33	25.6	0.19	68	-	-	1.00
2.17	0.47	4.8	0.37	25.4	0.16	62	-	-	1.08
4.04	0.46	4.6	0.39	23.3	0.15	57	-	-	1.15
6.70	0.50	3.4	0.37	19.8	0.13	51	-	-	1.20
9.65	0.51	4.6	0.40	21.8	0.09	54	-	-	1.03
12.78	0.48	4.1	0.40	18.7	0.12	47	-	-	1.19
15.64	0.50	4.4	0.41	18.9	0.10	47	-	-	1.14
18.27	0.54	4.7	0.40	20.3	0.06	52	-	-	1.15

Table A25. Normalized preexponential factors and decay times retrieved from the analysis of the excimer fluorescence decays of Py(8.65)-SNP quenched by nitromethane in water. λ_{ex}= 346 nm and λ_{em}= 510 nm.

[Nitromethane] (mM)	a_1	τ_1 (ns)	a_2	τ_2 (ns)	a_3	τ_3 (ns)	χ^2
0.00	0.50	5.1	0.30	43	0.20	87	1.09
0.81	0.50	5.1	0.27	40	0.22	82	1.24
2.17	0.51	5.4	0.30	44	0.19	84	1.11
4.04	0.50	4.8	0.26	36	0.25	77	1.11
6.70	0.51	5.2	0.29	40	0.20	79	1.10
9.65	0.51	5.1	0.29	40	0.19	78	1.14
12.78	0.51	5.0	0.25	35	0.24	71	1.07
15.64	0.51	4.9	0.27	35	0.22	71	1.17
18.27	0.53	4.7	0.27	34	0.20	70	1.11

Table A26. Normalized preexponential factors and decay times retrieved from the analysis of the monomer fluorescence decays of Py(10)-SNP quenched by nitromethane in water. λ_{ex}= 346 nm and λ_{em}= 375 nm.

[Nitromethane] (mM)	a_1	τ_1 (ns)	a_2	τ_2 (ns)	χ^2
0.00	0.34	29.7	0.14	91	1.09
0.67	0.30	24.6	0.13	73	1.16
1.87	0.31	25.6	0.11	67	1.12
3.70	0.35	24.1	0.09	64	1.10
5.81	-	-	-	-	-
8.23	0.34	20.7	0.06	61	1.20
10.25	0.37	18.4	0.08	54	1.21
12.26	0.37	19.9	0.06	59	1.01
14.30	0.37	18.5	0.07	55	1.12
20.77	0.36	17.9	0.05	54	1.19

Table A27. Normalized preexponential factors and decay times retrieved from the analysis of the excimer fluorescence decays of Py(10)-SNP quenched by nitromethane in water. λ_{ex}= 346 nm and λ_{em}= 510 nm.

[Nitromethane] (mM)	a_1	τ_1 (ns)	a_2	τ_2 (ns)	a_3	τ_3 (ns)	χ^2
0.00	0.52	5.1	0.28	40	0.21	86	1.12
0.67	0.53	5.5	0.30	45	0.17	90	1.12
1.87	0.53	5.0	0.29	43	0.17	88	1.12
3.70	0.52	5.2	0.22	82	0.26	38	1.13
5.81	-	-	-	-	-	-	-
8.23	0.56	5.3	0.27	40	0.17	82	1.08
10.25	0.53	5.2	0.26	37	0.21	76	1.01
12.26	0.54	4.7	0.24	33	0.22	74	1.11
14.30	0.53	5.4	0.28	38	0.19	77	1.02
20.77	0.54	5.0	0.27	35	0.20	73	1.05

Table A28. Normalized preexponential factors and decay times retrieved from the analysis of the monomer fluorescence decays of molecular pyrene quenched by nitrotoluene in water. λ_{ex}= 338 nm and λ_{em}= 375 nm.

[Nitrotoluene] (mM)	a_1	τ_1	a_2	τ_2	χ^2
0.00	0.25	16.1	0.75	134	0.99
0.03	0.25	16.4	0.75	133	1.12
0.09	0.25	16.9	0.75	132	1.10
0.17	0.25	15.9	0.75	131	1.03
0.27	0.26	16.3	0.74	130	1.12
0.38	0.27	16.2	0.73	129	1.02
0.50	0.27	16.2	0.73	127	1.14
0.63	0.27	15.9	0.73	125	1.13
0.75	0.28	16.3	0.72	124	1.08
0.87	0.27	15.7	0.73	122	1.05

Table A29. Normalized preexponential factors and decay times retrieved from the analysis of the monomer fluorescence decays of Py(0.06)-SNP quenched by nitrotoluene in water. λ_{ex}= 346 nm and λ_{em}= 375 nm.

[Nitrotoluene] (mM)	a_1	τ_1 (ns)	a_2	τ_2 (ns)	χ^2
0.00	0.13	46	0.87	142	0.99
0.03	0.15	47	0.86	142	1.12
0.05	0.15	52	0.85	142	0.98
0.08	0.14	46	0.86	140	1.11
0.11	0.16	46	0.84	140	0.97
0.15	0.17	52	0.83	141	1.14
0.19	0.16	50	0.84	138	1.12
0.24	0.16	47	0.84	137	1.12

Table A30. Normalized preexponential factors and decay times retrieved from the analysis of the monomer fluorescence decays of Py(2.65)-SNP quenched by nitrotoluene in water. λ_{ex}= 346 nm and λ_{em}= 375 nm.

[Nitrotoluene] (mM)	a_1	τ_1 (ns)	a_2	τ_2 (ns)	χ^2
0.00	0.18	58	0.82	113	1.06
0.01	0.16	53	0.84	110	1.07
0.02	0.15	49	0.85	108	0.96
0.05	0.19	54	0.81	109	1.10
0.08	0.15	48	0.85	106	1.09
0.11	0.13	39	0.87	104	0.96
0.14	0.15	44	0.86	102	1.11
0.17	0.14	39	0.86	101	1.05

Table A31. Normalized preexponential factors and decay times retrieved from the analysis of the excimer fluorescence decays of Py(2.65)-SNP quenched by nitrotoluene in water. λ_{ex}= 346 nm and λ_{em}= 510 nm.

[Nitrotoluene] (mM)	a_1	τ_1 (ns)	a_2	τ_2 (ns)	a_3	τ_3 (ns)	χ^2
0.00	0.53	5.4	0.22	41	0.22	89	1.10
0.01	0.55	5.6	0.28	49	0.17	99	1.18
0.02	0.57	5.3	0.24	46	0.19	92	1.13
0.05	0.56	5.3	0.23	44	0.21	90	1.07
0.08	0.56	5.4	0.21	41	0.24	87	1.02
0.11	0.54	4.8	0.23	41	0.23	87	1.06
0.14	0.54	5.0	0.25	43	0.22	89	1.08
0.17	0.54	4.6	0.22	39	0.24	86	1.21

Table A32. Normalized preexponential factors and decay times retrieved from the analysis of the monomer fluorescence decays of Py(8.65)-SNP quenched by nitrotoluene in water. λ_{ex}= 346 nm and λ_{em}= 375 nm.

[Nitrotoluene] (mM)	a_1	τ_1 (ns)	a_2	τ_2 (ns)	a_3	τ_3 (ns)	a_4	τ_4 (ns)	χ^2
0.00	0.47	1.9	0.24	8.6	0.16	35	0.13	96	1.14
0.01	0.48	1.6	0.23	7.0	0.17	30	0.13	93	0.99
0.04	0.45	1.7	0.25	7.5	0.17	32	0.14	93	1.01
0.06	0.15	5.5	0.67	7.8	0.10	28.3	0.08	90	1.07
0.11	0.48	1.6	0.19	7.3	0.18	28.7	0.15	90	1.05
0.13	0.54	1.2	0.20	6.9	0.14	31	0.12	90	1.09
0.16	0.82	0.5	0.09	6.1	0.05	30	0.04	90	1.23
0.19	0.44	2.1	0.22	10.3	0.18	34	0.17	91	1.02
0.22	0.42	2.2	0.20	9.0	0.20	31	0.18	89	1.16

Table A33. Normalized preexponential factors and decay times retrieved from the analysis of the excimer fluorescence decays of Py(8.65)-SNP quenched by nitrotoluene in water. λ_{ex}= 346 nm and λ_{em}= 510 nm.

[Nitrotoluene] (mM)	a_1	τ_1 (ns)	a_2	τ_2 (ns)	a_3	τ_3 (ns)	χ^2
0.00	0.50	5.1	0.27	41	0.23	82	1.16
0.01	0.48	4.7	0.27	38	0.24	81	1.06
0.04	0.50	4.7	0.26	38	0.24	79	1.10
0.06	0.48	5.0	0.31	41	0.20	80	1.02
0.11	0.49	4.5	0.27	35	0.24	78	1.08
0.13	0.51	4.3	0.26	35	0.23	77	0.91
0.16	0.50	4.7	0.27	35	0.23	77	1.15
0.19	0.51	4.6	0.26	34	0.23	75	1.16
0.00	0.50	4.5	0.27	33	0.23	75	1.01

Table A34. Normalized preexponential factors and decay times retrieved from the analysis of the monomer fluorescence decays of Py(10)-SNP quenched by nitrotoluene in water. λ_{ex}= 346 nm and λ_{em}= 375 nm.

[Nitrotoluene] (mM)	a_1	τ_1 (ns)	a_2	τ_2 (ns)	a_3	τ_3 (ns)	χ^2
0.00	0.26	13.8	0.15	41	0.07	95	1.16
0.01	0.25	10.3	0.19	33	0.09	92	1.19
0.02	0.20	6.4	0.13	27.0	0.06	86	1.08
0.04	0.25	9.6	0.18	33	0.08	92	1.02
0.06	0.26	11.5	0.17	36	0.09	93	1.08
0.09	0.26	11.6	0.15	35	0.09	90	1.03
0.12	0.25	12.2	0.16	35	0.10	89	1.13
0.15	0.26	10.1	0.16	35	0.08	92	1.02
0.18	0.25	9.3	0.18	31	0.10	86	1.08
0.22	0.25	12.3	0.15	34	0.10	86	1.05
0.25	-	-	-	-	-	-	-

Table A35. Normalized preexponential factors and decay times retrieved from the analysis of the excimer fluorescence decays of Py(10)-SNP quenched by nitrotoluene in water. λ_{ex}= 346 nm and λ_{em}= 510 nm.

[Nitrotoluene] (mM)	a_1	τ_1 (ns)	a_2	τ_2 (ns)	a_3	τ_3 (ns)	a_4	τ_4 (ns)	χ^2
0.00	0.30	3.0	0.25	8.5	0.30	49	0.14	94	1.10
0.01	0.41	3.9	0.16	12.4	0.32	52	0.11	97	1.04
0.02	0.47	4.7	0.14	21.3	0.33	59	0.06	108	1.05
0.04	0.03	5.4	0.53	5.4	0.29	40	0.22	83	1.14
0.06	0.36	2.6	0.23	9.1	0.27	46	0.14	88	1.11
0.09	0.51	5.2	0.30	40	0.19	85	-	-	1.11
0.12	0.35	4.8	0.87	4.8	0.28	36	0.20	80	1.17
0.15	0.52	4.9	0.29	38	0.19	82	-	-	1.15
0.18	0.53	4.8	0.29	37	-0.02	81	0.20	81	1.12
0.22	0.52	5.0	0.29	36	0.19	79	-	-	1.05
0.25	0.45	3.3	0.18	13.3	0.27	47	0.10	90	1.13

Table A36. Normalized preexponential factors and decay times retrieved from the analysis of the fluorescence decays of pyrene quenched by dinitrotoluene in water. λ_{ex}= 338 nm and λ_{em}= 375 nm.

[Dinitrotoluene] (mM)	a_1	τ_1 (ns)	a_2	τ_2 (ns)	χ^2
0.0	0.24	17.6	0.76	137	1.16
0.01	0.26	17.8	0.74	135	1.07
0.03	0.25	16.9	0.75	134	1.10
0.05	0.25	16.8	0.75	132	1.06
0.08	0.25	18.1	0.75	131	1.15
0.12	0.28	19.3	0.72	131	1.12
0.16	0.28	17.1	0.72	128	1.03
0.20	0.31	18.4	0.69	127	1.05

Table A37. Normalized preexponential factors and decay times retrieved from the analysis of the monomer fluorescence decays of Py(0.06)-SNPs quenched by dinitrotoluene in water. λ_{ex}= 346 nm and λ_{em}= 375 nm.

[Dinitrotoluene] (mM)	a_1	τ_1 (ns)	a_2	τ_2 (ns)	χ^2
0.00	0.15	57	0.85	146	1.05
0.003	0.16	58	0.84	146	1.06
0.01	0.14	44	0.86	143	1.13
0.02	0.16	54	0.84	143	1.20
0.03	0.16	47	0.84	142	1.13
0.05	0.17	47	0.83	142	1.10
0.06	0.17	47	0.83	141	1.06
0.07	0.18	49	0.82	141	1.23
0.08	0.18	47	0.82	140	1.13
0.09	0.16	42	0.83	138	1.13

Table A38. Normalized preexponential factors and decay times retrieved from the analysis of the monomer fluorescence decays of Py(2.65)-SNPs quenched by dinitrotoluene in water. λ_{ex}= 346 nm and λ_{em}= 375 nm.

[Dinitrotoluene] (mM)	a_1	τ_1 (ns)	a_2	τ_2 (ns)	a_3	τ_3 (ns)	χ^2
0.00	0.22	7.7	0.31	49	0.47	116	1.09
0.003	0.23	6.5	0.28	46	0.49	115	1.04
0.01	0.22	7.3	0.29	47	0.49	116	1.17
0.02	0.23	8.0	0.29	49	0.48	116	1.25
0.03	0.22	7.6	0.30	50	0.48	116	1.11
0.03	0.22	6.0	0.29	47	0.49	115	1.02
0.05	0.23	7.7	0.29	50	0.48	115	1.07
0.06	0.21	7.1	0.29	47	0.50	112	1.04
0.07	0.21	6.5	0.31	48	0.49	114	1.07
0.08	0.21	8.5	0.30	50	0.49	114	1.10

Table A39. Normalized preexponential factors and decay times retrieved from the analysis of the excimer fluorescence decays of Py(2.65)-SNPs quenched by dinitrotoluene in water. λ_{ex}= 346 nm and λ_{em}= 510 nm.

[Dinitrotoluene] (mM)	a_1	τ_1 (ns)	a_2	τ_2 (ns)	a_3	τ_3 (ns)	χ^2
0.000	0.44	5.1	0.29	49	0.27	91	0.95
0.003	0.44	5.0	0.29	48	0.27	91	1.06
0.008	0.45	5.0	0.34	52	0.22	95	1.03
0.016	0.46	4.9	0.31	50	0.24	93	1.06
0.025	0.43	5.0	0.29	48	0.28	90	1.13
0.034	0.43	5.3	0.35	52	0.23	95	1.01
0.045	0.43	4.9	0.33	49	0.25	92	1.06
0.056	0.43	4.7	0.33	50	0.24	93	1.11
0.068	0.42	5.0	0.33	50	0.25	92	1.04
0.081	0.41	5.1	0.35	51	0.24	92	1.07

Table A40. Normalized preexponential factors and decay times retrieved from the analysis of the monomer fluorescence decays of Py(8.65)-SNPs quenched by dinitrotoluene in water. λ_{ex}= 346 nm and λ_{em}= 375 nm.

[Dinitrotoluene] (mM)	a_1	τ_1 (ns)	a_2	τ_2 (ns)	a_3	τ_3 (ns)	χ^2
0.000	0.45	12.4	0.38	39	0.17	92	1.13
0.002	0.48	12.9	0.37	41	0.15	96	1.03
0.007	0.44	12.1	0.37	36	0.19	89	1.03
0.014	0.60	17.9	0.35	62	0.05	122	1.15
0.023	0.39	9.3	0.40	32	0.21	86	1.08
0.033	0.44	11.2	0.38	38	0.18	91	1.06
0.043	0.62	20.2	0.36	68	0.03	145	1.13
0.054	0.44	9.7	0.37	35	0.19	87	0.98
0.065	0.42	12.2	0.38	36	0.21	88	0.90
0.075	-	-	-	-	-	-	-

Table A41. Normalized preexponential factors and decay times retrieved from the analysis of the excimer fluorescence decays of Py(8.65)-SNPs quenched by dinitrotoluene in water. λ_{ex}= 346 nm and λ_{em}= 510 nm.

[Dinitrotoluene] (mM)	a_1	τ_1 (ns)	a_2	τ_2 (ns)	a_3	τ_3 (ns)	χ^2
0.000	0.49	5.5	0.32	46	0.19	91	1.17
0.002	0.50	5.3	0.28	42	0.23	86	1.13
0.007	0.50	5.7	0.32	47	0.18	90	1.27
0.014	0.50	5.2	0.32	45	0.18	89	1.14
0.023	0.50	4.8	0.30	42	0.20	87	1.10
0.033	0.50	4.8	0.27	38	0.23	82	1.06
0.043	0.51	5.1	0.31	43	0.18	87	1.10
0.054	0.50	4.7	0.29	38	0.22	82	1.12
0.065	0.50	4.9	0.30	39	0.21	83	1.12
0.075	0.51	4.8	0.29	39	0.20	82	1.22

Table A42. Normalized preexponential factors and decay times retrieved from the analysis of the monomer fluorescence decays of Py(10)-SNPs quenched by dinitrotoluene in water. λ_{ex}= 346 nm and λ_{em}= 375 nm.

[Dinitrotoluene] (mM)	a_1	τ_1 (ns)	a_2	τ_2 (ns)	a_3	τ_3 (ns)	χ^2
0.000	0.53	11.8	0.34	37	0.14	97	1.10
0.003	0.45	8.0	0.39	27	0.16	88	0.96
0.005	0.51	11.4	0.35	35	0.14	97	1.01
0.009	0.49	12.1	0.35	34	0.17	94	1.10
0.016	0.56	12.9	0.30	40	0.14	98	1.12
0.024	0.47	8.3	0.37	28	0.17	88	1.07
0.033	0.52	11.8	0.31	34	0.17	91	1.06
0.044	0.53	12.4	0.33	38	0.15	98	1.04
0.054	0.54	12.0	0.31	38	0.15	95	1.00
0.065	0.52	11.9	0.33	37	0.15	96	1.07

Table A43. Normalized preexponential factors and decay times retrieved from the analysis of the excimer fluorescence decays of Py(10)-SNPs quenched by dinitrotoluene in water. λ_{ex}= 346 nm and λ_{em}= 510 nm.

[Dinitrotoluene] (mM)	a_1	τ_1 (ns)	a_2	τ_2 (ns)	a_3	τ_3 (ns)	χ^2
0.000	0.35	8.1	0.46	48	0.21	93	0.98
0.003	0.39	9.7	0.43	50	0.18	94	1.00
0.005	0.37	10.8	0.48	52	0.15	97	1.04
0.009	0.37	10.1	0.45	49	0.18	93	1.15
0.016	0.34	9.6	0.40	45	0.24	86	1.04
0.024	0.37	8.9	0.42	45	0.21	87	1.04
0.033	0.36	9.9	0.45	47	0.19	89	1.04
0.044	0.42	8.1	0.40	44	0.18	87	1.00
0.054	0.35	9.6	0.42	42	0.23	84	1.16
0.065	-	-	-	-	-	-	-

Table A44. Normalized preexponential factors and decay times retrieved from the analysis of the monomer fluorescence decays of Py(3.7)-SNPs quenched by trinitrotoluene in water. λ_{ex}= 346 nm and λ_{em}= 375 nm.

[TNT] (μM)	a_1	τ_1 (ns)	a_2	τ_2 (ns)	a_3	τ_3 (ns)	χ^2
0.0	0.23	6.0	0.26	38	0.50	101	1.481
0.2	0.22	6.1	0.27	37	0.52	101	1.181
0.4	0.22	5.1	0.28	37	0.50	101	1.093
0.9	0.22	8.5	0.29	46	0.49	103	1.157
1.4	0.22	9.6	0.27	44	0.51	102	1.157
2.2	0.21	7.4	0.29	43	0.50	102	1.023
3.0	0.21	5.8	0.29	39	0.50	101	1.121
3.9	0.21	6.8	0.29	41	0.50	101	1.129
4.9	0.17	8.1	0.28	38	0.55	100	1.047
5.8	0.20	6.2	0.28	38	0.52	100	1.095
6.6	0.21	7.2	0.27	41	0.52	100	1.097
7.6	0.20	5.6	0.27	36	0.54	98	1.193

Table A45. Normalized preexponential factors and decay times retrieved from the analysis of the excimer fluorescence decays of Py(3.7)-SNPs quenched by trinitrotoluene in water. λ_{ex}= 346 nm and λ_{em}= 510 nm.

[TNT] (μM)	a_1	τ_1 (ns)	a_2	τ_2 (ns)	a_3	τ_3 (ns)	χ^2
0.00	0.39	5.7	0.38	54	0.23	96	1.09
0.16	0.40	5.2	0.33	50	0.27	92	1.02
0.41	0.39	5.3	0.32	48	0.29	90	1.10
0.86	0.39	5.3	0.36	51	0.25	94	1.32
1.44	0.38	5.8	0.35	50	0.27	92	1.25
2.19	0.37	5.6	0.33	48	0.29	90	1.21
3.03	0.37	5.7	0.35	49	0.27	91	1.19
3.91	0.38	5.5	0.31	46	0.31	87	0.96
4.87	0.37	5.3	0.32	45	0.31	87	1.15
5.79	0.38	5.8	0.38	50	0.25	91	1.12
6.64	0.37	5.6	0.35	48	0.27	89	1.13
7.64	0.36	6.0	0.37	49	0.27	89	1.03

Table A46. Normalized preexponential factors and decay times retrieved from the analysis of the monomer fluorescence decays of Py(6.00)-SNPs quenched by trinitrotoluene in water. λ_{ex}= 346 nm and λ_{em}= 375 nm.

[TNT] (μM)	a_1	τ_1 (ns)	a_2	τ_2 (ns)	a_3	τ_3 (ns)	χ^2
0.00	0.36	6.0	0.38	38	0.27	98	1.26
0.13	0.34	8.0	0.38	40	0.28	100	1.08
0.45	0.32	6.0	0.38	35	0.30	97	1.09
0.80	0.32	6.4	0.37	36	0.30	97	1.08
1.51	0.30	6.6	0.38	36	0.32	97	1.06
2.25	0.31	7.3	0.40	40	0.29	100	1.17
3.05	0.30	6.4	0.37	35	0.33	96	1.12
3.87	0.31	6.3	0.38	38	0.31	98	1.05
4.63	0.30	7.3	0.37	38	0.33	98	1.08
5.36	0.30	6.6	0.37	36	0.33	97	1.14
6.15	0.30	6.5	0.38	37	0.33	98	1.13

Table A47. Normalized preexponential factors and decay times retrieved from the analysis of the excimer fluorescence decays of Py(6.00)-SNPs quenched by trinitrotoluene in water. λ_{ex}= 346 nm and λ_{em}= 510 nm.

[TNT] (μM)	a_1	τ_1 (ns)	a_2	τ_2 (ns)	a_3	τ_3 (ns)	χ^2
0.00	0.40	5.6	0.33	46	0.27	90	1.13
0.13	0.40	5.6	0.37	49	0.23	93	1.07
0.45	0.41	5.5	0.40	52	0.18	98	1.16
0.80	0.40	5.5	0.34	46	0.27	89	1.19
1.51	0.41	5.6	0.38	49	0.21	93	1.08
2.25	0.38	5.4	0.34	44	0.28	86	1.06
3.05	0.39	5.3	0.36	46	0.25	88	1.15
3.87	0.38	5.6	0.37	45	0.25	88	1.04
4.63	0.38	5.4	0.37	46	0.24	87	1.00
5.36	0.37	5.8	0.36	44	0.25	86	1.07
6.15	0.37	5.2	0.36	42	0.27	84	1.09

Table A48. Normalized preexponential factors and decay times retrieved from the analysis of the monomer fluorescence decays of Py(7.9)-SNPs quenched by trinitrotoluene in water. λ_{ex}= 346 nm and λ_{em}= 375 nm.

[TNT] (μM)	a_1	τ_1 (ns)	a_2	τ_2 (ns)	a_3	τ_3 (ns)	χ^2
0.00	0.44	5.1	0.30	31	0.26	96	1.15
0.19	0.42	4.6	0.31	28.7	0.27	96	1.12
0.56	0.44	4.1	0.30	28.4	0.26	96	1.12
1.09	0.41	4.0	0.31	27.4	0.29	96	1.21
1.76	0.39	4.7	0.31	28.5	0.30	96	1.13
2.53	0.48	4.3	0.30	27.1	0.31	95	1.08
3.37	0.37	4.5	0.31	28.1	0.32	96	1.07
4.20	0.35	5.4	0.31	29.9	0.33	98	1.18
5.06	0.33	5.1	0.32	29.0	0.35	97	0.99
5.88	0.32	5.1	0.32	29.3	0.37	96	1.09
6.71	0.33	6.6	0.30	31	0.38	97	1.08

Table A49. Normalized preexponential factors and decay times retrieved from the analysis of the excimer fluorescence decays of Py(7.9)-SNPs quenched by trinitrotoluene in water. λ_{ex}= 346 nm and λ_{em}= 510 nm.

[TNT] (μM)	a_1	τ_1 (ns)	a_2	τ_2 (ns)	a_3	τ_3 (ns)	a_4	τ_4 (ns)	χ^2
0.00	0.34	3.6	0.17	13.7	0.34	54	0.14	98	1.14
0.19	0.40	3.9	0.14	17.0	0.35	57	0.12	101	1.08
0.56	0.41	4.8	0.09	18.5	0.31	49	0.19	91	1.20
1.09	0.37	4.2	0.15	15.0	0.36	56	0.12	99	1.06
1.76	0.32	3.2	0.20	10.6	0.31	48	0.18	90	1.10
2.53	0.36	3.1	0.18	12.9	0.35	53	0.10	100	1.11
3.37	0.37	3.3	0.17	12.6	0.30	47	0.16	89	1.08
4.20	0.38	4.1	0.15	14.7	0.33	49	0.14	91	1.01
5.06	0.38	3.7	0.17	14.7	0.34	50	0.12	93	1.22
5.88	0.38	3.0	0.20	12.9	0.30	47	0.12	89	1.09
6.71	0.37	3.8	0.17	14.2	0.31	45	0.15	86	1.19

Table A50. Steady state (SS) spectra and Stern-Volmer plots of F_0/F (●) and τ_0/τ (○) as a function of [NM] for quenching studies conducted in DMSO.

Sample	Molecular Pyrene	Py(0.06)-SNP	Py(2.65)-SNP	Py(8.0)-SNP	Py(10)-SNP
SS spectra	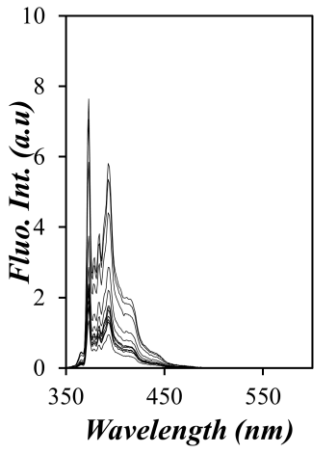	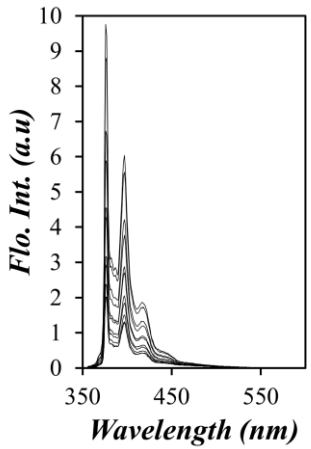	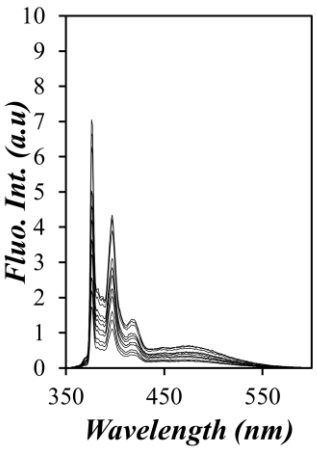	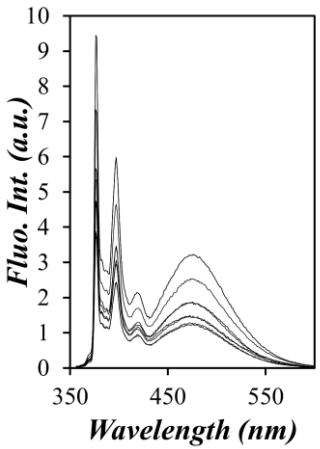	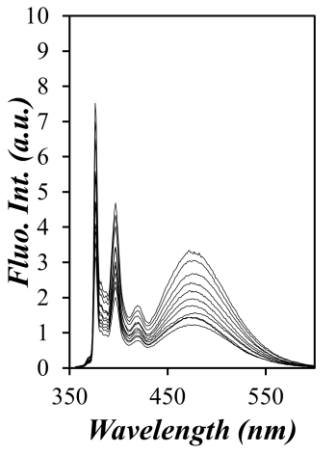

TRF decays	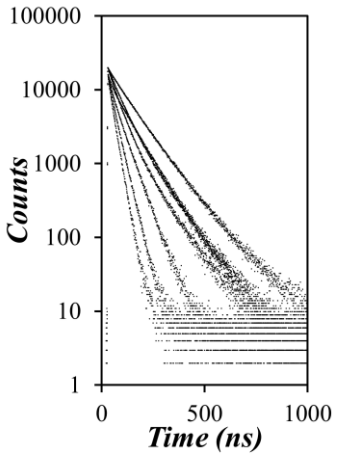	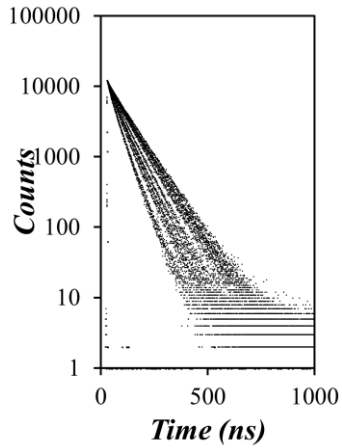	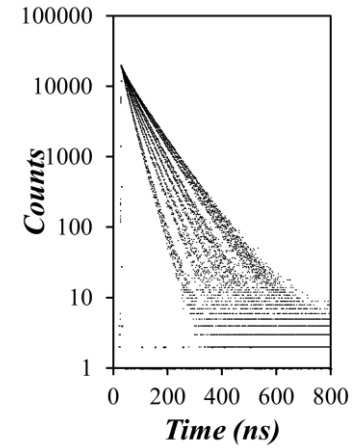	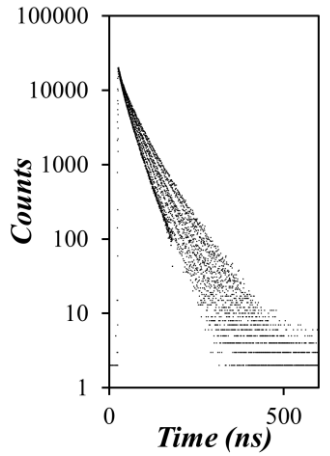	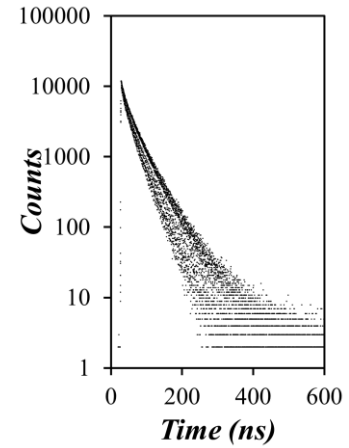
S-V plot	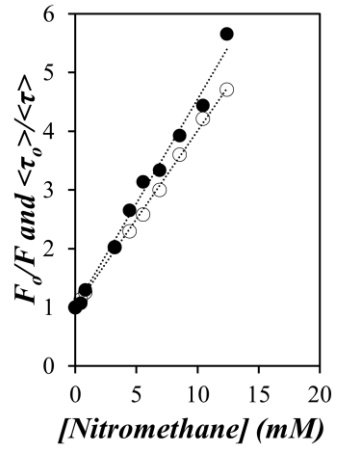	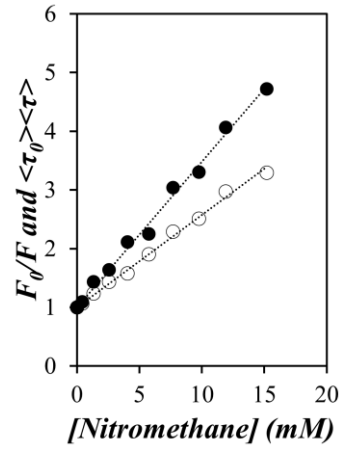	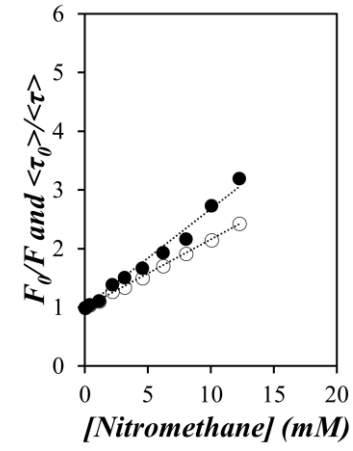	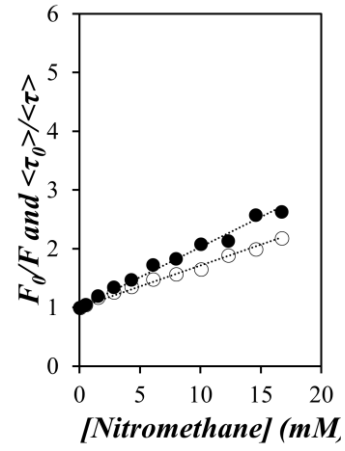	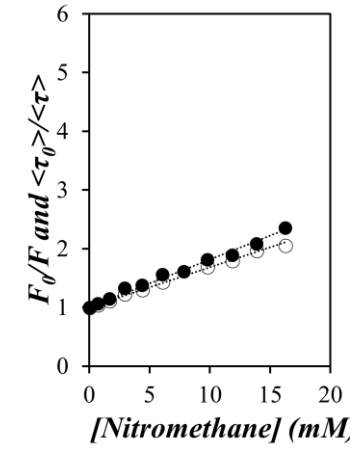

Table A51. Steady state (SS) spectra, time-resolved fluorescence decays, and Stern-Volmer plots of F_0/F (●) and τ_0/τ (○) as a function of [MNT] for quenching studies conducted in DMSO.

Sample	Molecular Pyrene	Py(0.06)-SNP	Py(2.65)-SNP	Py(8.0)-SNP	Py(10)-SNP
SS spectra	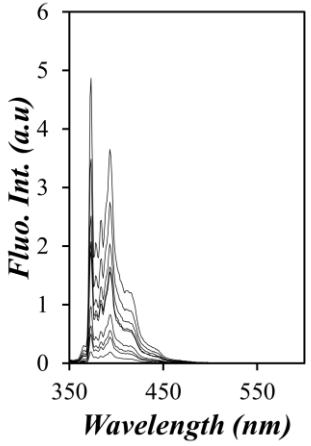	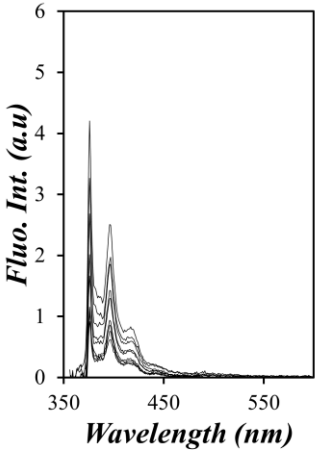	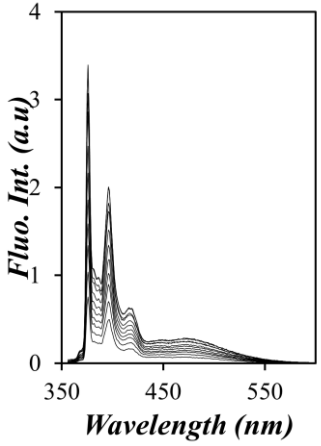	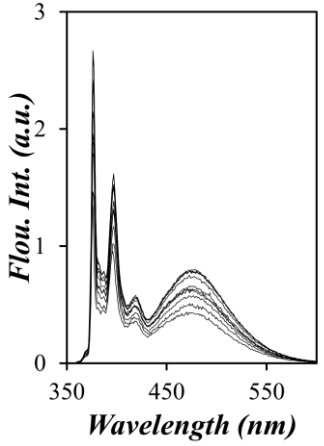	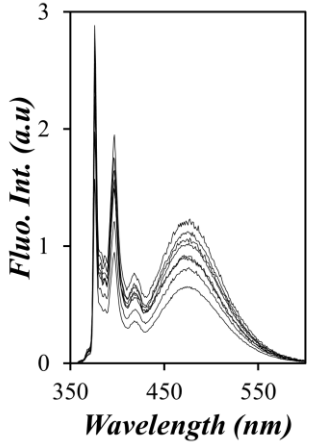

TRF decays	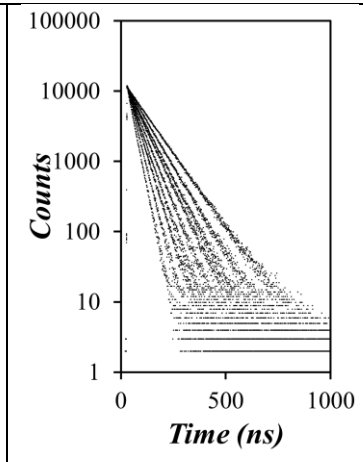	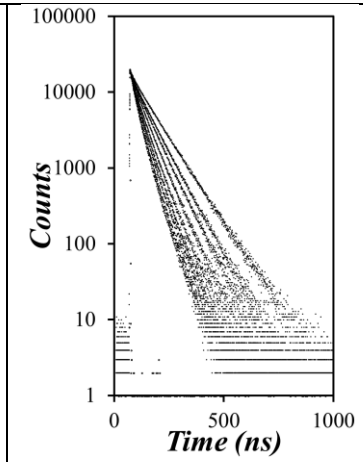	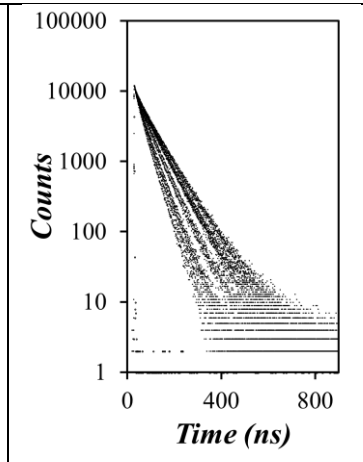	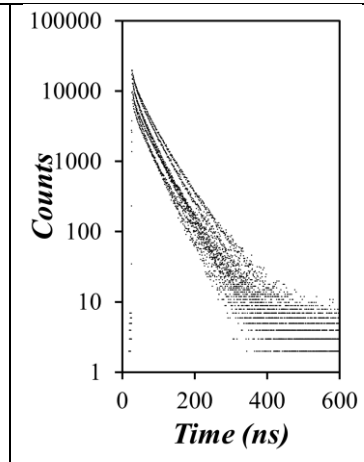	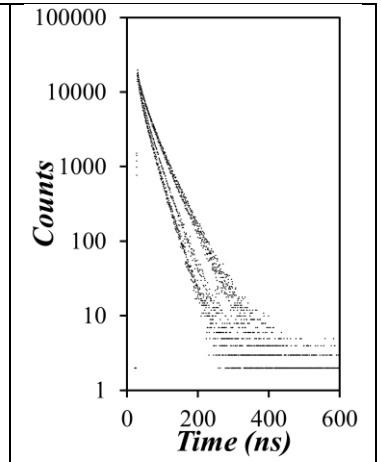
S-V plot	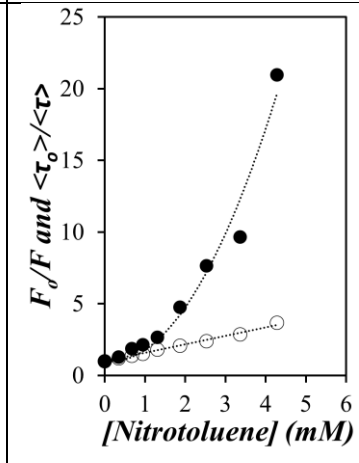	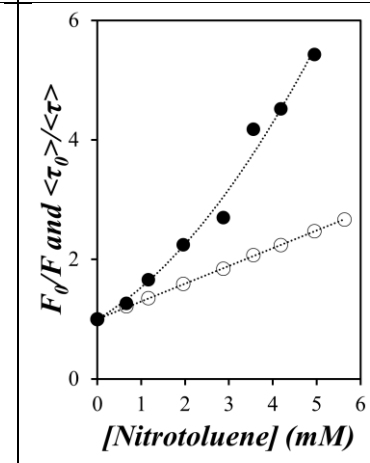	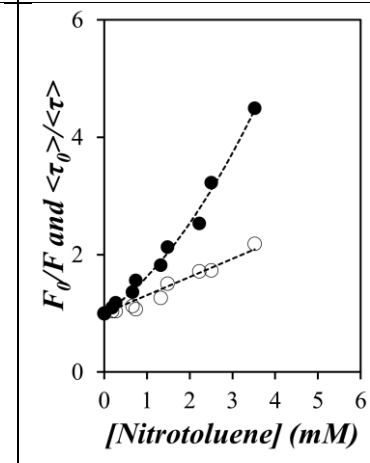	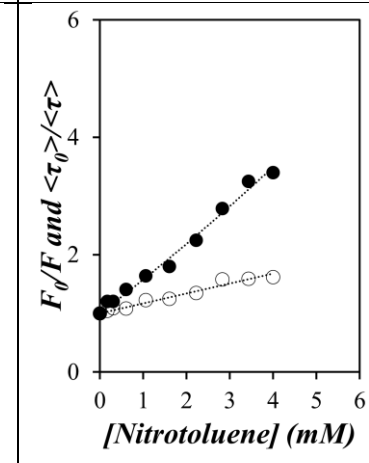	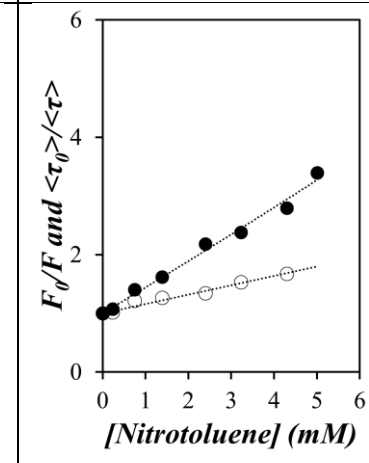

Table A52. Steady state (SS) spectra, time-resolved fluorescence decays, and Stern-Volmer plots of F_0/F (●) and τ_0/τ (○) as a function of [DNT] for quenching studies conducted in DMSO.

Sample	Molecular Pyrene	Py(0.06)-SNP	Py(2.65)-SNP	Py(8.0)-SNP	Py(10)-SNP
SS spectra	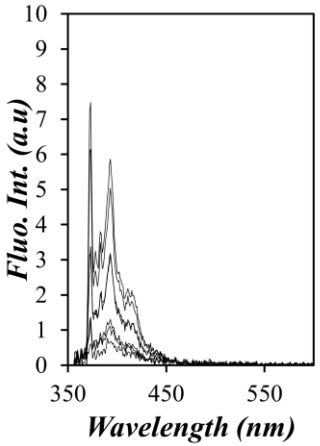	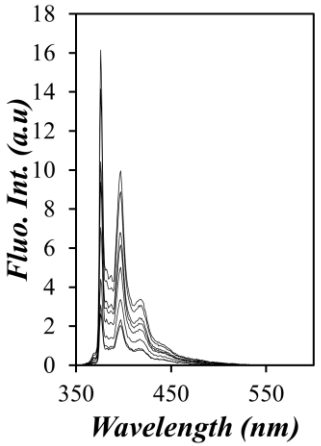	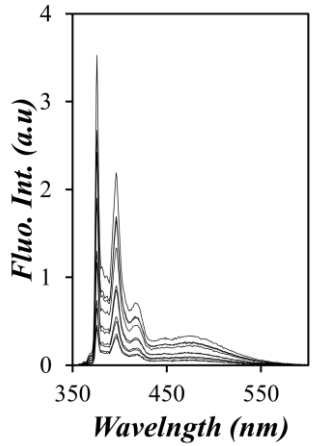	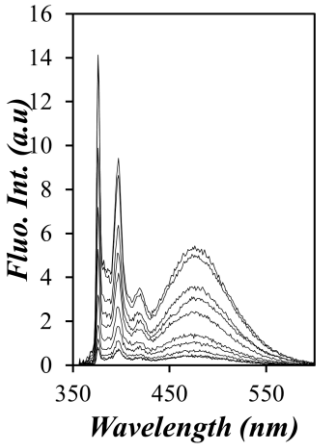	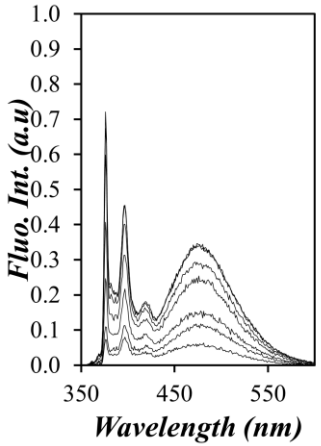
TRF decays	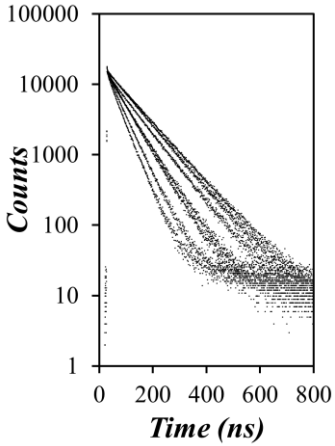	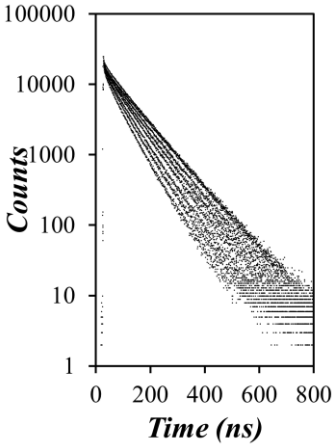	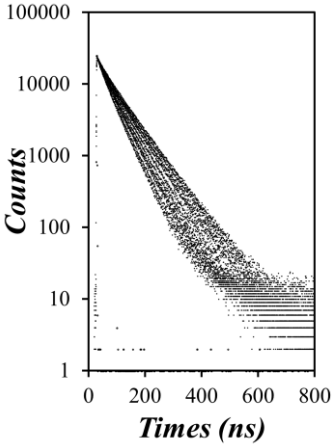	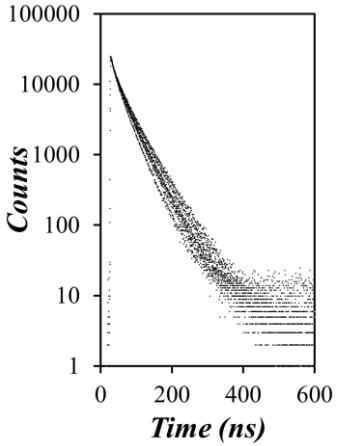	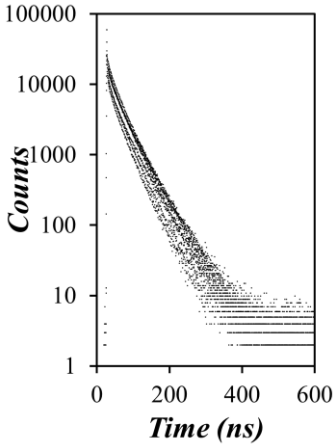

S-V plot	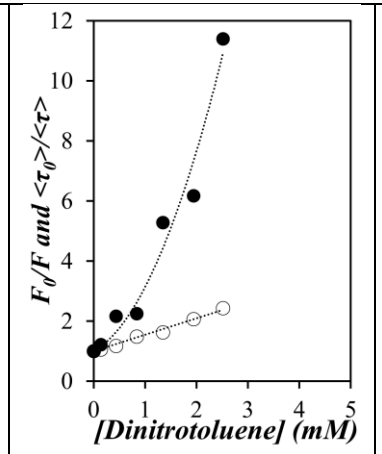 F_0/F and $<\tau_0>/<\tau>$ [Dinitrotoluene] (mM)	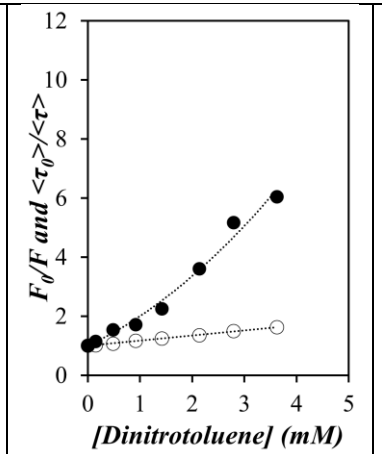 F_0/F and $<\tau_0>/<\tau>$ [Dinitrotoluene] (mM)	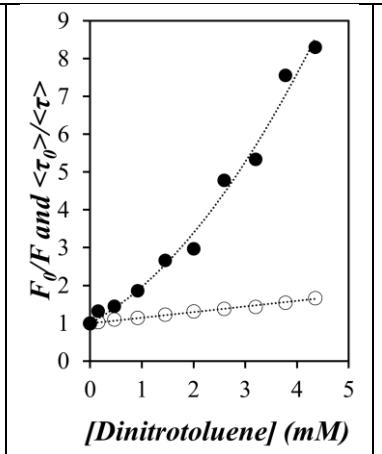 F_0/F and $<\tau_0>/<\tau>$ [Dinitrotoluene] (mM)	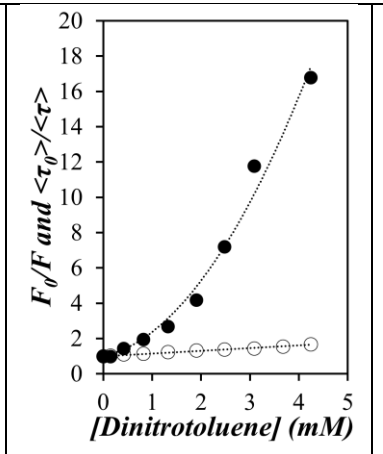 F_0/F and $<\tau_0>/<\tau>$ [Dinitrotoluene] (mM)	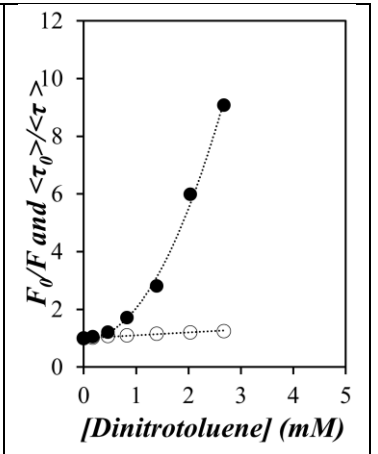 F_0/F and $<\tau_0>/<\tau>$ [Dinitrotoluene] (mM)

Table A53. Steady state (SS) spectra, time-resolved fluorescence decays, and Stern-Volmer plots of F_0/F (●) and τ_0/τ (○) as a function of [TNT] for quenching studies conducted in DMSO.

Sample	Py(0.06)SNP	Py(3.7)-SNP	Py(7.9)-SNP
SS spectra	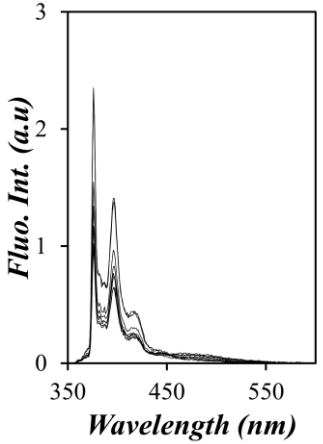	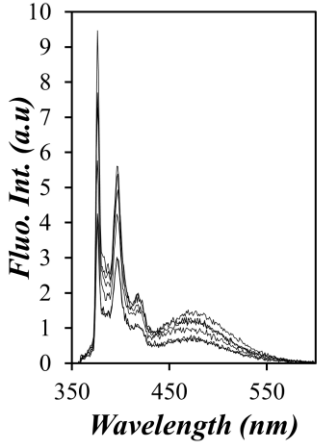	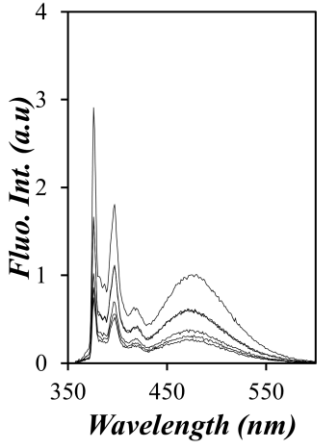
TRF decay 375 nm	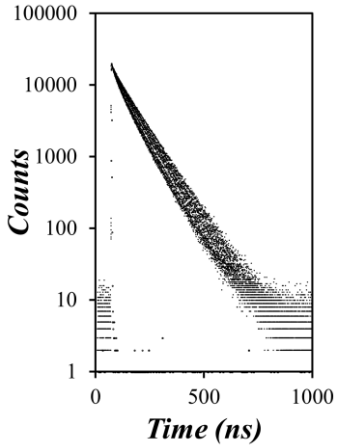	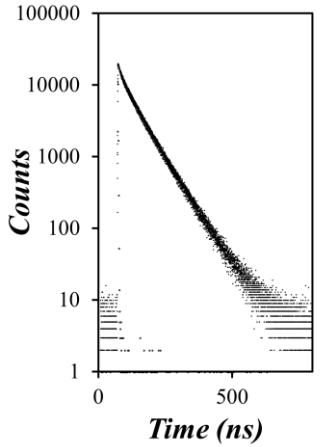	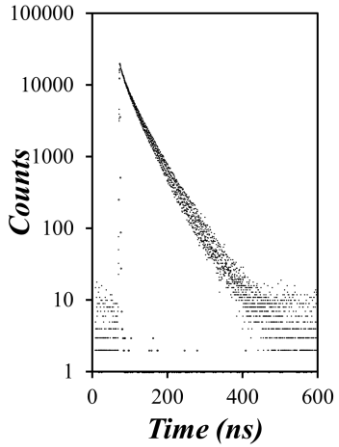

S-V plot at 375 nm	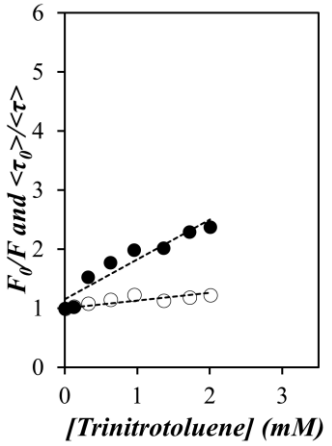	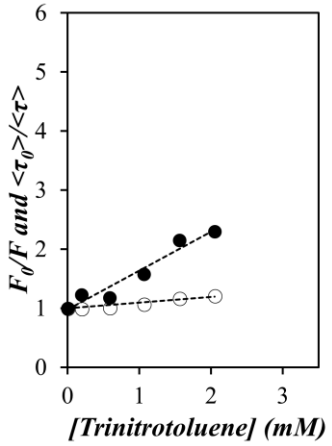	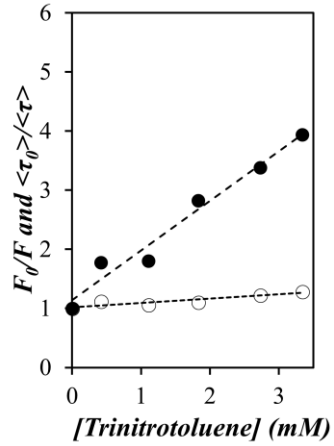

Table A54. Steady state (SS) spectra, time-resolved fluorescence decays, and Stern-Volmer plots of F_0/F (●) and τ_0/τ (○) as a function of [NM] for quenching studies conducted in milliQ water.

Sample	Molecular Pyrene	Py(0.06)-SNP	Py(2.65)-SNP	Py(8.0)-SNP	Py(10)-SNP
SS spectra	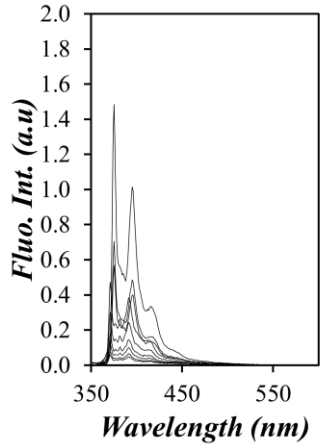	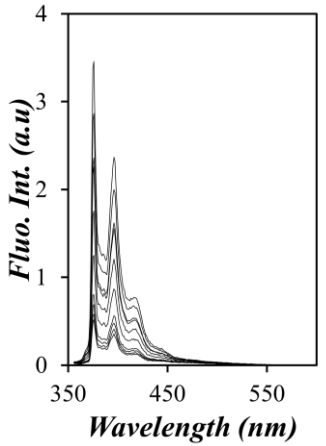	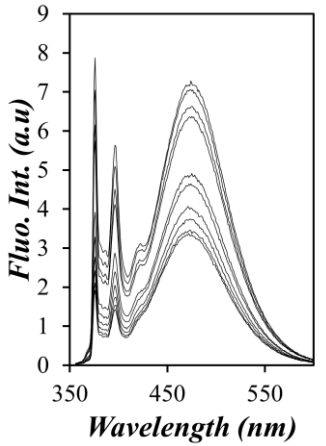	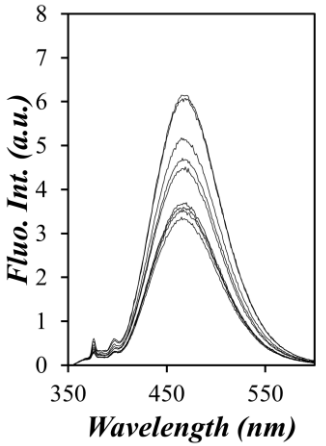	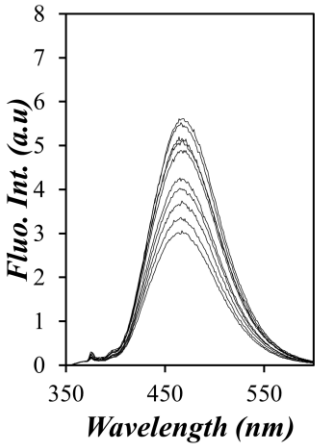
TRF decays	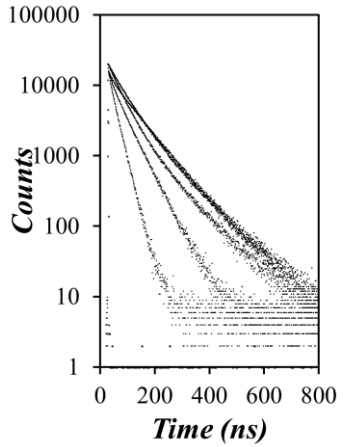	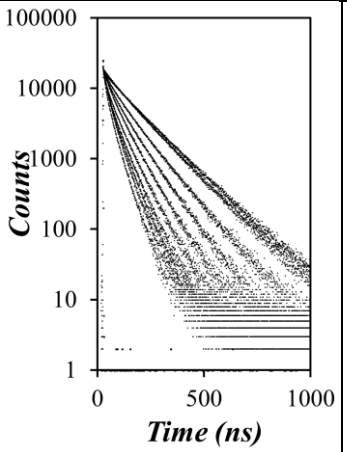	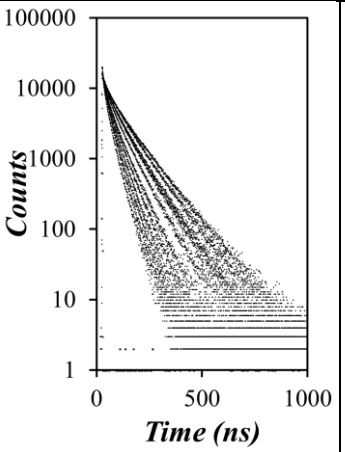	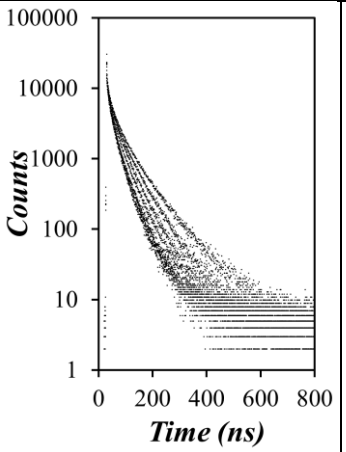	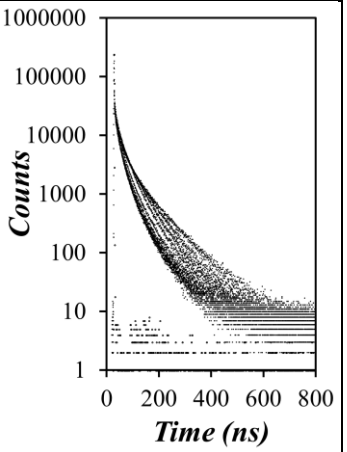

S-V plot	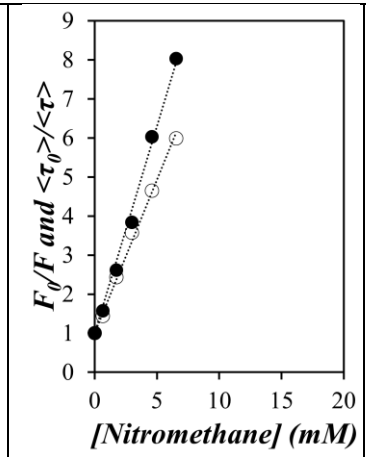	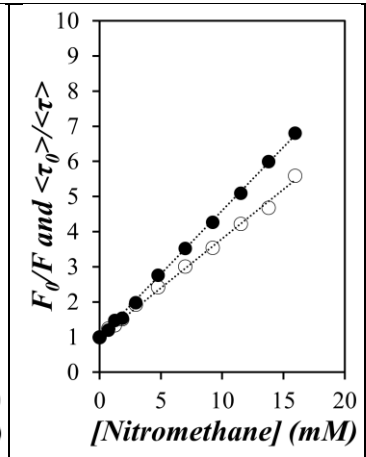	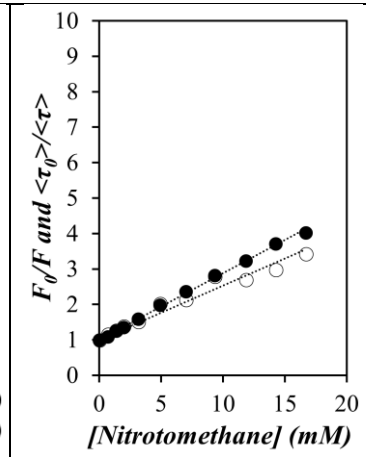	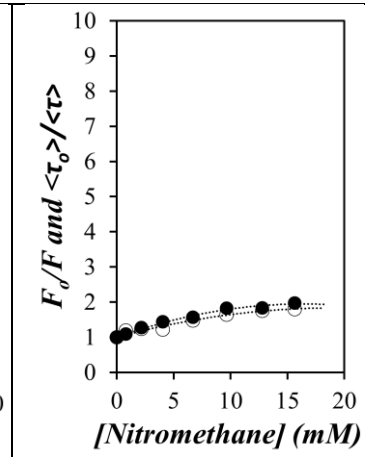	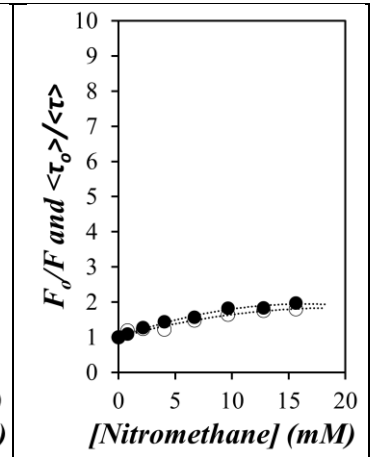
Modified S-V plot	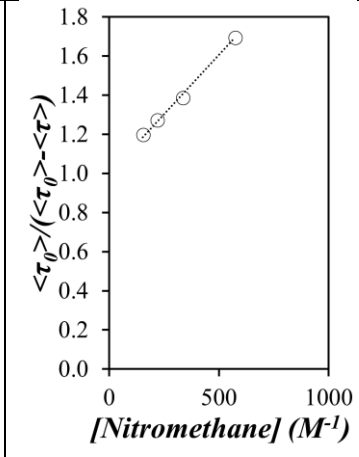	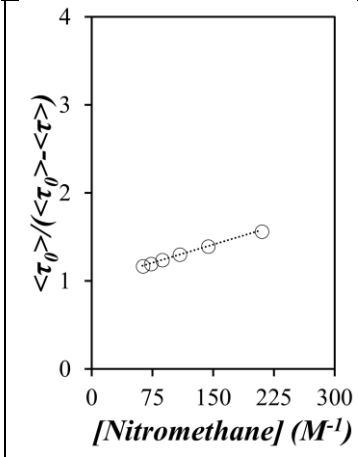	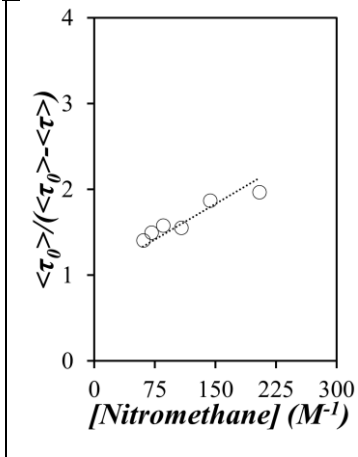	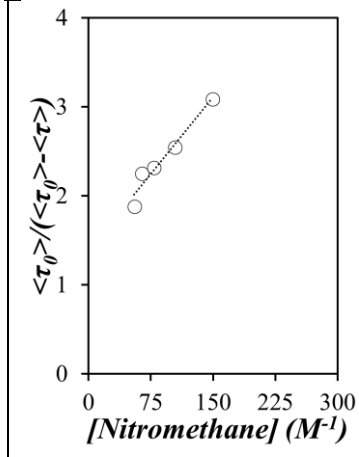	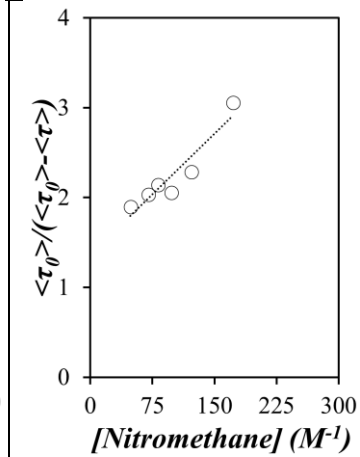

Table A55. Steady state (SS) spectra, time-resolved fluorescence decays, and Stern-Volmer plots of F_0/F (●) and τ_0/τ (○) as a function of [MNT] for quenching studies conducted in milliQ water.

Sample	Molecular Pyrene	Py(0.06)-SNP	Py(2.65)-SNP	Py(8.0)-SNP	Py(10)-SNP
SS spectra	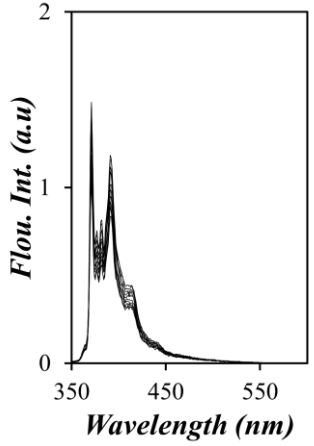	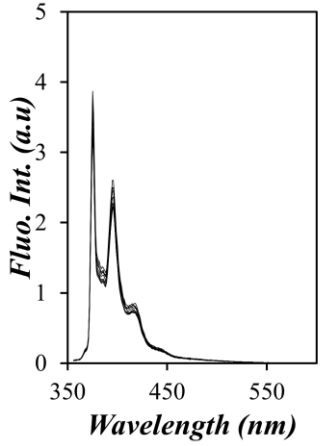	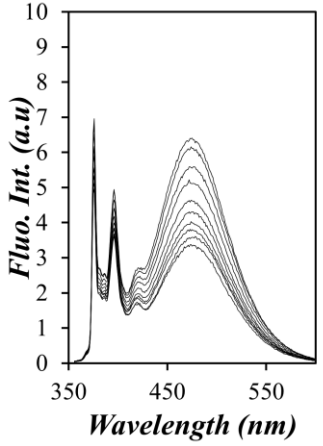	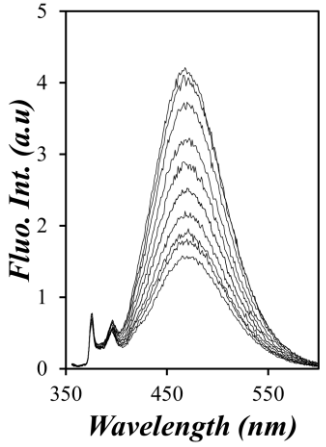	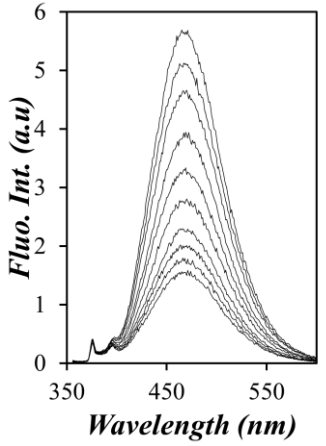
TRF decay at 375 nm	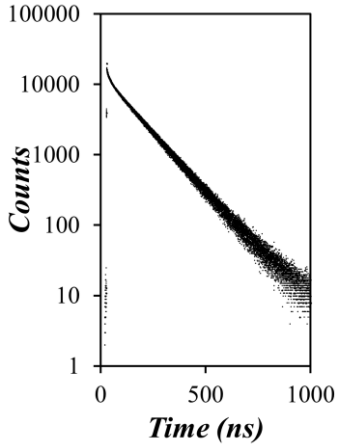	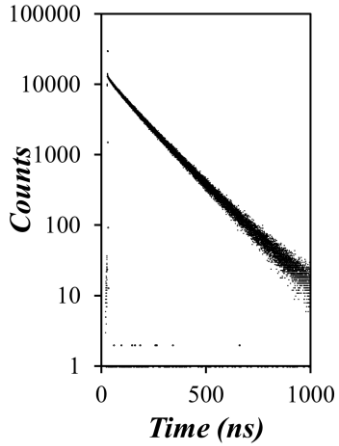	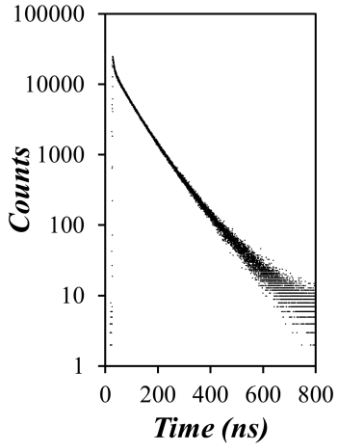	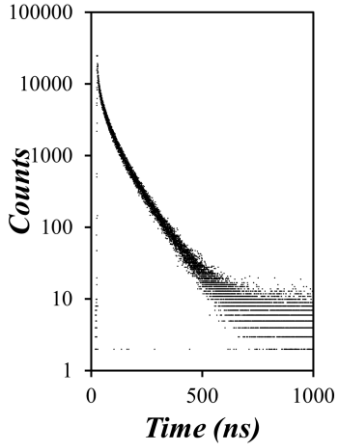	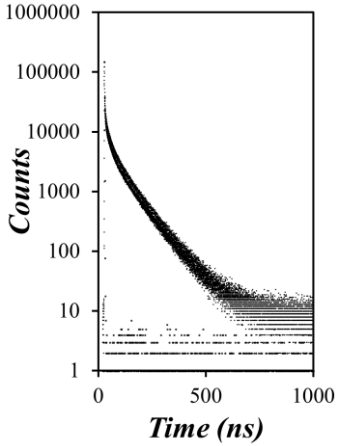

TRF decay at 510 nm			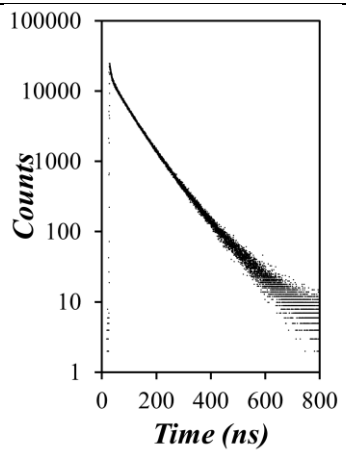	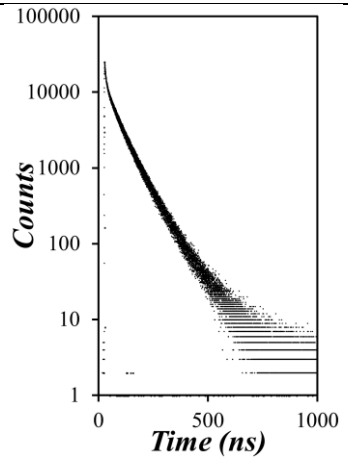	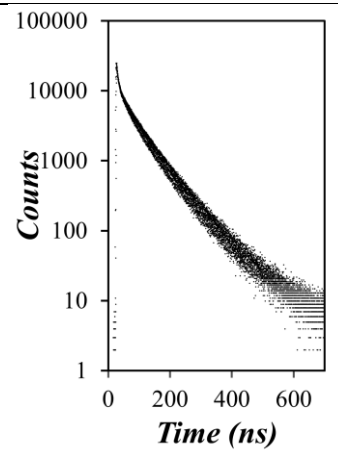
S-V plot at 375 nm	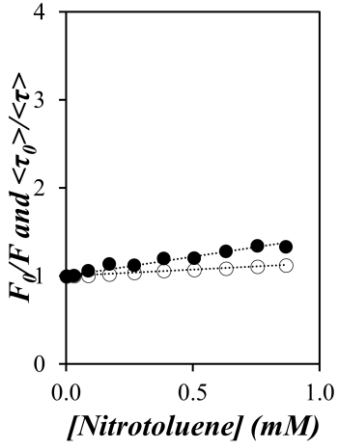	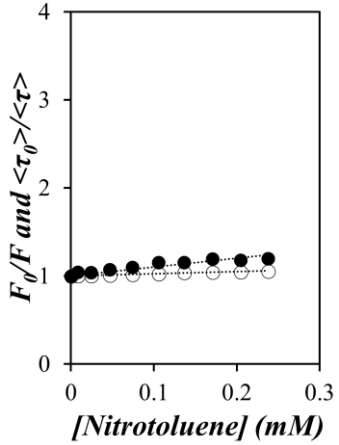	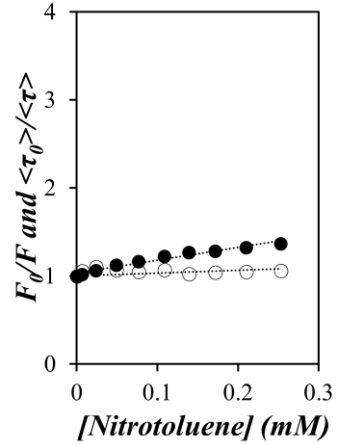	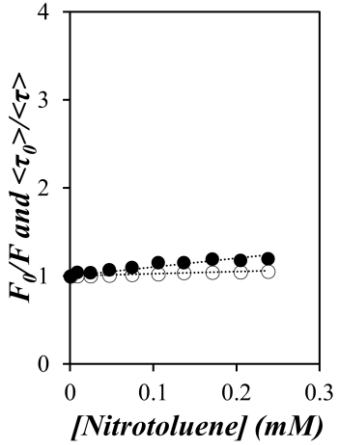	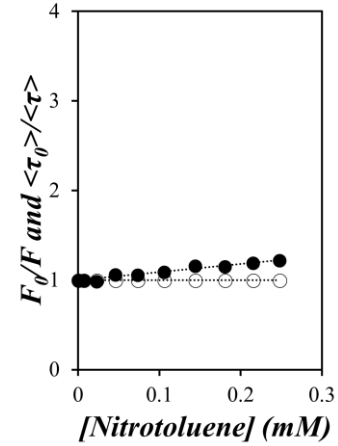

S-V plot at 510 nm			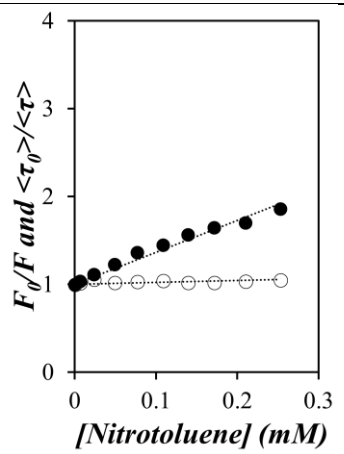	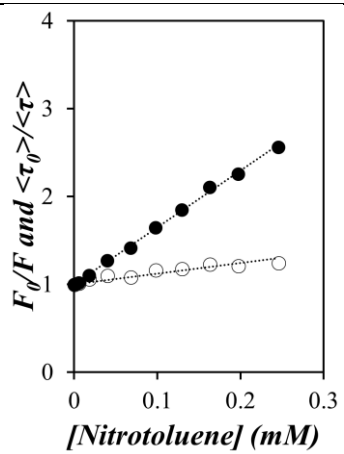	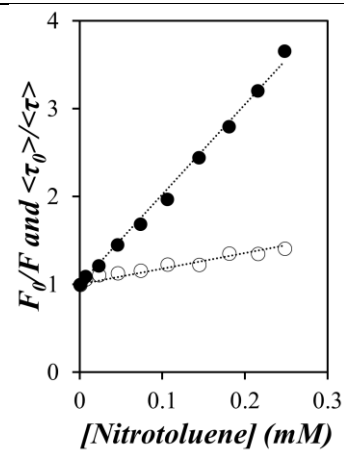

Table A56. Steady state (SS) spectra, time-resolved fluorescence decays, and Stern-Volmer plots of F_0/F (●) and τ_0/τ (○) as a function of [DNT] for quenching studies conducted in milliQ water.

Sample	Molecular Pyrene	Py(0.06)-SNP	Py(2.65)-SNP	Py(8.0)-SNP	Py(10)-SNP
SS spectra	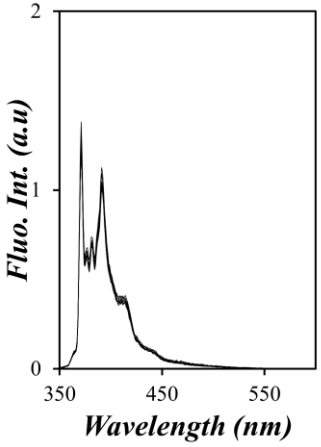	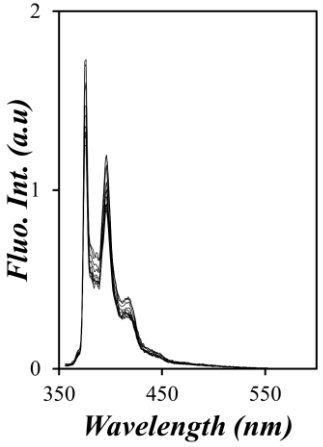	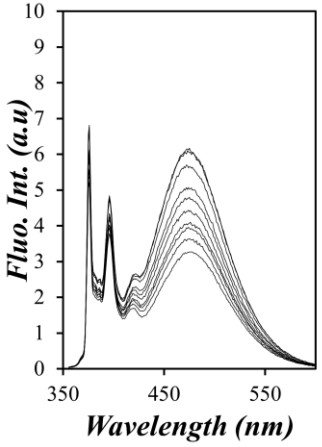	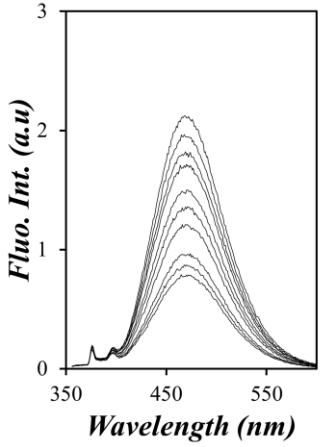	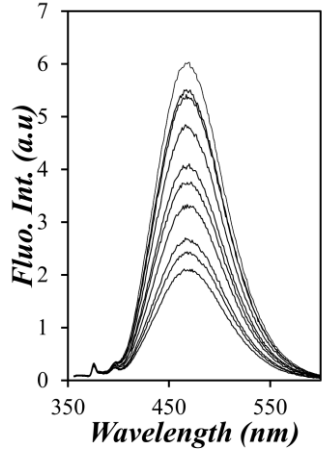
TRF decay at 375 nm	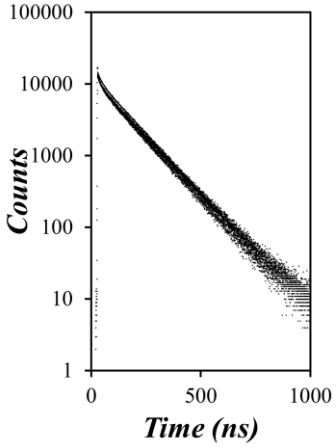	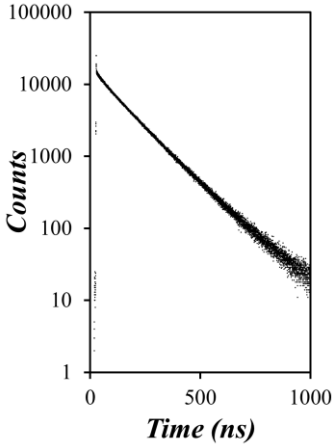	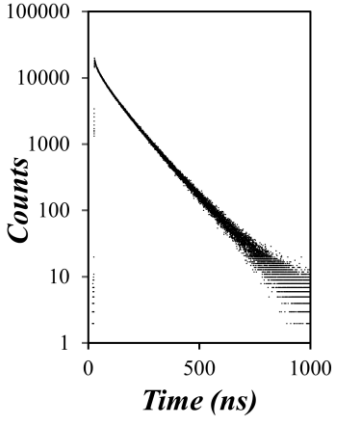	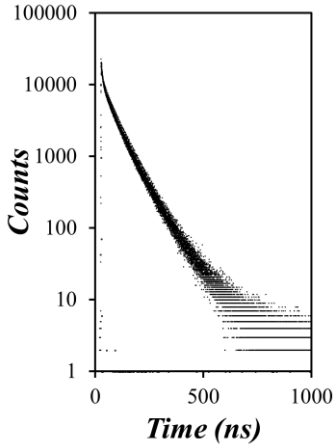	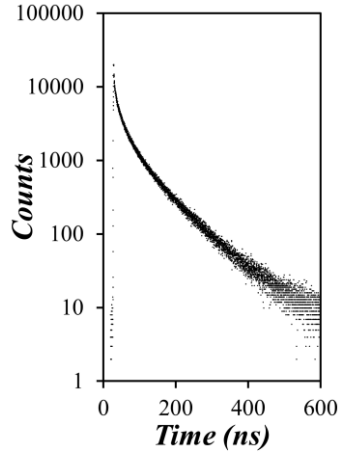

S-V plot at 375 nm	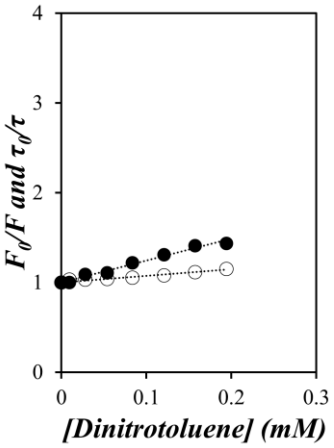	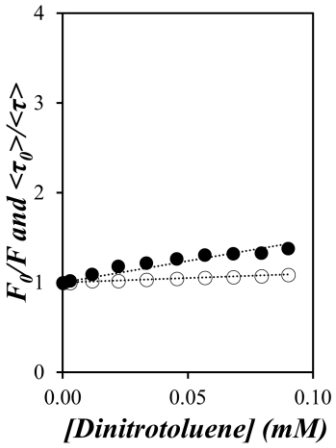	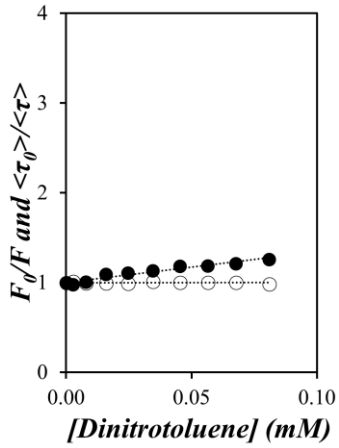	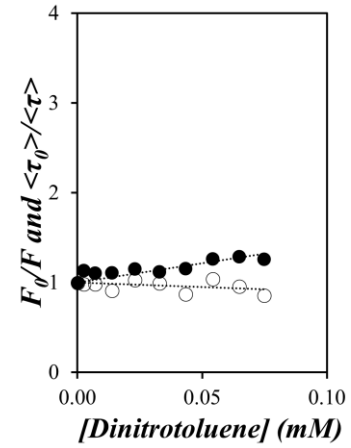	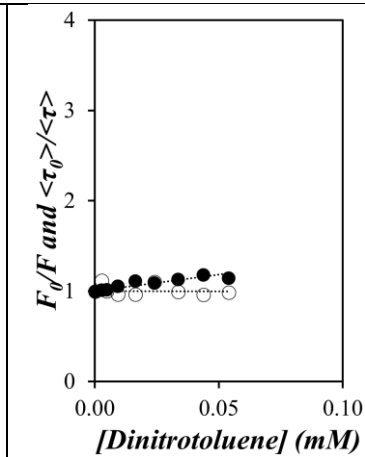
TRF decays at 510 nm			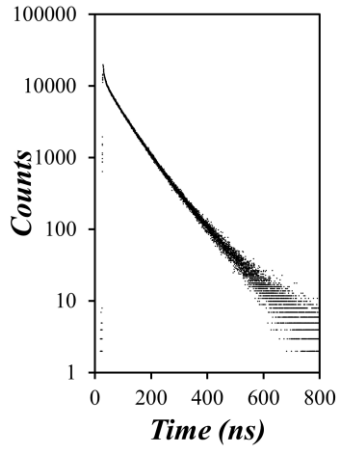	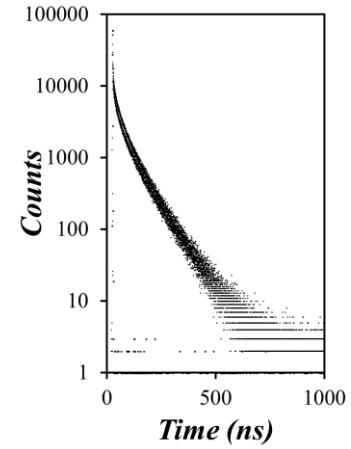	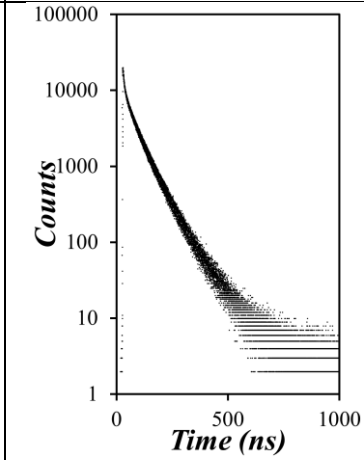

SV plot at 510 nm			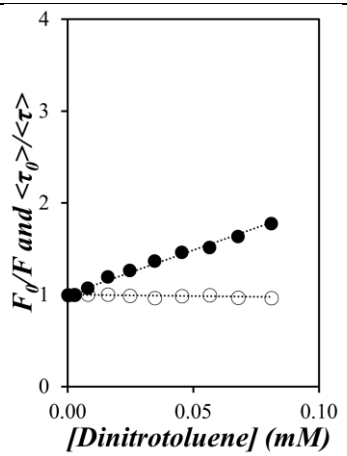	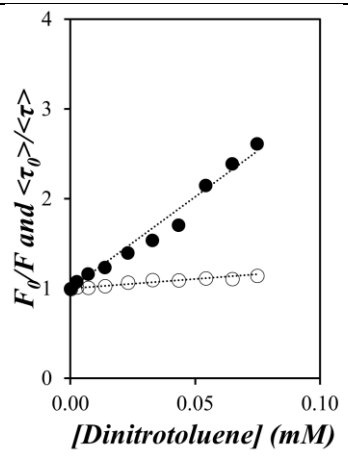	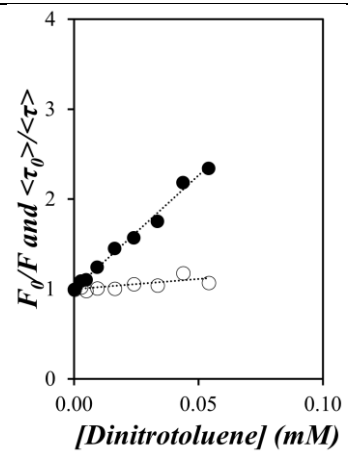

Table A57. Steady state (SS) spectra, time-resolved fluorescence decays, and Stern-Volmer plots of F_0/F (●) and τ_0/τ (○) as a function of [TNT] for quenching studies conducted in milliQ water.

Sample	Py(3.7)-SNP	Py(6.0)-SNP	Py(7.9)-SNP	Py(10.5)-SNP
SS spectra	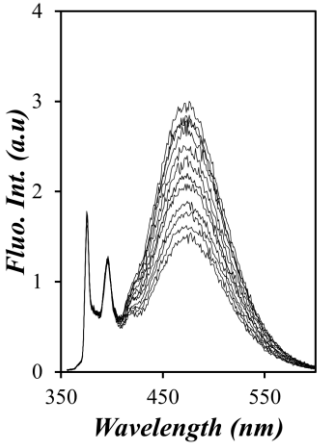	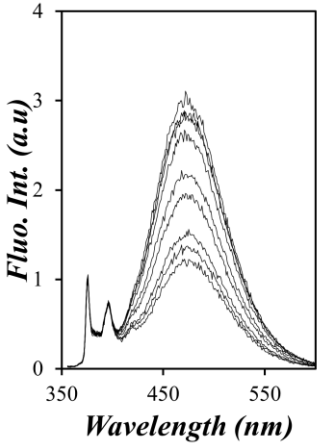	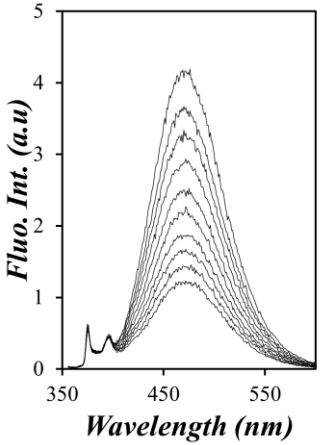	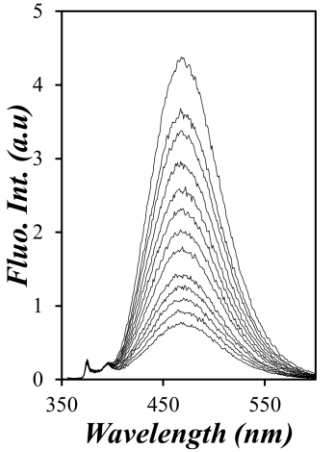
TRF decays 375 nm	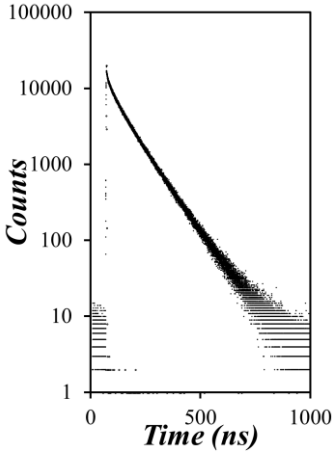	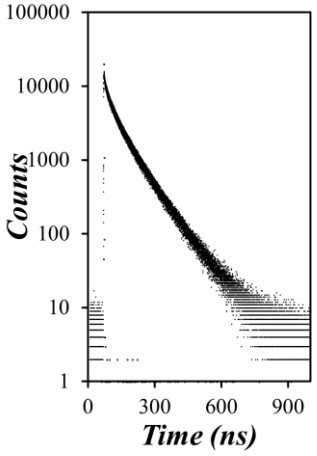	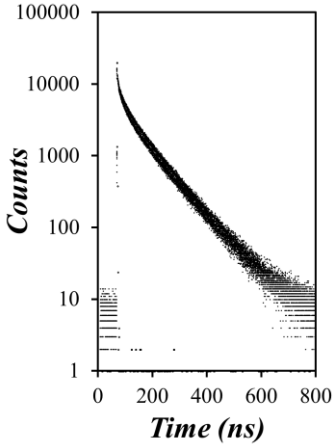	

S-V plot at 375 nm	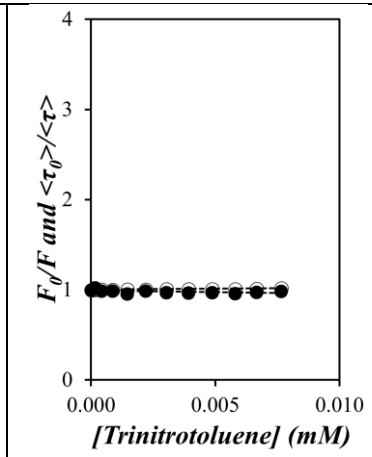	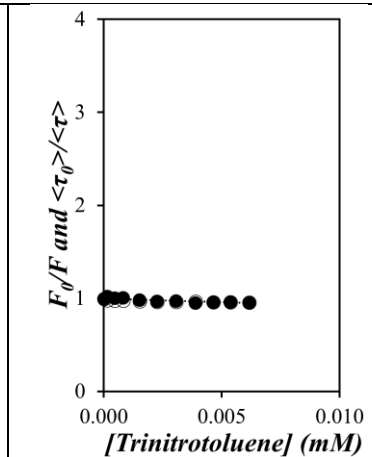	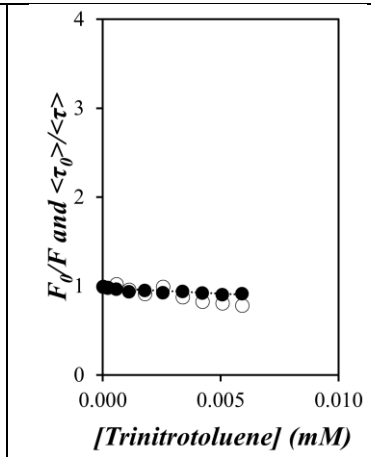	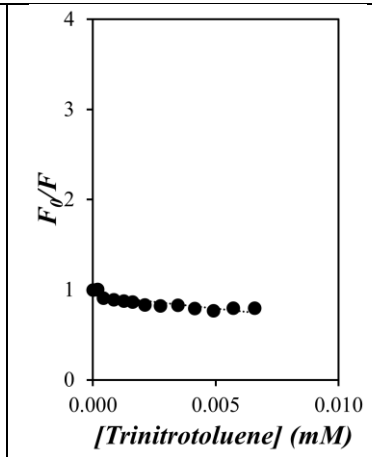
TRF decays at 510 nm	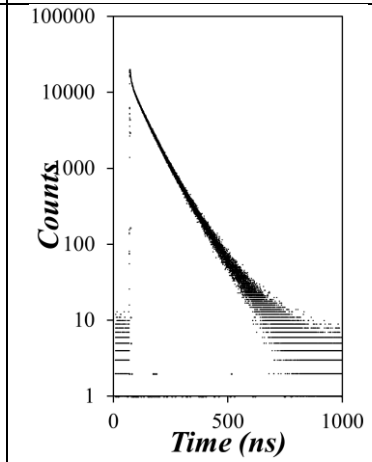	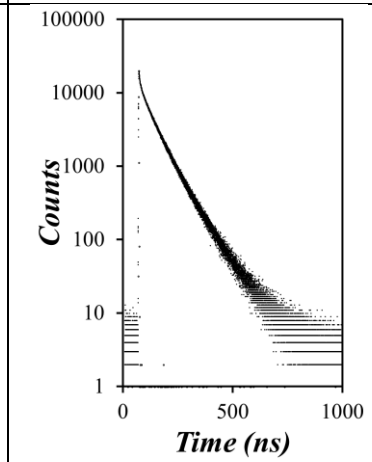	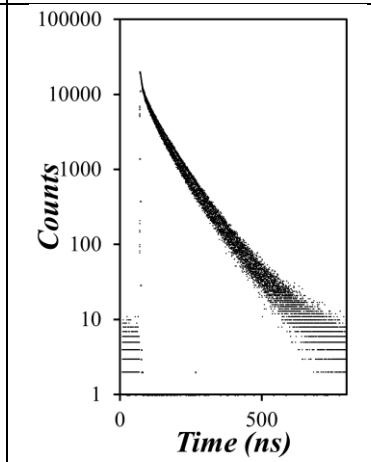	

S-V plot	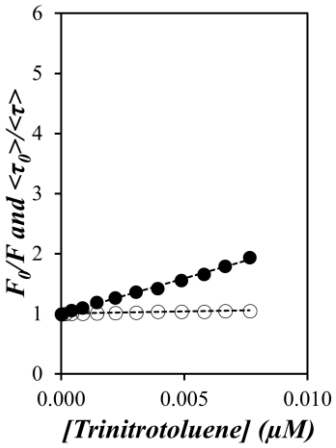	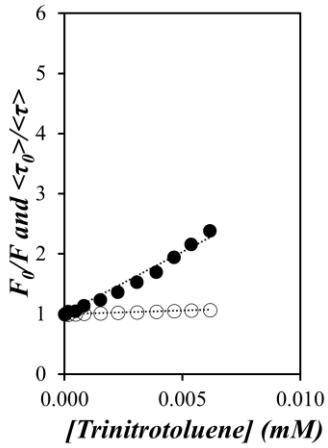	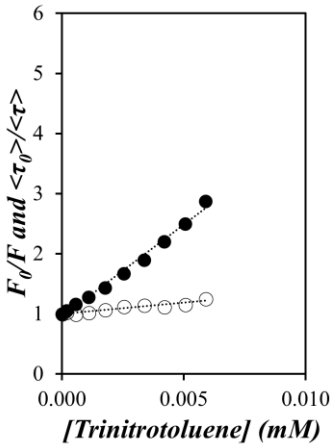	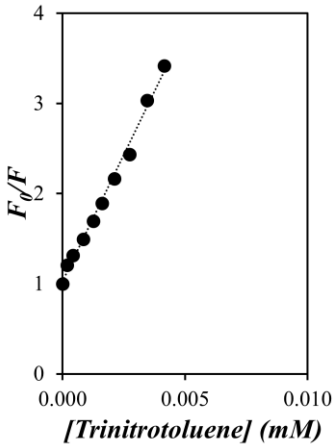

Table A58. Parameters obtained from the Michalis-Menten like equation fits.

Quencher	k_m **(s)**	**(**Δk_m**)**
MNT	0.0534	0.0076
DNT	0.39	0.06

Table A59. Parameters obtained from the Hills equation fits.

Sample Name	Quencher	y	Detection limit (ng/mm^2)	(ΔDL) (ng/mm^2)	k (ng/mm^2)	(Δk) (ng/mm^2)	h	(Δh)
Py(11)-SNP1	MNT	0.1	30	9	9	1	1.8	0.4
Py(11)-SNP1	TNT	0.1	1.4	0.6	0.17	0.04	1.0	0.2
Py(1)-SNP1	DNT	0.1	205	150	33	11	1.2	0.4
Py(4)-SNP1	DNT	0.1	118	45	13	2	1.0	0.2
Py(6)-SNP1	DNT	0.1	141	93	23	7	1.2	0.4
Py(8)-SNP1	DNT	0.1	20	13	3.8	1.1	1.3	0.5
Py(11)-SNP1	DNT	0.1	11	5	3.6	0.8	1.9	0.7
Py(36)-SNP1	DNT	0.1	7	3	2.7	0.6	2.4	1.0
Py(6)-SNP2	DNT	0.1	62	45	14.4	4.5	1.5	0.7
Py(39)-SNP2	DNT	0.1	11	5	1.6	0.4	1.2	0.3
Py(6)-Amy	DNT	0.1	132	87	11.6	3.7	1.0	0.3
Py(4)-Sty(10)-SNP1	DNT	0.1	32	17	11.2	2.8	2.1	0.9
Py(15)-Sty(10)-SNP1	DNT	0.1	28	20	5.3	1.7	1.3	0.5

Table A60. Comparison of detection limits reported in the literature since 2010 presented in order from most to least recent.

Year	Analyte Detection limit	Optical sensor type and detection method	REF#
2018	K_s of $8.4 \cdot 10^4$ M^{-1}, and a response time of 300 s to achieve over 89% quenching efficacy	A series of emissive polythiophene (PT) derivatives were made. Their quenching efficiencies were characterized in $CHCl_3$ by monitoring the decrease in fluorescence intensity with increasing concentration of NACs quenchers. Picric acid was found to be the best quencher. Films of the PT derivatives, made by drop casting the chlorobenzene polymer solution onto quartz plates, were characterized by monitoring the quenching efficiency as a function of exposure time to picric acid vapors.	Ref #68
2018	Picric acid, 0.20 ng per mm^2 with 65% quenching.	A series of dibenzothiophene derivatives were synthesized. Films of the dibenzothiophene derivatives adsorbed onto 1 × 1 cm^2 cotton tissues via immersion in chloroform-polymer solutions for 24 hours and subsequently dried at room temperature under vacuum. NACs were added directly onto the films and detection limits were determined by visual inspection.	Ref #30
2018	TNT, $K_{sv} = 1.3 \cdot 10^5$ M^{-1}	2-Bromoethyl methacrylate polymer microbeads were synthesized, and a pyrene derivative was link to the microbeads via azide functionalization and click chemistry. Dispersion of the pyrene linked microbeads (0.05 g/L) were made in water and NACs were progressively added to the dispersions. Stern-Volmer plots were made and the Stern-Volmer constant, $K_{sv,}$ was determined. Note K_{sv} is equivalent to $k_q \times \tau_0$.	Ref: #26
2018	TNT, detection limit is 1 drop of a 0.1 g/L solution	Two novel polytriphenylamine derivatives were synthesized with aggregation induced emission active tetraphenylethylene units in the backbone and side chains via Yamamoto-type coupling. Paper sensors were made by drop-coating polymer solutions onto filter papers and drying with a gentle flow of air. TNT solutions were prepared and dropped onto the fluorescence paper strips. The detection limit was determined by visual inspection.	Ref: #21
2018	TNT, 0.5 nM TNT induces noticeable change in the fluorescence intensity of the paper strips.	A polyethylene imine protected copper nanocluster (PEI CuNC) was prepared. Strip of Whatman #35 filter papers were coated via 1 hour incubation in an aqueous PEI CuNC solution. The prepared PEI CuNC coated paper strips were soaked in TNT solutions with various concentrations. Detection limit was determined by visual inspection.	Ref: #18
2017	Detected 0.5 μM TNT in aqueous	The drop method was employed to coat cellulose filter papers with carbon quantum dots. The prepared films were then	Ref: #16

	solution with almost 100% quenching	dipped into aqueous TNT solutions for 10 seconds. The detection limit was determined by visual inspection.	
2017	TNT, found K_{SV} values of $2.0 \cdot 10^3$ and $4.1 \cdot 10^3$ M^{-1} for P1, and P2, respectively	Carbazole based linear (P1) and hyperbranched (P2) conjugated polymers were synthesized via Sonogashira coupling. The polymers were characterized in dichloromethane (DCM) solutions by monitoring the fluorescence intensity with increasing concentration of TNT. Stern-Volmer plots were made and the Stern-Volmer constant, $K_{sv,}$ was determined in DCM for both polymers	Ref: #11
2017	A detection limit of 50 ppm for TNT was determined.	Block copolymers of poly (2-hydroxyethl methacrylate-co-pyrene-butyric acid hydroxyethyl methacrylate was made. The polymers were adsorbed onto cellulose filter papers via immersion of filter paper in a polymer solution in methanol for 10 s at room temperature. Methanol was evaporated, the filter paper was cut into test strips and 5 µL of aqueous NACs solutions was deposited onto the filter paper. The detection limit was determined by visual inspection.	Ref: #38
2017	TNT, 0.14 ng per mm^2	Polyaniline was synthesized. Filter paper was immersed in a polyaniline ethanol-acetonitrile solution for 1 hour at room temp. A gloved finger was dipped into 40 µL of TNT solution with a known concentration, and then pressed onto a polyaniline coated filter paper. The detection limit was determined by an infrared camera.	Ref: #37
2016	TNT, 1 ng per mm^2 poly(triphenyl ethene)	Two aggregation-induced emission active polymer, namely poly(triphenyl ethene) and pol(tetraphenyl ethene) were prepared. A known amount of NAC per unit area of filter paper was deposited onto filter paper. A layer of poly(triphenyl ethene) in THF/H_20 (1:9 v/v) was spray-coated onto NAC contaminated filter paper.	Ref: #22
2015	TNT, 5×10^{-5} M in water with complete quenching.	A copolymer of styrene and styrene functionalized with pyrene was synthesized, and electrospun into a fluorescent nanofiber membrane (FNFM). The FNFM was dipped into 1:1 H_2O:acetonitrile solution mixtures with different TNT concentrations. The membrane was incubated at room temperature in these solutions for 10 minutes. The detection limit was determined by visual inspection.	Ref:# 27
2015	Determined a K_{SV} value of $1.8 \cdot 10^5$ M^{-1} for TNT	Pyrene-labeled polyether sulfone was electrospun onto a quartz plate. The film was then immersed in milliQ water. Quencher dissolved in water was progressively added to the cuvette and the fluorescence intensity of the excimer (I_E) was measured. A Stern-Volmer plot was constructed and was used to determine K_{sv}.	Ref: #25
2014	Over 80% quenching was observed after a 5-minute exposure time to TNT vapors	Pyrene was encapsulated in organically modified silica networks. Several films with varying thickness were prepared by spin coating. The films were enclosed in a vial with the	Ref: #10

		headspace saturated with TNT at room temperature and the quenching efficacy was monitored as a function of time.	
2012	Determined K_{SV} to be $2.5 \cdot 10^5$ M^{-1} for picric acid loaded with 0.110 mmol per g of tetraphenylethene	A series of mesoporous silica was functionalized with varying amount of aggregation-induced emission active tetraphenylethene. The functionalized mesoporous silica was dispersed in water and the fluorescence intensity was monitored with increasing amounts of picric acid dissolved in water. Stern-Volmer plots were constructed and K_{SV} was determined.	Ref: #20
2011	Determined K_{SV} to be $1.2 \cdot 10^5$ M^{-1} for TNT	Several donor-acceptor conjugated polymers were prepared with diethylamine phenyl (donors) and 2,1,3-beznothiadiazole (acceptors). Films of these polymers were prepared by spin coating the polymer solutions in organic solvents onto dried quartz plates. The quartz plate were immersed in water and the quencher was added to the solution. The K_S for TNT was determined.	Ref: #69
2010	Determined K_{SV} to be $1.5 \cdot 10^5$ M^{-1} for picric acid quenching experiments conducted in 50% THF and 50% water solution.	Hyperbranched poly(silyenephenylene) polymer particles were prepared. Quenching studies were carried out in THF, and THF-Water mixtures and the photoluminescent intensity was monitored with increasing amounts of picric acid in either THF or THF-water mixtures.	Ref: #49

Derivation of the Stern-Volmer Equation for the quenching of Py-SNPs

The pyrene labels and the SNPs were, respectively, soluble and dispersible in DMSO. The random distribution of the pyrene labels inside the Py-SNPs resulted in the formation of pyrene-rich and pyrene-poor domains where excimer formation occurred at different rates. Consequently, the process of pyrene excimer formation could be described by Equation S1 where a population of pyrene Py_i found in the Py-SNPs was excited to generate Py_i* and form excimer upon encounter with a ground-state pyrene. In Equation S1, k_i is a pseudo-unimolecular rate constant of excimer formation corresponding to a specific local concentration of pyrene labels around Py_i* inside the Py-SNP, and τ_M and τ_E are the natural lifetimes of the pyrene monomer and excimer, respectively.

$$\begin{array}{ccccc} \mathrm{Py_i} + h\nu & \longrightarrow & \mathrm{Py_i}^* + \mathrm{Py} & \xrightarrow{k_i} & (\mathrm{Py_iPy})^* \\ & & \downarrow \tau_M^{-1} & & \downarrow \tau_E^{-1} \end{array} \quad \text{(S1)}$$

Addition of a quencher Q to a dispersion of Py-SNP in DMSO induced the quenching of the pyrene species Py_i* with a rate constant k_q according to the reaction scheme shown in Equation S2.

$$\begin{array}{ccccc} \mathrm{Py_i} + h\nu & \longrightarrow & \mathrm{Py_i}^* + \mathrm{Q} & \xrightarrow{k_q} & \mathrm{Py_i} + \mathrm{Q} \\ & & \downarrow \tau_M^{-1} & & \end{array} \quad \text{(S2)}$$

Based on the two reaction schemes given in Equations S1 and S2, the concentration of the species Py_i* could be described by Equation S3, which after integration yielded Equation S4.

$$\frac{d[Py_i^*]}{dt} = -\left(\frac{1}{\tau_M} + k_i + k_q[Q]\right)[Py_i^*] \quad \text{(S3)}$$

$$[Py_i^*]_{(t)} = [Py_i^*]_o \times \exp\left[-t\left(\frac{1}{\tau_M} + k_i + k_q[Q]\right)\right] \quad \text{(S4)}$$

The fluorescence decay of the pyrene labels could then be obtained by accounting for all pyrene species in the dispersion as done in Equation S5.

$$[Py^*]_{(t)} = \sum_{i=1}^{\infty}[Py_i^*]_o \times \exp\left[-t\left(\frac{1}{\tau_M} + k_i + k_q[Q]\right)\right] \quad \text{(S5)}$$

The intensity (I), equivalent to the number average lifetime ($<\tau>_N$), of the fluorescence emitted by the pyrene labels was then obtained by integrating Equation S5 from time t equal to zero to infinity as shown in Equation S6.

$$I = <\tau>_N = \int_{t=0}^{\infty} [Py^*]_{(t)}\, dt = \sum_{i=1}^{\infty} [Py_i^*]_o \times \frac{1}{\frac{1}{\tau_M} + k_i + k_q[Q]} \tag{S6}$$

The Stern-Volmer equation was obtained by taking the ratio of the fluorescence intensity without quencher (I_o) over that with quencher (I). Since I is given by Equation S6, I_o or $<\tau>_{No}$ could be easily calculated by setting Q equal to zero in Equation S6 to yield Equation S7.

$$\frac{I_o}{I} = \frac{<\tau>_{No}}{<\tau>_N} = \frac{\sum_{i=1}^{\infty} [Py_i^*]_o \times \frac{1}{\frac{1}{\tau_M} + k_i}}{\sum_{i=1}^{\infty} [Py_i^*]_o \times \frac{1}{\frac{1}{\tau_M} + k_i + k_q[Q]}} = \frac{\sum_{i=1}^{\infty} [Py_i^*]_o \times \frac{1}{\frac{1}{\tau_M} + k_i}}{\sum_{i=1}^{\infty} [Py_i^*]_o \times \frac{1}{\frac{1}{\tau_M} + k_i} \times \frac{1}{1 + \frac{k_q}{\frac{1}{\tau_M} + k_i}[Q]}} \tag{S7}$$

Taking advantage of the fact that quenching is highly efficient, the ratio $k_q/(1/\tau_M + k_i)$ is expected to be much smaller than unity which enabled the expansion of Equation S7 into Equation S8.

$$\frac{I_o}{I} = \frac{<\tau>_{No}}{<\tau>_N} = 1 + k_q[Q] \frac{\sum_{i=1}^{\infty} [Py_i^*]_o \times \frac{1}{\left(\frac{1}{\tau_M} + k_i\right)^2}}{\sum_{i=1}^{\infty} [Py_i^*]_o \times \frac{1}{\frac{1}{\tau_M} + k_i}} = 1 + k_q[Q] <\tau>_{Wo} \tag{S8}$$

In Equation S8, $<\tau>_{Wo}$ is the weight average lifetime of the pyrene labels. Consequently, plotting the ratio of the number average lifetimes $<\tau>_{No}/<\tau>_N$ as a function of quencher

concentration was expected to yield a straight line whose slope equals $k_q \times \langle\tau\rangle_{Wo}$. Straight lines were obtained in all quenching experiments for the $\langle\tau\rangle_{No}/\langle\tau\rangle_N$ ratios and the quenching rate constant k_q was calculated by dividing the slope by $\langle\tau\rangle_{Wo}$. This procedure was applied to obtain all k_q values presented in Figure 8.

Determination of response times, detection limits, and their errors

A) Response times and errors: All quenching studies conducted with chemical vapour were conducted with 0.5×0.5 cm^2 Py-CFPs coated with Py(11)-SNP1 as described in the experimental section (Chapter 2). The quenching efficiency given as $(1-\frac{F}{F_0})\times 100\%$ was plotted as a function of exposure time (t). The data were well described by a hyperbola which could be parameterized with Equations 6 and S9, similar to the Michalis Menten equation typically used to describe enzyme kinetics.[70]

$$E_Q = (1-\frac{F}{F_0})\times 100\% = \frac{t}{k_m + t} \qquad \text{(S9)}$$

The method of propagation of error, commonly used in statistics, was employed to determine the error on the detection limit.

B) Detection limits and errors: All quenching studies where the quencher was directly deposited onto the Py-CFPs were modeled with the Hill equation, shown in Equations 7 and S10. The Hill equation, formulated by Archibald Hill, was initially derived to model the sigmodal binding of O_2 to hemoglobin.[71] It was found to describe the decrease in the fluorescence intensity plotted as a function of the mass of quencher deposited on the Py-CFP expressed in ng of quencher per mm^2. All experimental data was fitted using OriginPro by using random guesses for h and k, and

minimizing the error in y with the fitted function.

$$/\, y = 1 - \frac{x^h}{x^h + k^h} \tag{S10}$$

The detection limit was obtained by finding the value of x in Equation S10 that would result in a value of y equal to 0.1 which corresponded to a 90% quenching efficiency. This was achieved by inverting Equation S10 as shown in Equation S11.

$$f(x) = k \times \exp[\frac{1}{h} \times Ln(\frac{1-y}{y})] \tag{S11}$$

The method of propagation of error was applied to determine the error on x.